ROLE OF GRM1 IN ALTERING GLUTAMATE METABOLISM AND BIOAVAILABILITY

By

RAJ D. SHAH

A dissertation submitted to the

School of Graduate Studies

Rutgers, The State University of New Jersey

In partial fulfillment of the requirements

For the degree of

Doctor of Philosophy

Graduate Program in Toxicology

Written under the direction of

Dr. Suzie Chen

And approved by

_____

_____

_____

_____

_____

New Brunswick, New Jersey

May 2020

ABSTRACT OF THE DISSERTATION

Role of GRM1 in Altering Glutamate Metabolism and Bioavailability

By RAJ D. SHAH

Dissertation Director:

Suzie Chen

Altered metabolic activity has been implicated in several types of cancer including malignant melanoma. Previously, we have illustrated the role of a neuronal receptor, metabotropic glutamate receptor 1 (GRM1), in the neoplastic transformation of melanocytes *in vitro* and spontaneous development of metastatic melanoma *in vivo*. Glutamate, the natural ligand of GRM1, is one of the most abundant amino acids in humans and the predominant excitatory neurotransmitter in the central nervous system. The overall goal of this dissertation is to determine how ectopic GRM1 expression leads to the rewiring of metabolic processes, especially in glutamate metabolism, and how this may contribute to deregulated tumor cell proliferation. Using a set of isogenic melanoma cell lines, we demonstrated correlations between GRM1 and glutaminase (GLS) expression. Metabolomics revealed that $GRM1^+$ melanoma cells exhibit elevated levels of glutaminolytic mitochondrial tricarboxylic acid (TCA) cycle-related amino acids and intermediates, especially glutamate. The increased intracellular pool size of glutamate could be a direct result of increased conversion of glutamine to glutamate via the activity of GLS. Furthermore, principle component analysis revealed that modulation of GRM1 in

the aforementioned set of isogenic melanoma cells causes metabolic perturbations that overlap with GRM1 expression levels. It has been well known that glutaminolysis is primarily responsible for increased glutamate production in tumors. Using a rational drug-targeting strategy, we critically evaluate metabolic bottlenecks with the goal to cut off tumor glutamate bioavailability. In cultured $GRM1^+$ melanoma cell lines, CB-839, a potent, selective, and orally bioavailable inhibitor of GLS suppressed cell proliferation while riluzole, an inhibitor of glutamate release, promoted apoptotic cell death *in vitro* and *in vivo*. Combined treatment with CB-839 and riluzole treatment proved to be superior to single agent treatment, restricting glutamate bioavailability and leading to severe suppression of tumor cell proliferation *in vitro*. Most importantly, disruption of GRM1 signaling through combined actions of CB-839 and riluzole significantly suppressed tumor growth in two independent xenograft mouse models of melanoma, with no obvious symptoms of toxicity detected. Molecular analysis of excised tumor specimens demonstrated enhanced suppression of ERK and AKT phosphorylation with the combination of CB-839 and riluzole. Using LC-MS analysis, we determined that the blood plasma concentration of unbound riluzole is substantially higher in male mice compared to females possibly clarifying why riluzole treatment displays a superior response in males. Finally, we established that GLS overexpression, in $GRM1^+$ cell lines, ensues at least in part, through the deep-rooted mTORC axis, as seen through pharmacological inhibition of mTOR phosphorylation and subsequent downregulation of GLS. These insights, combined with our data, support the rationale to target glutamate bioavailability and may aid in the identification of novel metabolic targets to combat $GRM1^+$ human neoplasia.

ACKNOWLEDGEMENTS

I would like to express my sincerest gratitude to my mentor and thesis advisor, Dr. Suzie Chen, who has guided me through this dissertation and has helped transform this "pair of hands" into an independent scientist. Your door is always open and you have always listened to what I have to say as if I was your equal. Your vigorous support, guidance and mentorship have been essential to my scientific career growth as an independent scholar as well as an individual. I am in the Susan Cullman Laboratory for Cancer Research (LCR) because 8 years ago, you took a chance on me and gave me numerous opportunities as an undergraduate, technician and graduate student. Whoever I am today is because of you. Whatever success I can find in the future, I will owe every single bit of it to you. I can proudly say that I have the best dissertation advisor anyone can possibly have.

I would like to sincerely thank my committee members, Dr. Cheryl Dreyfus, Dr. Shengkan Jin, Dr. Lori White, and Dr. Renping Zhou for giving me great advice and insight, and for contributing to my understanding of cancer biology. I learn a lot from our conversations during committee meetings. I would like to express my special thanks to Dr. Philip Furmanski, Dr. Nan Joo Suh and Dr. Renping Zhou for their morale-boosting words. They have given me invaluable guidance over the years.

To all the past and present members of the Chen lab, especially Dr. Brian Wall, Jairo Sierra and Robert Cerchio, all of you have been extremely supportive and encouraging. I want to thank undergraduate students, Andrew Boreland and Darling Rojas - both of them have been major assets to this project. Their meticulous efforts in assisting with various experiments have been endless. The environment in our lab has been inspiring

and tremendously collaborative. I will miss every single one of you and will cherish these memories for life.

To all of my colleagues here at LCR, past and present: Dr. Chetan Rane, Dr. Trushar Rathod, Dr. Prasad Subramaniam, Dr. Alex Bott, Naing Lin "Paul" Shan, Dr. Joseph Wahler, Dr. Soumyashree Das Gupta. All of you have been fellow research companions and friends – thank you for making my time in the department enjoyable. I am grateful for the time we have spent together, and I will miss you all.

To the LCR staff, past and present: Deborah Stalling, Erica Dipaola, Bobbie Busch, Annette Dinisio, Dorothy Wong, Vi Dan, Amy Loughman. Your immense support with my teaching assistantship, administrative paperwork or any other responsibility has made this journey a pleasant one.

Last but most important, I would like to thank all my family members whose guidance and unconditional love has been the cornerstone of my success. To my wife, my best friend and the love of my life, Mosam Shah, I cannot explain how grateful I am to have you in my life. Your support has been unconditional throughout this process. This dissertation is as much your effort as mine.

DEDICATION

I would like to dedicate this dissertation to my family whose affection and support has carried me this far.

ACKNOWLEDGEMENT OF PUBLICATIONS

This dissertation is composed, in part, of three research articles that have been listed below and thereby acknowledged. I am the co-first author of these articles. All of the data and writing reused in this thesis represents my original work, except a few key metabolomic analyses that were conducted by our collaborator, Dr. Filipp. His contributions have been indicated as necessary.

Singh SJ*, **Shah R***, Olmstead K, Filipp FV and Chen S. *Targeting Glutamine Metabolism in Melanoma.* Manuscript submitted for publication.

Shah R*, Singh SJ*, Eddy K, Filipp FV and Chen S. *Concurrent Targeting of Glutaminolysis and Metabotropic Glutamate Receptor 1 (GRM1) Reduces Glutamate Bioavailability in GRM1$^+$ Melanoma.* Cancer Research, 2019. **79**(8): p. 1799-1809.

Pelletier JC, Chen S, Bian H, **Shah R**, Smith GR, Wrobel J and Reitz AB. *Dipeptide Prodrugs of the Glutamate Modulator Riluzole.* ACS Med Chem Lett, 2018. **9**(7): p. 752-756.

TABLE OF CONTENTS

LIST OF FIGURES

Introduction

Melanoma

In the United States, cancer is the second leading cause of death and is expected to surpass heart disease in several years [1]. Cancer of the skin is by far the most common of all cancers, with increasing frequency for the past three decades. It includes basal cell carcinoma (BCC), squamous cell carcinoma (SCC) and melanoma. Although melanoma accounts for only ~5% of all skin cancers, it causes an overwhelming majority of skin cancer related fatalities. Melanoma is the most aggressive, malignant and dangerous form of skin cancer. According to the American Cancer Society, approximately 100,350 new cases of invasive melanoma will be diagnosed and 6,850 deaths will occur in 2020 [2]. Generally, women are more susceptible to melanoma than men before age 50, interestingly, the incidence rates in men are double and even triple than women by age 65 and older [2]. Among racial groups, melanoma is more common among Caucasians than any other ethnic group [2]. Melanoma is more likely to grow and metastasize, and patients frequently perish to metastatic, not primary tumors. The survival rate for patients varies depending on the stage of disease at time of diagnosis. For melanoma lesions that are detected early, have not penetrated deep into the epidermis and promptly removed, the 5-year survival rate is almost 100%. If the disease is more advanced when the melanoma has metastasized to other organs, the 5-year survival rate is only 20% [2]. Besides, analysis of over 27,000 melanoma patients suggests that as primary tumor thickness increases, there is a significant decrease in survival [3]. Depending on the different molecular mechanisms underlying the disease, melanoma is classified into four major subtypes: nodular, superficial spreading,

lentigo maligna and acral. The most common type of melanoma is superficial spreading melanoma, which accounts for 80% of all melanomas [4].

Melanoma arises from the aberrant transformation and uncontrolled proliferation of melanocytes, specialized melanin producing cells of the skin, and can develop anywhere on the skin [5]. Melanin protects the deeper layers of the skin from harmful ultraviolet (UV) light exposure [6, 7]. UV radiation, from the sun and of late from indoor tanning devices, damages DNA by inducing the dimerization of adjacent thymine nucleotides, thus interfering with DNA replication [6, 7]. While humans have cellular mechanisms to repair these dimers, mutations can occur and abolish the repair process. Accumulation of mutations in a cell's DNA is the primary cause of cellular transformation and subsequent tumorigenesis. With respect to melanoma, several oncogenes and tumor suppressors have been implicated in the initiation, progression, and maintenance of the disease; however, it remains one of the most difficult cancers to treat. Like other solid tumors, melanoma is genetically heterogeneous and thrives in an environment with many cell types with various metabolic profiles including immune cells, some of which generate a suppressive tumor microenvironment, permitting cancerous cells including melanoma cells to survive.

Genetic mutations associated with melanoma development

The mitogen-activated protein kinase (MAPK) and PI3K/AKT (also known as protein kinase B or PKB) pathways are frequently dysregulated in tumors, including sporadic melanoma. Activation of the MAPK pathway is crucial for mediating signal transduction cascades regulating tumor cell proliferation and invasion [8]. On the other hand, PI3K/AKT pathway activation leads to suppression of apoptosis in tumor cells,

thereby promoting survival [9]. The MAPK and PI3K/AKT pathways cooperate with each other in the transduction of survival signals [10]. The discovery of the most common mutation (V600E) in the *RAF* gene encoding the serine/threonine protein kinase BRAF (BRAF) in 60% of melanomas was a monumental step in the quest for developing targeted therapy against the disease. A single-base missense substitution resulting in a T to A transition at nucleotide 1799 causes the substitution of a valine for a glutamic acid at codon 600 (V600E) of the kinase domain [11, 12]. Other less common mutations such as V600K, V600R and V600M are known to occur in a low percentage of cancer patients [13]. NRAS, a member of the RAS family of oncogenes, is mutated only in ~15-20% of melanoma cases [14]. Curtin *et al*. postulated that NRAS activates both PI3K/AKT and MAPK pathways, while BRAF only activates MAPK in melanoma pathogenesis [15]. In melanoma, tumor suppressor genes such as PTEN, or INK4A are lost in many cases. Both BRAF and NRAS require another stimulus, such as loss of PTEN for BRAF and inactivating mutations in INK4A for RAS to yield transformed melanoma cells [16, 17]. The PTEN tumor suppressor is known to antagonize the PI3K/AKT pathway; therefore, its loss results in dysregulated expression of AKT.

Normal melanocyte differentiation and proliferation are under the control of the microphthalmia-associated transcription factor (MITF). MITF plays a role in lineage commitment of melanocytes and melanoma [18]. MITF expression is essential for melanoma cell proliferation and survival [19]. With integrative genomic analysis, it is found to be amplified in ~16% of melanomas. $BRAF^{V600E}$ mutation together with ectopic expression of MITF has been shown to transform primary melanocytes into malignant melanoma [20]. In addition, MITF also stimulates the cell cycle regulator, INK4A, for

efficient melanocyte differentiation [21]. $p16^{INK4A}$ (INK4A) and $p14^{ARF}$ (ARF) are two proteins encoded by the cyclin-dependent kinase inhibitor 2A (CDKN2A), both of which demonstrate tumor suppressive activity. To date, CDKN2A remains the main high risk gene involved in susceptibility to melanoma [22]. Mutations in CDKN2A are found in ~20% of melanoma-prone families. Deletion of INK4A and ARF is a common genetic lesion detected in ~50% of primary tumors and nearly all human melanoma cell lines [23].

G protein coupled receptors and cellular transformation

Guanine nucleotide binding-protein coupled receptors (GPCRs) compromise the largest known family of cell surface receptors which mediate a variety of cellular responses. GPCRs can bind to a wide variety of endogenous ligands including ions, amines, purines, lipids, peptides, and proteins [24]. A GPCR and its associated downstream signal transduction is activated upon binding of its ligand to the ligand-binding site in the extracellular domain - a subsequent conformational change is induced in the intracellular loops of the transmembrane region. Which downstream signaling pathway is turned on is dependent on the type of guanine nucleotide binding protein (G-protein) to which the receptor is coupled [25]. The heterotrimeric G-protein subunits consist of G_{α}, $G_{\beta,}$ and G_{γ}, which are situated at the intracellular domain of the GPCR and function as dimers. The inactive form of the receptor is bound to guanine diphosphate (GDP). The conformational change upon activation results in the exchange of GDP with guanine triphosphate (GTP) of the associated G-protein within the intracellular domain of the GPCR. This phosphate exchange alters the affinity of the G-protein with the GPCR and results in the dissociation of that G-protein [26, 27].

GPCRs are divided into the following five families depending on their sequence and structural homology: rhodopsin, secretin, glutamate, adhesion and Frizzled/Taste2 [28, 29]. Our group exclusively focuses on the glutamate receptor family of GPCRs. Glutamate, the predominant excitatory neurotransmitter in the central nervous system (CNS), exerts its signaling properties on glutamate receptors. Glutamate receptors are divided into two major classes: ionotropic glutamate receptors (iGluRs) and metabotropic glutamate receptors (GRMs). The iGluR subfamily regulates synaptic transmission of the central nervous system (CNS), which plays a role in the flow of cations across the plasma membrane of neuronal cells allowing for the depolarization and influx of calcium [30]. iGluRs mediate rapid transient synaptic transmission. Based on their sequence similarities, electrophysiological and pharmacological properties, iGluRs are sub-categorized into NMDA (N-methyl-D-aspartate), AMPA (α-amino-3-hydroxyl-5-methyl-4-isoxazole-propionate) and kainate receptors (KAR) [31-33]. AMPA receptors evoke excitatory postsynaptic potentials and mediate fast synaptic transmission. In contrast, kainate and NMDA receptors mediate slower synaptic transmission and exert their effects on plasticity. The discussion on metabotropic glutamate receptors is continued in the next section.

GPCRs have been known to have oncogenic properties since the identification of the oncogene, *Mas,* by Wigler and colleagues in 1986 [34]. Wild type *Mas* is able to transform murine NIH3T3 fibroblasts with weak foci forming ability *in vitro* but strong tumorigenicity *in vivo* [34]. The lack of mutations in *Mas* was the first documented study of a normal GPCR being tumorigenic through ectopic expression alone. Not long after, a study on the effects of an ectopically expressed serotonin GPCR in NIH3T3 cells revealed that wild type GPCRs have the potential to become tumorigenic when exposed to an excess

of locally produced or circulating ligands and agonists in the cellular microenvironment [35]. These findings were further supported by the observation that ectopically expressed human muscarinic acetylcholine receptors, which share sequence homology with both the *mas* and serotonin receptors, also exhibited transforming potential in NIH3T3 cells under similar conditions [36]. Both of the aforementioned studies noted that maintenance of the transformed phenotype requires the continued presence of the agonist. Another study by Allen *et al*. reported that constitutively activating mutations in GPCRs were sufficient to enhance their ability to alter normal signaling cascades and induce neoplastic transformation in an agonist-independent manner [37]. In the past decade, numerous studies have linked GPCRs to cancer associated mechanisms such as metastasis and immune evasion. A recent publication is the first to report a correlation between methylation of GPCR genes and cancer cell progression [38]. Together these findings place a new focus on the oncogenic potential of GPCRs, how dysregulation might occur, and their influence on signaling pathways involved with the malignant phenotype.

Metabotropic glutamate receptor 1 (GRM1) as an oncoprotein

An emerging hallmark for many malignancies is the aberrant expression and function of metabotropic glutamate receptors (GRMs). GRMs are characterized by their seven transmembrane domain structure and their ability to modulate downstream cellular signaling when activated by their ligands/agonists. The GRM family consists of 8 different subtypes (GRM1-8) that are subdivided into 3 different groups based on their sequence homology and coupling to small G-proteins. Group I GRMs consist of GRM1 and GRM5. Upon activation, Group I GRMs stimulate phospholipase C via $G_{q/11}$, leading to the

formation of two second messengers, inositol 1,4,5-triphosphate (IP3) and diacylglycerol (DAG). In contrast, Group II and Group III GRMs are negatively coupled via $G_{i/o}$ to adenyl cyclase, leading to 3'-5'-cyclic adenosine monophosphate (cAMP) formation. The natural ligand of all GRMs, including GRM1, is glutamate - one of the key neurotransmitters in the mammalian central nervous system responsible for excitatory synaptic signaling in the brain. Normally, GRM1 participates primarily in post-synaptic transmission and its absence results in severe deficits in learning and memory, as shown in GRM1-knockout mice [39]. These mice have also been shown to have reduced long-term potentiation and mild ataxia [40]. It is now known that different GPCRs including GRM1 can mediate and support tumor growth by excessive production or accumulation of ligand by tumor cells themselves [35]. A recent report by Gelb *et al*. has proposed that the GRM1 receptor behaves like a dependence receptor creating dependence on glutamate for sustained growth and viability of human melanomas expressing GRM1 [41].

Our group was the first to establish a heretofore-unknown component of melanoma pathogenesis: melanocytes ectopically expressing metabotropic glutamate receptor 1 (GRM1) leads to melanocyte transformation *in vitro* and spontaneous malignant melanoma formation in a transgenic mouse model, TG-3 [42-45]. Molecular analysis of the TG-3 model suggested that the raised, heavily pigmented lesions developed in the ear (pinnae), eyelid, perianal region and snout due to hyper-proliferation of melanocytes, a consequence of insertional mutagenesis by a transgene insertion into intron 3 of the gene coding for GRM1 with concomitant deletion of about 70kb of host sequence [46]. In order to distinguish whether the aberrant expression of GRM1 in tumors was a cause or a consequence of melanoma, a new transgenic line (E line) was constructed. It was

engineered to express GRM1 in melanocytes under the regulation of a melanocyte-specific promoter, dopachrome tautomerase (DCT). This new E transgenic line displayed similar onset and progression of melanoma as observed for TG-3. Other groups have meanwhile confirmed these findings through the production of an inducible GRM1-driven transgenic murine model where the expression of GRM1 is conditionally activated by a neuron-specific enolase (NSE) in melanocytes [47]. They also demonstrated that continuous expression of GRM1 is essential for maintaining tumorigenicity and its transformed phenotype [47]. We and others have shown that GRM1 activation through glutamate binding and downstream signaling activates the MAPK and PI3K/AKT pathways in melanoma [48, 49] (Figure 1). Specifically, glutamate-stimulated activation of GRM1 causes a conformational change in the receptor followed by GTP hydrolysis. GRM1 is preferentially coupled to $G_{\alpha q}/G_{\alpha/11}$ G-proteins that, upon activation, results in the stimulation of phospholipase C (PLC), causing hydrolytic cleavage of phosphatidylinositol-4,5-bisphosphate (PIP_2) and subsequently giving rise to two second messengers: diacylglycerol (DAG) and inositol-1,4,5-triphosphate (IP_3) [50]. IP_3 promotes increased calcium release from the endoplasmic reticulum whereas DAG activates protein kinase C (PKC). These events result in activation of two of the most commonly deregulated signaling cascades in cancer, MAP kinase and PI3K/AKT [51]. Results from earlier studies have shown that treatment of tumor cells with a GRM1-agonist, L-quisqualate, results in augmented phosphorylation of MEK and ERK [52], which are two integral components of the MAP kinase pathway. Furthermore, the idea that this activation of the MAP kinase pathway is dependent on functional GRM1 was demonstrated by the absence of MAPK activity in cells pre-treated with either a non-competitive GRM1 antagonist, BAY 36-7620

or a competitive GRM1 antagonist, LY367385, followed by stimulation with a GRM1-agonist, L-quisqualate [51, 53].

GRM1 has been extensively studied in order to evaluate its involvement in tumorigenesis. Findings by numerous groups illustrated GRM1 as a potential target for the treatment of breast cancer by showing that reduced GRM1 expression and activation resulted in a diminished growth of breast cancer cells both *in vitro* and *in vivo* [54-56]. Subsequently, GRM1 has been identified as a novel endogenous regulator of inflammation in several triple negative breast cancer (TNBC) cells [57]. Another study has demonstrated the transformative properties of GRM1 in immortalized mouse mammary epithelial cells (iMMECs), which was used as a model system to study breast cancer [58]. The oncogenic potential of GRM1 was also demonstrated in mouse kidney epithelial cells. These cells, when transfected with GRM1, resulted in tumor formation *in vivo*. Furthermore, siRNA-mediated downregulation of GRM1 in transformed kidney epithelial cells impaired tumor growth *in vivo* [59]. Interestingly, RNAi-mediated suppression of GRM1 expression was also associated with decreased invasion *in vitro* and inhibition of tumor cell settling *in vivo* in a pancreatic ductal adenocarcinoma (PDAC) mouse model [60]. The effects of GRM1 antagonists have also been demonstrated in Kaposi's sarcoma herpesvirus (KSHV) associated malignancies [61]. Furthermore, the therapeutic effects of GRM1 silencing have been illustrated in a glioblastoma model *in vitro* and *in vivo*, as demonstrated by knockout and inhibition experiments [62-64]. Taken together, numerous types of cancers have been linked to GRM1 since the initial report in melanoma; however, much work remains to understand how GRM1 expression is activated and pave the road to cell transformation and tumorigenesis.

Melanoma treatments

Chemotherapies and targeted therapies

For patients diagnosed with primary melanoma, surgical removal of the tumor(s) provides the best chance of definitive cure. Late stage melanoma is difficult to treat due to the fact that there is a high genomic variability of heterogeneous tumors [65]. The understanding of how various genetic mutations are associated with the onset and progression of melanoma allows for innovation and subsequent implementation of novel therapeutic strategies targeting specific oncogenes. Within the last decade, much progress has been made in the treatment of metastatic melanoma. Earlier studies have shown that treatment with Sorafenib (BAY 43-9006), a general multi-kinase inhibitor, resulted in inhibition of melanoma cell proliferation *in vitro* and *in vivo* [8] after which its effectiveness was assessed via clinical trials [66]. However, its Phase 2 randomized clinical trial was discontinued in advanced melanoma patients due to little or no antitumor activity [67]. Then, a highly selective small molecule inhibitor, Vemurafenib/Zelboraf (PLX4720/PLX4032), against cells that harbor the most common mutation in melanoma, mutated $BRAF^{V600E}$, was initially reported to have therapeutic effects in patients with advanced melanoma [68-71]. However, most patients who initially responded eventually acquired resistance. Its effectiveness was marred by patient relapse within 8-12 months [71, 72]. The treatment responses were so short-lived likely due to the reactivation of the MAPK pathway or other mutations [10, 48, 72, 73]. Combining BRAF inhibitors with other small molecule inhibitors that target other components of the MAPK pathway such as MEK and ERK appears to be an improvement over single-agent therapy but also has increased toxicity [10, 74, 75]. It is noteworthy that until recently, it had not been possible to develop

an inhibitor towards RAS [76]. Christensen *et al*. reported on a $KRAS^{G12C}$ inhibitor that demonstrates pronounced tumor regression in multiple KRAS-mutant tumor models [77]. Despite the nominal successes described above, responders to these therapies only represent a minority of patients.

Immunotherapies

Melanoma is one of the most immunogenic types of cancers, hence making it a strong candidate for immune checkpoint blockade (ICB) therapy [78]. In the past five years, immune checkpoint inhibitors have become the cornerstone of treatment for melanoma. Monoclonal antibodies against programmed cell death protein 1 (PD-1), nivolumab and pembrolizumab, and cytotoxic T lymphocyte-associated 4 (CTLA4), ipilimumab, block proteins that assist cancer cells to evade T-cell mediated death. Immunotherapies such as anti-CTLA4 or anti-PD-1/anti-PD-L1 antibodies, which specifically target suppressive immune molecules, have shown better response rates and some improvement in patient survival with advanced melanoma [79]. For instance, anti-PD-1 antibodies including pembrolizumab and nivolumab have response rates in the range of 30-40% and improved median overall survival [80]. However, meta-analysis of clinical trial data has shown that only a small proportion of melanoma patients were responsive to single agent monoclonal antibodies against PD-1/PD-L1 [81]. It has been demonstrated that the programmed cell death receptor 1, PD-1 and programmed cell death ligand 1, PD-L1 checkpoint axis act as a negative regulators of the host's immune response [82]. In normal physiology, this axis is used to protect the host against auto-immunity [83]. Cancer cells use this axis to their advantage to escape immune system surveillance [82, 84]. Cancer cells including melanoma cells upregulate PD-L1 expression on the cell surface [78, 84].

T-lymphocytes with surface expression of PD-1 interacts with PD-L1 on the tumor cells, leading to T-cell exhaustion, causing dysfunction of the immune system in detecting and eliminating the tumor cells [84]. Velasco and colleagues' analysis of patient treatment outcomes suggest that as a single agent therapy, anti-PD-1/ anti-PD-L1, might not be as effective as a combination therapy. Resistance to anti-PD-1 therapy may be due to lack of inflammation, downregulation of antigen presentation, and/or lack of PD-L1 expression in the tumor microenvironment (TME). Utilizing various permutations of drugs in combination with anti-PD-1/anti-PD-L1 might improve patients' responsiveness to immune checkpoint blockade (ICB) therapy [81]. It is not surprising that various combinatorial studies utilizing different immune checkpoint or molecular inhibitors targeting single or multiple pathway(s) have been one of the most sought-after clinical trials in human cancers including melanoma.

Targeting GRM1 to combat melanoma

Since the oncogenic potential of GRM1 in cancer especially in melanoma is well characterized, some progress has been made by translating laboratory findings into the clinic. We demonstrated approximately 80% human melanoma cell lines and 60% of human melanoma biopsies have GRM1 expression at both mRNA and protein levels independent of NRAS/BRAF genotypes, while normal human melanocytes do not [48]. Suppression of GRM1 expression by silencing RNA has led to a reduction in tumor cell growth *in vitro* and tumor progression *in vivo* [53, 85]. Riluzole, a glutamate export reducer that is FDA-approved for the treatment of Amyotrophic Lateral Sclerosis (ALS) [86, 87], has been shown to suppress the growth of GRM1 expressing melanoma cells *in vitro*, *in vivo,* and in clinical trials due to suppression of the MAP kinase and PI3K/AKT pathways

[88]. It decreases the available ligand required to stimulate glutamate receptors and functionally acts as an inhibitor of GRM1. Riluzole has been reported to indirectly antagonize glutamate receptors by inhibiting glutamate release as well as the inactivation of voltage-gated Na^+ channels [89]. The inhibition of glutamate release is thought to alter the autocrine loop sustained in GRM1 expressing melanoma cells as these cells are addicted to glutamate and have been shown to release significantly higher levels of extracellular glutamate compared to cells lacking GRM1 [51]. We translated our pre-clinical results to Phase 0 and Phase 2 single agent riluzole clinical trials in late-stage melanoma patients [90, 91]. Despite significant decreases in FDG-PET scans, a decrease in MAPK and PI3K/AKT signaling cascade molecules in post-treatment samples plus stable disease in about 46% of the patients, it is apparent that single-agent therapeutic strategies are unlikely to have a long lasting beneficial effects in melanoma patients [91]. To elucidate the cytotoxic effects of riluzole, we analyzed samples post riluzole treatment in human specimens from a completed Phase 0 riluzole single agent trial and excised *G*RM1 expressing melanoma samples [90]. Our recent clinical trials demonstrated that all late-stage melanoma patients express GRM1 and thus findings from our GRM1 models are expected to be applicable to more patients. Interestingly, a melanoma patient-derived xenograft (PDX) utilizing tissue from a patient that became resistant to BRAF inhibition also exhibited GRM1 in the initial passage (P0) tumor and much higher levels at P2, suggesting a growth advantage for $GRM1^+$ cells. In addition to single agent therapy, we also seek to combine riluzole with other drugs to enhance the response rate. In a Phase 1 trial, the joint administration of riluzole and sorafenib, a multi-target kinase inhibitor, synergistically reduced the growth of wild-type or $BRAF^{V600E}$ tumors in patients with

advanced melanoma cells [92]. A phase 2 combinatorial trial utilizing both riluzole and sorafenib was recently completed (unpublished).

The clinical use of riluzole is characterized by extensive hepatic metabolism and an exceptionally high level of patient-to-patient variability in drug exposure, due to variable first pass elimination effects caused by heterogeneous expression of the cytochrome P450 isoform CYP1A2. This is one of the reasons that many patients with ALS do not benefit from riluzole because it is metabolized quickly. Such high variability makes it exceedingly difficult to establish the pharmacokinetic and pharmacodynamic relationships needed to develop well-optimized dosing regimens for riluzole treatment. To circumvent the first pass metabolism by CYP1A2, we adopted a prodrug approach where the exocyclic nitrogen in riluzole's chemical structure is masked as a functional group not anticipated to be recognized by CYP1A2 as a substrate for oxidation. In collaboration with Fox Chase Chemical Diversity Center Inc, we have prepared and evaluated over 300 peptide prodrugs encompassing three generations of structural modifications, supported by Phase 1 and 2 SBIR grants and we have identified a top candidate, FC-4157 (Troriluzole®) [93]. The entire portfolio of ~300 glutamate modulator prodrugs, has since been acquired by Biohaven Pharmaceuticals for further clinical development and commercialization. Recently, as part of a Phase 1b trial, patients with advanced solid tumors were treated with increasing doses of troriluzole and the maximum tolerated dose (MTD) was established [94].

The partial success of these therapies targeting GRM1 has demonstrated that targeting glutamate receptors in cancer can have clinically positive implications. This makes glutamate receptors and their downstream effector molecules compelling candidates

for further investigation with regards to their role in carcinogenesis and their potential as therapeutic targets. Ultimately, this will help us augment our knowledge pertinent to GRM1 and gain new insights into basic mechanisms regulating cancer cell biology.

Cancer cell metabolism

Cancer cells are constantly adapting to the hosts' defense by manipulating intrinsic and extrinsic biological pathways. Hanahan and Weinberg have classified these manipulations into eight biological components: sustaining proliferative signaling, evading growth suppressors, resisting cell death, enabling replicative immortality, inducing angiogenesis, activating invasion and metastasis, reprogramming of energy metabolism and evading immune destruction [95]. Within the last two decades, *reprogramming of energy metabolism* has become a popular and valuable therapeutic cancer target to study. Cell metabolism, simply defined, is the set of complex biochemical processes occurring in a cell required to sustain life. Due to their utterly plastic nature, cancer cells may utilize a plethora of pathways for energy production [96]. Metabolic pathways are composed of numerous steps that are highly regulated, and it is possible for metabolites formed in one pathway to feed into other biosynthetic pathways [97]. In cancer, these pathways differ depending on the tissue of origin and are often rewired allowing tumor cells to sustain hyper-growth and proliferative states.

Aerobic glycolysis "Warburg effect"

Cancer cells employ a different metabolic strategy than normal cells to satisfy their energy requirements and sustain cellular proliferation. Under aerobic conditions, normal cells acquire their energy primarily from the conversion of glucose to pyruvate by a process known as glycolysis which occurs in the cytosol (Figure 2). The pyruvate then enters the

tricarboxylic acid (TCA) cycle where it converts into carbon dioxide in the mitochondria via oxygen-consuming cellular respiration [98, 99]. However, under hypoxic conditions where oxygen is not readily available, cells prefer to rely more on anaerobic glycolysis, which converts glucose into lactate instead of pyruvate, resulting in decreased availability of pyruvate for mitochondrial respiration (oxidative phosphorylation). It has been noted, however, that cancer cells often produce large amounts of lactate regardless of the availability of oxygen and this form of metabolism is referred to as "aerobic glycolysis," or the "Warburg effect" [98, 100, 101]. This phenomenon was first observed in 1924 by the Nobel laureate and German scientist, Otto Warburg, thereby famously recognized by his name. While aerobic glycolysis is considerably less efficient than cellular respiration in terms of adenosine triphosphate (ATP) generation, 2 ATP versus 36 ATP respectively, when the cell microenvironment is nutrient rich, aerobic glycolysis can generate more ATP by producing it at a faster rate [102]. It has been suggested, however, that the reason for this 'metabolic switch' is not to increase ATP production since the amount of ATP in a proliferating cell is not significantly different from a resting cell, but rather to provide the building blocks for macromolecular synthesis [103, 104].

Tricarboxylic acid (TCA) cycle

Under aerobic conditions, pyruvate, the end product of glycolysis, enters the mitochondria to be oxidized to acetyl CoA which combines with oxaloacetate to start the TCA cycle and oxidative phosphorylation [96]. One predominant metabolic rewiring activity distressing the TCA cycle is that many cancer cells exhibit remarkable dependence on glutamine and cannot survive with glutamine deprivation [105]. This phenomenon is often referred to as 'glutamine addiction'. Experimental evidence suggests that glutamine

is the major respiratory fuel for energy production in tumor cells [106]. Glutamine is the most abundant amino acid in human blood [107, 108]. In addition to being a nitrogen donor for protein and nucleotide synthesis, glutamine provides for anaplerosis to refill the mitochondrial carbon pool. During periods of rapid growth, the demand for glutamine surpasses its supply in many cancer cells [109]. It has been demonstrated that tumor cells can utilize glutamine for citrate production through the reversal (reductive carboxylation) of the TCA cycle [110]. First, glutamine is de-aminated to glutamate, via glutaminase (GLS), which is then converted to α-ketoglutarate. Next, α-ketoglutarate undergoes reductive carboxylation to generate isocitrate by isocitrate dehydrogenase (IDH). At last, isocitrate is catalyzed by aconitase to produce citrate which is converted to acetyl CoA by ATP citrate lyase [111]. Overall, both glutamine and glucose may provide the carbon skeletons and co-factors such as NADPH and ATP, for cancer growth and survival.

Factors that can affect cancer cell metabolism

Earlier, only genomic modifications that result in the activation of oncogenes, loss of tumor suppressors or mitochondrial DNA mutations were expected to regulate cancer cell metabolism. Lately, it has been recognized that the metabolic phenotype of cancer cells can also be influenced by several non-genetic factors. As the number of neoplastic cells increases in the tumor, nutrient and oxygen availability gradually begins to decrease. This triggers the formation and growth of new blood vessels, that are poorly formed and inefficient [112]. Subsequent changes in the availability of nutrients are known to have a significant impact on actively proliferating carcinomas. Moreover, contrary to the traditional view that cells can take up and utilize nutrients whenever their reserves are depleted, nutrient uptake is strictly regulated by growth factor signaling [113]. In addition

to nutrient availability, metabolism could also be modulated by the surrounding tumor microenvironment (TME) of the cancer cell. Hypoxic conditions in the TME could turn on a transcriptional program that could theoretically change the metabolic profile of cancer cells [114, 115]. There have been reports suggesting that the molecular basis for the shift from oxidative to reductive glutamine metabolism in mammalian cells is linked to HIF-1α activity [116]. An area that has distorted the viewpoints of multiple experts is the questionable contribution of stromal cell-generated metabolites to the tumor and whether these metabolites promote or inhibit tumor advancement. Taken together, these insights throw light on some intrinsic and extrinsic factors that disrupt metabolism, all of which can have important implications in cancer development and progression.

Glutamate and cancer

The role of glutamate in normal and cancer cells

Glutamate is the most abundant and multifaceted biomolecule that plays a fundamental role in multiple metabolic processes and signaling in human cells. Glutamate, the predominant excitatory neurotransmitter in the central nervous system (CNS), is also involved in several non-neuronal cellular functions through interaction with different receptors [61]. Glutathione (GSH), an important scavenger of reactive oxygen species (ROS) found in all human cells, is made up of glutamate, glycine and cysteine. Tumor cells express elevated levels of antioxidant proteins such as GSH for detoxification [117], further endorsing the importance of glutamate. Post conversion to α-ketoglutarate by glutamate dehydrogenase (GLDH), glutamate may enter the TCA cycle to supply intermediates for cell growth [96]. Evidence points to the involvement of glutamate in cancer progression and regulation of the TME [118]. Moreover, supplementation of glutamic acid in

conditioned media stimulated proliferation in slow growing melanoma cells [119], indicative of a growth advantage. This likely has to be attributed to the fact that abundant glutamate in the TME supports efficient carbon utilization for anabolism and growth [109, 120]. Furthermore, glutamate antagonists have been shown to limit tumor growth, migration and invasiveness in human tumors including breast, colon, lung and astrocytoma, showing their anticancer potentials [121]. Interestingly, one of the most noticeable reprogramming events in cancer cell metabolisms is the preferential utilization of glutamate for reductive metabolism even under normoxic conditions. Recently, several reports have linked resistance to BRAF inhibitors with augmented glutamine dependency [122-124], suggesting that altered glutamate-dependent anabolic pathways may be central to acquiring drug resistance in some cancers including melanoma.

Glutaminolysis

In the late 1950s, it was found that some cancer cells could not survive in the growth media without the addition of exogenous glutamine, suggesting that tumor cells are highly dependent on glutamine for survival and growth [125]. Experimental evidence shows that glutamine is the major respiratory fuel for energy production in tumor cells [126]. The ability of glutamine to satisfy the bioenergetic needs and provide intermediates for macromolecular synthesis required for cell growth is important in tumor cell metabolism [106]. Thus, the metabolism of glutamine is considered another important hallmark besides the “Warburg effect” in tumor cell metabolism. In humans, glutamine has the highest concentration in the blood plasma relative to other amino acids, ranging from concentrations of 0.5 to 1 mM [104, 120]. Due to its extracellular abundance, glutamine is transported into the cell via the SLC1A5 (ASCT2) transporter [127-129]. The internalized

glutamine is then oxidized through the loss of its amide group to form glutamate, by a mitochondrial-associated enzyme called glutaminase (GLS) [130, 131]. GLS is an amidohydrolase that is often referred to as the "key gatekeeper" of glutamate-driven glutaminolysis [132]. The reverse reaction is catalyzed by another enzyme, glutamine synthetase (GS), which catalyzes the conversion of glutamate back into glutamine, and has been implicated in cancers such primary liver cancer and hepatocellular carcinoma [133, 134]. Byproducts of the "glutaminase" reaction are used for synthesis of purines, pyrimidines, NAD^+ cofactors, amino-sugars, glutathione, and non-essential amino acids (NEAA) such as alanine, asparagine and phosphoserine [128, 129, 135].

The human genome encodes two distinct isoforms of glutaminases in mammals, kidney-type glutaminase (KGA) and liver-type glutaminase (LGA). Different isoforms of each enzyme arise from alternative splicing and surrogate promoter mechanisms [136]. KGA which has ubiquitous distribution is encoded by the *GLS1* gene on chromosome 2 whereas LGA, mainly expressed in liver tissues, is derived from the *GLS2* gene on chromosome 12. KGA exists as two splice variants through alternative splicing: one expressing the full length form of the *GLS1* gene which retains the acronym KGA and the other is termed as kidney glutaminase isoform C (GAC) which has a 71 residue shorter carboxy-terminus [132]. Numerous evidence implicates that upregulation of KGA, especially GAC (jointly referred to as GLS henceforth), plays a critical role in tumor proliferation throughout various types of cancers, such as glioma, lymphoma, non-small cell lung cancer, prostate cancer and triple-negative breast cancer [137-140]. Furthermore, downregulation or inhibition of GLS has slowed the proliferation of these tumor cells [140, 141]. GLS inhibition has been shown to enhance the effectiveness of chemotherapy [142]

and also improve the efficacy of other targeted therapies [143, 144], suggesting the critical role of targeting GLS in an attempt to improve overall patient response. Elevated GLS levels are functionally linked to the oncogenic transcription factor, Myc. Myc-induced cell growth [145] has emerged as an important player in numerous cancer types [137]. The vital role of glutamate in cancer cell proliferation suggests that glutaminolytic enzymes could be attractive targets for therapy.

Cancer cells amplify the release of extracellular glutamate

The role of glutamatergic signaling in tumor biology has been increasingly studied in a variety of malignancies including neuronal tumors, melanoma, breast cancer, prostate cancer, etc. Melanoma cells release excess glutamate into the extracellular environment to warrant constitutive activation of the GRM1 receptor [51]. Moreover, several later studies conducted in different cancer models supported these findings when they detected a more than threefold increase in extracellular glutamate from GRM1 expressing cells compared with controls [53, 58, 59]. A study by Briggs *et al*. has proposed that large amounts of extracellular glutamate, secreted by triple-negative breast cancers, has the potential to inhibit cystine uptake by the cystine-glutamate antiporter (xCT) system [146]. This intracellular depletion of cysteine can increase HIF-1α expression due to the inactivation of the main HIF-1α prolyl-hydroxylase [146]. HIF-1α prolyl-hydroxylases are responsible for the degradation of HIF-1α. Others have reported that the molecular basis for the rewiring of anabolic glutamate metabolism in mammalian cells is linked to HIF-1α activity [116]. HIF-1α could also be activated by the PI3K/AKT/mTOR signaling pathway [147], which is upregulated in numerous cancers including $GRM1^{+}$ melanoma cells.

It is well known that stem cells of the neural crest give rise to the cells of the central nervous system (CNS), including astrocytes, glia, and neurons [148]. Melanocytes of the skin also arise from the neural crest stem cells. Due to the similar origin of the CNS cells and melanocytes, Prickett and Samuels proposed that they may share similar signaling pathways important for homeostasis, proliferation, growth, and overall survival [149]. Glioma, a cancer arising from glia cells in the brain, uses glutamate as an autocrine or paracrine signal to promote cellular migration and invasion [150]. Results from a recent study by Pei *et al*. indicate that glutamatergic signaling may provide positive feedback through metabolic reprogramming and genetic switching to accelerate glioma duplication and progression [151]. Glioma cells release excess glutamate through the xCT antiporter, which causes the excitotoxic death of neurons and permits tumor cell expansion [152, 153]. Also noteworthy is the evidence that glutamate-secreting glioma cells exhibit a distinct growth advantage [154]. It was previously reported that the brain is a common site for a secondary melanoma tumor to arise once it becomes metastatic [155]. Therefore, it is interesting to note that when this occurs excess glutamate released by melanoma may further promote tumor growth in a similar fashion to glioma by inducing excitotoxicity [51]. One of the possible ways for these cells to obtain enough glutamate for subsequent release is by elevating the consumption of glutamine into cells followed by conversion to glutamate via GLS. In addition, enhanced glutamate release has been observed in both breast cancer and prostate cancer cell lines, further supporting the importance of glutamatergic signaling in the malignant phenotype [118].

Use of glutamine and glutamate as prognostic biomarkers

The identification of a reliable predictive clinical biomarker is crucial for precision medicine. Predictive biomarkers are biological molecules detected in most patients and are frequently correlated with treatment responses [156]. Personalized/precision medicine is the future for most disease treatments, and it is essential to identify clinically relevant biomarkers, which can be easily applied in the clinic. Most pre-clinical cancer studies only assess for the efficacy of drug(s) on tumor progression, but it is crucial to also identify predictive biomarkers for treatment responses. Identification of these biomarkers will give clinicians the opportunity to make suitable and rational decisions in therapeutic options.

A prognostic tool that has recently been developed measures glutamine addiction in patients [129]. First, a patient is injected with radioactive ^{18}F-labeled 2*S*, 4R stereoisomer of 4-fluoroglutamine (^{18}F-glutamine), followed by a position emission tomography/computed tomography (^{18}F-glutamine-PET/CT) scans, in contrast to the conventional ^{18}F-glucose (FDG-PET/CT) scan which measures the Warburg effect [129, 157, 158]. ^{18}F-glutamine-PET/CT scans are useful in clinics to stage cancer, assess treatment responses, and predict the prognosis of the disease [158]. The development of this tool was only possible due to the understanding that cancer cells exhibit increased glutamine uptake via the SLC1A5 transporter [158]. Furthermore, ^{18}F-glutamine-PET/CT scans have been proposed as a possible tool to monitor the efficacy of glutamine-targeted therapies [129].

Sufficient levels of amino acids in systemic circulation are necessary to satisfy the bioenergetic needs of tumor cells in addition to providing intermediates for macromolecular synthesis [106]. Specifically, amino acids such as glutamine, glutamate,

aspartic acid, and serine are crucial for DNA synthesis, angiogenesis and protein content amplification [159]. During the process of transformation, the increase in demand for these amino acids leads to increased consumption and subsequent lower bioavailability in cancer patients [160]. In African American and Caucasian American patients with prostate cancer, serum glutamate levels directly correlated with Gleason score [161]. Likewise, plasma levels of glutamate are increased in colorectal carcinoma patients and in patients who have acquired immunodeficiency syndrome (AIDS) [162]. Other studies by Vanhone *et al.* and Rodriguez-Tomas *et al*. elucidate a clinical application to utilize systemic glutamate bioavailability where they use blood plasma glutamate concentration for the diagnosis of lung cancer with higher specificity [163, 164]. Interestingly, while investigating whether glutaminases function as prognostic biomarkers in human cancers, Saha *et al*. revealed that GLS and GLS2 expression can differentially modulate the clinical outcomes depending on the type of cancer [165]. Similar to how patients who carried the mutated BRAF genotype were found to display improved response to vemurafenib therapy [156, 166], certain levels of glutamate in the blood could also provide insights into the potential responsiveness of these patients to glutamatergic inhibitors. Metabolic and signaling activities of these biomarkers could pave the way for better prognostic tools and potential therapeutic interventions.

Targeting glutamine metabolism in cancer

Many cancer cells exhibit a phenomenon called “glutamine addiction”, in which they increase their uptake of glutamine via the SLC1A5 transporter [127, 129]. To complement this, cancer cells elevate their GLS levels [128, 129, 167-169]. Overexpression of GLS allows for increased glutamine metabolism, thereby providing a

means for the tumor cells to replenish the citric acid cycle and produce molecules required for anabolic growth. This fundamental insight that basic research has provided to the understanding of the glutaminolysis pathway has allowed for the development of various inhibitors, specifically GLS inhibitors such as BPTES, CB-839 and compound 968.

Inhibitors of glutaminase

GLS is the most well-studied and also the rate-limiting enzyme in the glutaminolysis pathway. Numerous inhibitors against GLS have been developed, such as Bis-2-(5-phenylacetamido-1,2,4-thiadazol-2yl) ethyl sulfide (BPTES), CB-839, and compound 968. These have been shown to allosterically inhibit GLS [129, 170]. BPTES is specific for the kidney-type glutaminase isoform [171]. The mechanism of action of BPTES occurs by the compound binding to the dimer interface of GLS, thereby inhibiting the tetramerization of GLS subsequently leading to its inactivation [129, 170]. BPTES has also been shown to suppress cancer cell growth *in vitro* and *in vivo* [170]. Even though BPTES is a potent inhibitor of GLS, the pharmacokinetic analysis of this compound has revealed that it has poor solubility and bioavailability thus limiting its potential for clinical use. This led to the development of CB-839 (Telaglenastat®) by Calithera Biosciences [128]. CB-839, first reported by Gross *et al*., is a selective, noncompetitive and potent inhibitor for GLS that has displayed antiproliferative efficacy in many cancers, including melanoma, breast cancer, leukemia/lymphoma, and kidney cancer [172-174]. The recent crystal structure analysis showed that the terminal electron-withdrawing trifluoromethoxy not only increases the integral lipophilicity but also improves the electronegativity of the pyridazinyl nitrogen atoms resulting in strengthened hydrogen bond interaction [175]. In particular, CB-839 is the only small molecule inhibitor of GLS that is being evaluated in a

clinical setting, currently in phase 1 and 2 clinical trials [176]. Additionally, another member of the GLS allosteric inhibitor family is compound 968. Compound 968 was shown to block oncogenic transformation of fibroblasts, while also displaying antiproliferative effects on cancer cells without affecting their normal counterparts [137]. The mechanism of action is through the binding of compound 968 at the monomeric interface of GLS, in comparison with BPTES and CB-839 which bind at the dimer interface [170]. CB-839 and BPTES are known to exclusively inhibit both products of the *GLS1* gene, GAC and KGA. However, the pan-glutaminase inhibitor compound 968 targets protein forms of both *GLS1* and *GLS2* (LGA) and has recently been utilized to suppress luminal-type breast cancer growth by inhibiting the previously underappreciated LGA [177]. In ovarian cancer cells, GLS inhibition enhances the effectiveness of chemotherapy [142] and also improves the efficacy of other targeted therapies [143, 144], suggesting the critical role of targeting GLS in an attempt to improve overall patient response. Moreover, the accumulation of glutamine, as a result of GLS inhibition, has been shown to induce divergent metabolic programs to overcome tumor immune evasion [178]. This has been linked to enhanced anti-tumor activity of PD-1 and PD-L1 antibodies by overcoming blockade of T cell activation [179]. Taken together, GLS inhibitors have shown great pre-clinical promise across cancers; however, resistance is a major hurdle of monotherapy regimes [176].

Resistance to glutaminase inhibition

As a monotherapy, GLS inhibition can be overcome by tumors cells through compensatory mechanisms, specifically against glutamate deprivation through different permutations of asparagine synthetase, a glutamate/cystine antiporter (xCT), or pyruvate

carboxylases [180-182]. To overcome GLS inhibition, tumor cells have been shown to upregulate asparagine synthetase, leading to an increase in asparagine concentrations which regulates the uptake of certain amino acids, mammalian target of rapamycin complex 1 (mTORC1) activation, and protein and nucleotide synthesis [182]. Additionally, breast cancer cells have shown to be viable even under glucose deprivation, in conjunction with a dysfunctional xCT antiporter leads to the sustenance of mitochondrial respiration [180]. It is possible that xCT expression is downregulated in CB-839 resistant cells to demote any further glutamate export. The third mechanism of resistance is the upregulation of pyruvate carboxylase [129, 181]. Pyruvate carboxylase plays a role in the conversion of pyruvate into oxaloacetate [129, 181]. In relation to glutamate-deprived cells, it can replenish the citric acid cycle and has been upregulated in CB-839-resistant cancer cells [129, 181]. In fact, Parlati and colleagues have suggested that pyruvate carboxylase expression strongly correlates with resistance to CB-839 and that it can rescue cells from GLS inhibition by supporting anapleurotic utilization of glucose [183]. Additionally, it is possible that the environment and metabolic milieu accompanying the tumor is responsible for the apparent resistance to glutaminase inhibition [184, 185]. Looking towards the future, it might be beneficial for patients to be treated with a combinatorial drug regime that targets two or more proteins within the glutaminolysis pathway. Taking these resistant mechanisms into consideration accentuates the importance of developing a multifaceted approach towards targeting cancer cell metabolism.

How is glutaminase regulated in cancer?

The regulation of GLS in cancer remains to be fully elucidated. Several studies have proposed different mechanisms by which GLS is regulated (Figure 3). Gao *et al.*

unfolded the indirect link between c-Myc, a well-known oncogenic transcription factor, and glutamine metabolism. c-Myc has been implicated in both activation and repression of numerous cellular functions, especially metabolism. Elevated level of c-Myc protein transcriptionally suppresses two microRNAs, miR-23a and miR-23b, which target GLS mRNA. As a result, upregulated expression of mitochondrial GLS induces increasing amounts of glutamate and glutamate-derived metabolites into the TCA cycle to sustain neoplastic progression [145]. Liu and colleagues shine light on the correlation between c-Myc overexpression and the mammalian target of rapamycin (mTOR) signaling pathway, which is a critical intracellular regulator of the cell cycle. mTOR serves as the catalytic subunits of two multi-protein complexes termed as the mTOR complex 1 (mTORC1) and complex 2 (mTORC2). Liu *et al*. called for the requirement of an intact mTORC1 axis in c-myc driven hepatocarcinogenesis, eluding to a possible target for treatment [186]. Rapamycin, a specific inhibitor of mTORC1 activity, is useful in the treatment of certain cancers. However, studies have proposed that prolonged rapamycin treatment can considerably reduce levels of mTORC2 [187]. To get around this, everolimus was developed. Compared with the parent compound rapamycin, everolimus is more selective for the mTORC1 protein complex, with no effect on the mTORC2 complex [188]. Both rapamycin and everolimus have displayed inhibitory effects on the growth, proliferation, and survival of tumors including melanoma, with minimal toxicity [189]. Interestingly, it has been found that the mTORC1/c-Myc axis also regulates GLS expression in pancreatic cancer [190].

Numerous reports have exposed alternate mechanisms underlying GLS-mediated pathogenesis. Rathore *et al.* discovered that NF-κB, which is initially defined as a nuclear

factor that binds to the B site of the immunoglobulin κ light chain gene enhancer in B lymphocytes, exhibited similar mechanisms to switch glutamine from a non-essential amino acid to a major energy source [191]. In a human T-lymphocytic cell line, Jurkat, p65 subunit of NF-κB binds to miR-23a and recruits the histone deacetylase (HDAC) to suppress downstream gene expression, which results in enhanced glutamine consumption [191]. Zhao *et al.* found that interferon-α (IFN-α) induced phosphorylation of Signal Transducer and Activator of Transcription 1 (STAT1), which then binds to GLS promotor resulting in enhanced *GLS1* transcription [192]. Lukey *et al.* unveiled a vital role of the transcription factor c-Jun in metabolic reprogramming. As the product of oncogene *JUN*, c-Jun directly binds to the GLS promoter which increases gene expression in breast cancer cells [193]. Uncovering unique complex networks of GLS regulation that are specific to each cancer type introduces potential for new therapeutics via a "bench to bedside" approach [194].

Section I: Determine the relationship between GRM1 and its subsequent signal transduction cascade and altered glutamate bioavailability

Aim 1: Rationale

Glutamate is the predominant excitatory neurotransmitter in the central nervous system. It was previously believed that glutamate-mediated signals were limited to the central nervous system, however, increasing pieces of evidence propose this signaling mechanism to also be present in peripheral tissues and is required for normal function [195]. Aberrant expression of GPCRs and the availability of abundant glutamate in the surrounding environment have been shown to induce the transformation of normal cells to malignancy [35]. These earlier studies led us to discover elevated levels of extracellular glutamate in several melanoma cell lines *in vitro*. Our previous findings illustrate that GRM1-expressing melanoma cells release excess glutamate into the extracellular matrix resulting in constitutive activation of the receptor [51]. To date, the role of GRM1-mediated glutamatergic signaling in altering cancer cell metabolism in melanoma has not been thoroughly investigated. We hypothesize that glutamatergic signaling cascades mediated by GRM1 in GRM1-expressing melanoma cells are responsible for altering glutaminolytic glutamate production subsequently leading to deregulated tumor cell growth and survival. In addition to glutamate being the natural ligand of GRM1, our interest in exploring the effects of altered glutamate bioavailability was based on previous studies demonstrating increased resistance to targeted therapy as a result of augmented glutamine dependency in melanoma cells [122, 123]. In melanoma, resistance to targeted therapy has also been

shown to result in the induction of oxidative phosphorylation and mitochondrial biogenesis, further justifying our interest in altered metabolism [196, 197].

Materials and Methods

Cell lines

Patient-derived human melanoma cell lines C8161, C81-61, UACC903, and 1205LU were provided by Drs. Mary J.C. Hendrix (Children's Memorial Research Center, Chicago, IL), Jeffrey Trent (The Translational Genomics Research Center, Phoenix, AZ), and Meenhard Herlyn (Wistar Institute, Philadelphia, PA). C81-61 is an early stage melanoma cell line, which does not express endogenous GRM1. C8161 is a malignant metastatic melanoma cell line from the same patient as C81-61 but with hyperactive GRM1. Several stable C8161 TetR siGRM1 knockdown clones were generated, and for the current study clone B22-20 was used and maintained in 1 μg/ml blasticidin and 10 μg/ml hygromycin [198]. Induction of siRNA against GRM1 was carried out by incubating the cells with 10 ng/ml of doxycycline for 4 days. Stable C81-61 GRM1-6 ($GRM1^{OE}$) clone that expresses elevated GRM1 levels compared to parental cell lines was selected with 10 μg/ml blasticidin [199]. Together, the panel of human cell lines, C81-61 ($GRM1^{-}$), C8161si ($GRM1^{KD}$), C81-61OE ($GRM1^{OE}$), and C8161 ($GRM1^{+}$) provide a patient-derived isogenic progression model of NRAS/BRAF wild type melanoma.

The 1205LU (ATCC CRL-2812) model is derived from lung metastases of primary melanoma lesion WM793B cells (ATCC CRL-2806) after subcutaneous injection into immune deficient mice. 1205LU cells are highly invasive and exhibit spontaneous metastasis to the lung and liver [200]. The WM793B line was established from skin taken from the primary melanoma of a vertical growth phase (VGP) lesion taken from the

sternum of a patient on 01/07/1983. These cell lines were cultured in RPMI-1640 medium supplemented with 10% fetal bovine serum (FBS). hTERT/CDK^{R24C}/p53^{DD} (AR7119; immortalized normal human melanocytes) cells were provided by Dr. David Fisher (Harvard Medical School, Boston, MA) and maintained in Medium 254 with human melanocyte growth supplements (M-254, Invitrogen, Carlsbad, CA) [20]. All cell lines were maintained at 37 ºC in a humidified 5% CO_2 incubator.

Reagents and antibodies

CB-839 (PubChem CID: 71577426) and riluzole (PubChem CID: 5070) were purchased from Selleckchem (Houston, TX). CB-839 and riluzole were dissolved in dimethyl sulfoxide (DMSO, Fisher Scientific) as 50 mM and 100 mM stock solutions, respectively, and used in treatments at the indicated concentrations. Anti-GLS antibody was purchased from Novus Biologicals (NBP1-58044, Littelton, CO). Monoclonal α-tubulin antibody was purchased from Sigma Aldrich (T6074, St. Louis, MO). Anti-GRM1 antibody was purchased from Lifespan BioSciences (LS-C354444, Seattle, WA).

Cell lysate protein extraction

Culture media was aspirated and cells were washed twice with cold 1X PBS. Extraction buffer (10:1 Laemmli Sample Buffer: β-mercaptoethanol mixture) was added to the plates dropwise in varying amounts depending on the cell number; for example: for 500,000 cells on a 60 mm plate, 130 µL of extraction buffer was added. The cells were then scraped and collected in a centrifuge tube. The samples were heated for 10 minutes at 99°C and then centrifuged at 14,000 rpm for 10 minutes at 4°C. The supernatant containing the whole cell protein lysate was then transferred into a new tube to be analyzed by immunoblot.

Western immunoblot

Sodium dodecyl sulfate polyacrylamide gel electrophoresis (SDS-PAGE) gels were prepared according to the percentage of the gels using double deionized water, 30% acrylamide, resolving (3 M Tris-HCl, pH 8.8) and stacking (0.5 M Tris-HCl, pH 6.8) buffer, 10% sodium dodecyl sulfate (SDS), 1.5% ammonium persulfate (APS) and N, N, N', N'-tetramethylethylenediamine (TEMED). 10 μL of a reference ladder protein marker (Precision Plus Protein Standard--Bio-Rad Cat# 161-0374, Hercules, CA) was used to determine the size of the band. After the lysates were denatured at 95ºC for five minutes, 15 μL of each sample corresponding to each cell line was added to the remaining wells. The protein lysates were electrophoresed at approximately 140 volts for 1.5 hours. The gel containing the proteins was then transferred at 180 mA for two hours onto a nitrocellulose membrane (GVS North America Cat# 1215471) which was layered between Whatman paper and sponges. Post transfer, the nitrocellulose membrane was separated from the gel and stained with Ponceau S solution (Sigma) to affirm completion of protein transfer. The membrane was then cut depending on the size of the protein of interest and blocked for 30 minutes with 0.25% milk (nonfat dry milk and 50 mM Tris-HCl, pH 7.6, 150 mM NaCl, 0.1% Tween-20). The membrane containing the target proteins were left to incubate overnight on a rocker in the cold room in a solution containing 0.25% non-fat milk and the respective primary antibody. The next day, it was washed twice with TBST, incubated on a rocker for one hour at room temperature with the respective secondary antibody, either anti-rabbit (1: 5000, Dky x Rb IgG, Millipore Cat# AP182P) or anti-mouse IgG (1: 5000, Sigma Cat# A4416-1mL) in 0.25% w/v milk (1X TBS, 0.1% Tween-20). The membrane was then washed with TBST five times. Western horseradish peroxidase substrate

(Millipore Cat# WBLUF0100) was applied drop wise to the membrane and covered for 3 minutes in the dark to probe the membrane before being resolved. The computer program Genesys (Syngene) was used to take an image of the membrane and exposure time was determined based on the intensity of the target protein. The band intensities were quantified using ImageJ computer software.

Cell proliferation/viability (MTT) assay

Cell proliferation was ascertained using MTT reagent [51]. All cell lines were cultured in RPMI-1640 medium, which contains 0.02 g/L of glutamate, supplemented with 10% FBS. Briefly, each cell line was cultured in 96-well culture plates (~2500 cells per well) followed by treatment with vehicle (DMSO), CB-839 or/and riluzole at varying concentrations. At indicated time points, 10 μL of Thiazolyl Blue Tetrazolum Bromide (Sigma Cat# M5655) in 1XPBS (MTT solution 1) was added and incubated for 4-6 hours at 37°C. 100 μL of MTT solution 2 [(10% Sodium dodecyl sulfate (SDS) in 0.01M HCl)] was added and incubated overnight at 37°C. The number of viable cells was determined by measuring absorbance (at 560 nm with a reference wavelength of 750 nm) using a 96-well plate reader (Infinite M200 Tecan USA, Durham, NC).

Glutamate determination in conditioned media

Glutamate concentration in the conditioned media was measured after 0, 2 or 4 days in culture with glutamate-free MEM using the Glutamine/Glutamate Determination Kit (GLN1, Sigma-Aldrich) according to the manufacturer's instructions. The determination of L-glutamate was done by measuring the dehydrogenation of L-glutamate to α-ketoglutarate accompanied by the reduction of NAD^+ to NADH. The conversion of NAD^+ to NADH was determined by measuring absorbance at 340 nm using a 96-well plate reader

(Infinite M200 Tecan USA, Durham, NC). The amount of NADH is proportional to the amount of glutamate in each sample.

Quantifying the intracellular pool of metabolites

This experiment was performed in collaboration with Dr. Fabian Filipp (University of California, Merced, CA). The metabolomics procedure described below, including GCMS, was executed by Dr. Filipp's laboratory.

100,000 cells per well were seeded in replicate (n=6) in 6-well plates (657160, Greiner Bio-One, Kremsmünster, Germany) in DMEM (10-017, Corning Cell-Gro, Manassas, VA) supplemented with 10% FBS, 1% Penicillin-Streptomycin (30-002-CI, Corning Cell-Gro, Manassas, VA), and 1% MEM Non-Essential Amino Acids (25-025-C, Corning Cell-Gro, Manassas, VA). 24 hours following seeding, media was aspirated and replaced with MEM (Corning Cell-Gro, Manassas, VA), supplemented with 1 g/L D-Glucose (0188, Amresco, Solon, OH), 2 mM L-Glutamine (G3126, Sigma Merck, Darmstadt, Germany), 10% FBS, and 1% MEM Vitamins (25-020-CI, Corning Cell-Gro, Manassas, VA). Following 24 hours incubation in supplemented MEM, 5 µL of supernatant containing conditioned media was transferred to micro centrifuge tubes (MT-0200-BC, Biotix, San Diego, CA) with 1 mL of cold extraction buffer consisting of 50% methanol (A452, Fisher Scientific, Fair Lawn, NJ) in ultrapure (18.2 MΩ x cm) water with 20 µM L-Norvaline (N7627 Sigma Merck, Darmstadt, Germany) and 20 µM DL-Norleucine (N1398, Sigma Merck, Darmstadt, Germany) and dried by vacuum centrifugation in a speedvac concentrator (DNA120OP115, Savant, Thermo Fisher Scientific, Waltham, MA) overnight. The remaining media was aspirated and the cells washed quickly with cold 0.9% sodium chloride in ultrapure water (Amresco) and placed

on ice. To each well, 1 mL of cold extraction buffer was added, the cells scraped on ice and the entire solution was then transferred to a pre-chilled micro centrifuge tube. Tubes were then frozen in liquid nitrogen, thawed, and placed in a digital shaking dry bath (8888-0027, Thermo Fisher Scientific, Waltham, MA) set to 1100 rpm for 15 min at 4°C. Samples were then centrifuged for 15 min at 4°C and 12500 g in a refrigerated centrifuge (X1R Legend, Sorvall, Thermo Fisher Scientific, Waltham, MA) using a fixed-angle rotor (F21-48x1.5, Sorvall, Thermo Fisher Scientific, Waltham, MA). Supernatants were transferred to new micro centrifuge tubes and dried by vacuum centrifugation overnight.

Dried, extracted cell samples or media supernatants were derivatized by the addition of 20 µL of 2.0% methoxyamine-hydrochloride in pyridine (MOX, TS-45950, Thermo Fisher Scientific, Waltham, MA) followed by 90 min incubation in a digital shaking dry bath at 30°C and 1100 rpm. Then 90 µL of N-methyl-N-trimethylsilyltrifluoroacetamide (MSTFA, 394866-10X1ML, Sigma Merck, Darmstadt, Germany) was added and samples incubated at 37°C and 1100 rpm for 30 min before centrifugation for 5 min at 14,000 rpm and 4°C. The supernatant was transferred to an auto sampler vial (C4000LV3W, Thermo Fisher Scientific, Waltham, MA) with screw cap (C5000-53B, Thermo Fisher Scientific, Waltham, MA) for analysis by gas chromatography (GC, TRACE 1310, Thermo Fisher Scientific, San Jose, CA) coupled to a triple-quadruple GC mass spectrometry system (QQQ GCMS, TSQ8000EI, TSQ8140403, Thermo Fisher Scientific, San Jose, CA).

Gas chromatography mass spectrometry (GCMS)

Samples were analyzed on a QQQ GCMS system equipped with a 0.25 mm inner diameter, 0.25 µm film thickness, 30 m length 5% diphenyl/95% dimethyl polysiloxane

capillary column (Trace GOLD TG-5MS, 26098-1420, Thermo Fisher Scientific, Waltham, MA) and run under electron ionization at 70 eV. The GC was programed with an injection temperature of 250°C and split less injection volume of 1.0 µL. For media samples, a 1:20 split injection was used. The GC oven temperature program started at 50°C for 1 min, rising to 300°C at 10 K/min with a final hold at this temperature for 6 min. The GC flow rate with helium carrier gas (HE, HE 5.0UHP, Praxair, Danbury, CT) was 1.2 mL/min. The transfer line temperature was set at 290°C and the ion source temperature at 295°C. A range of 50-600 m/z was scanned with a scan time of 0.25 seconds.

Metabolites were identified using Trace Finder (Version 3.3, Thermo Fisher Scientific, Waltham, MA) based on in-house libraries of metabolite retention times and fragmentation patterns. Identified metabolites were quantified using the selected ion count peak area for specific mass ions, and standard curves generated from reference standards run in parallel. Peak intensities were normalized for extraction efficiency using L-norvaline as an internal standard. The mean and standard deviation for each quantified metabolite was calculated for each cell line and treatment condition. A univariate t-test was used to compare the means for each metabolite and cell line.

TGS melanoma model of ectopic expression of GRM1

The original transgenic founder strain 3 (TG-3) with hyperactive *Grm1*$^{+}$ was crossed with hairless SKH-1 mice to arrive at the TGS strain—brother-sister littermates have been mating since the year 2000. TG-3 mice were established as a result of a classic case of insertional mutagenesis that led to the ectopic expression of Grm1 in melanocytes. TG-3 mice spontaneously develop metastatic melanoma with 100% penetrance. SKH-1 is an uncharacterized/nonpedigreed hairless strain of mice. The goal was to make the

pigmented lesions visible on the TGS mice in the absence of fur. TGS mice were genotyped by DNA extraction from the tails and subsequent PCR of the *Grm1* locus [46].

Apoptosis and necrosis assay

1205LU cells seeded in a 96-well clear bottom plate at a density of 50,000 cells per well and incubated in RPMI with 10% FBS for 24 hours before treatment with vehicle (DMSO), 10 µM riluzole, 0.5 µM CB-839, and 10 µM riluzole + 0.5 µM CB-839. The experiment was conducted twice in triplicates for each time point and concentration (n=6). A commercially available Apoptosis/Necrosis Detection Kit (blue, green, red) (ab176749, Abcam) was utilized to determine whether apoptosis and/or necrosis was induced by the treatments. Reagents included 50 mL Assay Buffer, 200 µL of Apopxin Green Indicator (100X), 100 µL of 200X 7-AAD, and one vial of CytoCalcein Violet 450, requiring the addition of 100 µL of DMSO to prepare a 200X stock solution. The protocol was performed as per the manufacturer's instructions. Briefly, cells were washed twice with 100 µL of Assay Buffer and resuspended in 200 µL of Assay Buffer. A cocktail mix containing 2 µL of Apopxin Green Indicator (100X), 1 µL of 7-AAD 200X, and 1 µL of CytoCalcein 450 200X Stock solution was added to each well. The plate was then incubated in the dark at room temperature for 40 minutes. Following incubation, each well was washed twice with 100 µL of Assay Buffer and then replaced with 100 µL of Assay Buffer. Numerical readings were taken on a SpectraMax fluorescence 96-well microplate reader as well as images captured on a Confocal fluorescence microscope. Blue fluorescence will signify healthy cells, green will demonstrate apoptotic cells, and red will display necrotic cells.

Results

Elevated circulating plasma glutamate levels in a Grm1-driven TGS melanoma model

We derived TGS mice from crosses between melanoma-prone TG-3 [46, 47, 201, 202] with hairless SKH-1. Onset and progression of the pigmented lesions are very similar in TG-3 and TGS mice; in the absence of hair, the pigmented lesions are readily visible in TGS mice. Homozygous TGS mice that harbor two copies of the disrupted endogenous *Grm1* gene succumb to large tumor burden by 4-5 months old; we had to sacrifice them per Rutgers IACUC, thus, they are not included in our studies. Heterozygous *Grm1*$^{+/-}$ TGS mice with only one copy of the disrupted endogenous *Grm1* are viable, show highly pigmented tumors and bear large tumor burden by 11-12 months of age, indicating that Grm1 signaling stimulates melanomagenesis in a gene-dosage-dependent manner. An image addressing the visual (phenotypic) difference between heterozygous a TGS mouse and a wild type TGS mouse is shown in Figure 5A. We examined circulating plasma glutamate levels in 2.5-month old wild type (no disrupted *Grm1*), heterozygous and homozygous TGS mice and the differences were not statistically significant (Figure 4). We also compared glutamate levels in circulating blood plasma between 4.5-month old wild type and heterozygous TGS mice and no significant fluctuations were detected (Figure 4) although an increasing trend begins to appear with disrupted Grm1 expression. Successively, when comparing glutamate levels in circulating blood plasma between 6-month old heterozygous TGS and wild type mice, heterozygous TGS mice showed elevated glutamate levels (Figure 5B), suggesting aberrant Grm1 expression may promote an increase in its natural ligand, glutamate, in circulation to ensure constitutive activation of

Grm1 receptor; similar observation was made in *in vitro* cultured cells [51]. These results suggest a time-dependent increase in blood plasma glutamate levels.

Elevated GLS detected in GRM1^{+} human melanoma cell lines

Ectopic expression of GRM1 is sufficient to induce cellular transformation *in vitro* and spontaneous melanoma development *in vivo* [46]. To investigate a possible relationship between GRM1 expression, altered glutamate bioavailability and glutaminase (GLS), we first confirmed GRM1 expression in C8161, UACC903, and 1205LU human melanoma cells, plus immortalized normal human melanocytes, hTERT/CDK^{R24C}/p53^{DD} (AR7119). C8161 is a malignant human melanoma cell line that expresses wild type BRAF. UACC903 and 1205LU are other malignant melanoma cell lines that harbor the BRAF^{V600E} mutation. C8161, UACC903, and 1205LU demonstrated significantly elevated levels of GRM1 and GLS compared to hTERT/CDK^{R24C}/p53^{DD} cells with almost undetectable GRM1 and very low GLS expression (Figure 6).

No correlation between GRM1 and GLS expression in patient tumor samples

Our findings suggest that GRM1 expression is correlated with GLS expression in human melanoma cell lines. In an attempt to strengthen this argument outside of a limited selection of cell lines, we performed analysis on melanoma patient tumor specimens utilizing the newly developed GEPIA tool. GEPIA is a web server for cancer and normal gene expression profiling that uses RNA sequencing data from the TCGA database [203]. We found no correlation between GRM1 and GLS (Pearson's correlation coefficient = 0.085). The log-scale axis for visualization is displayed in Figure 7. 461 melanoma patient tumor samples were examined for this analysis. It is noteworthy that the small fraction of patient tumors that are GRM1-positive also express elevated levels of GLS. These results

should be inspected with caution as it is difficult to procure surrounding normal tissue for comparative evaluation.

Altered intracellular metabolite levels in a GRM1-driven melanoma progression model

GRM1-expressing melanoma patients share a common metabolic dysregulation of glutamatergic signaling. In order to understand and quantify the metabolic phenotype of $GRM1^+$ cells, we profiled an isogenic cellular melanoma model by GCMS (Figure 8). We analyzed both overexpression of GRM1 in a GRM1 low background (parental C81-61 and C81-61OE) and suppression of GRM1 in a GRM1 high background (parental C8161 and C8161si). While manipulation of GRM1 expression levels failed to alter intracellular lactate concentration (Figure 8, 9A), higher levels of GRM1 correlated with significantly increased levels of intracellular citrate, α-ketoglutarate, aspartate, fumarate, malate, lysine and glutamate (Figure 8, 9B, 9C, 9D). This indicates that GRM1 expression does not increase lactate fermentation but does increase levels of TCA cycle intermediates. Several studies have shown that cells expressing GRM1 produce and release elevated amounts of glutamate [51, 53, 118, 161]. C81-61OE ($GRM1^{OE}$) and C8161 ($GRM1^+$) were clustered together characterized by elevated pool sizes of glutamate and tricarboxylic acid (TCA) cycle related metabolites (Figure 8). The increased intracellular pool size of glutamate could be a direct result of increased conversion of glutamine into glutamate via the activity of GLS. The clustering of cellular specimens was determined by the first two principle components. Principle component analysis converts the set of biochemically correlated metabolite variables into a set of linearly uncorrelated variables called principal components. Our principle component analysis plot represented more than 60% data in the first two principle components. The multidimensionality reduction plot visualizes the data

separation between tumorigenic and non-tumorigenic specimens as well as the metabolic switch and reversal that is induced by the genetic perturbations (Figure 8). Knockdown of GRM1 in tumorigenic C8161 causes a shift in the metabolic state that is similar to C81-61. In reverse, overexpression of GRM1 in non-tumorigenic C81-61 causes metabolic perturbation into a quadrant of the multidimensional space overlapping with C8161. Taken together, unsupervised clustering and principle component analysis showed metabolic similarity between tumorigenic C8161 ($GRM1^{+}$) and C81-61OE ($GRM1^{OE}$) specimens and non-tumorigenic C81-61 ($GRM1^{-}$) and C8161si ($GRM1^{KD}$).

Genetic modulation of GRM1 expression in cells alters GLS expression levels

Consistent with our observed elevated glutamate concentrations, a high level of expression for GLS was detected in $GRM1^{+}$ cells, but much less in AR7119, indicating a possible correlation between GRM1 and GLS expression levels (Figure 6). To investigate this further, we utilized a panel of isogenic cell lines, C81-61 ($GRM1^{-}$), C8161si ($GRM1^{KD}$), C81-61OE ($GRM1^{OE}$) and C8161 ($GRM1^{+}$). C81-61OE cells with high levels of GRM1 also had high levels of GLS protein when compared to C81-61 cells which displayed low protein levels of GRM1 and GLS (Figure 9E). This was confirmed in another clonal pair of isogenic cells where suppression of GRM1 protein in a GRM1-high background (parental C8161 and C8161si) resulted in significantly reduced levels of GLS protein (Figure 9E). These results suggest that GRM1 expression increases glutamate production by increasing GLS expression.

GLS inhibition reduces proliferation/viability of GRM1^{+} human melanoma cells

In *in vitro* tetrazolium-based proliferation/viability assays all three GRM1-expressing human melanoma cells, C8161, 1205LU, and UACC903 displayed modest efficacy in suppressing cell growth in the presence of CB-839 as compared with the control vehicle (DMSO) group regardless of their BRAF genotypes (Figure 10, 12A). It is noteworthy that a considerably higher concentration of CB-839 (10-50 μM) is required to observe a reduction in UACC903 cell proliferation, likely due to the presence of other driver mutations in addition to BRAF^{V600E}, considering that 1205LU cells also have the BRAF^{V600E} mutation (Figure 12A). Furthermore, to determine if GRM1 expression modulates the responsiveness to GLS inhibition, exogenous human GRM1 cDNA was introduced into an early stage melanoma cell line, C81-61, which does not express endogenous GRM1 (see profiling data in Figure 8 and 9). Characterization of several GRM1-expressing C81-61 clones confirmed that these clones were transformed and tumorigenic [199]. We compared the growth rate of the parental C81-61 cell line to the C81-61OE cell line in the presence of CB-839. A marked reduction in the cell proliferation of C81-61OE was seen with 0.5 μM CB-839 as compared to the vehicle (DMSO) control (Figure 10). Strikingly, very minute if any changes were detected in the growth of the parental C81-61 cells with analogous treatment conditions (Figure 10). These results suggest that GRM1 expression may influence the responsiveness of melanoma cells to GLS inhibition.

Combinatorial treatment with CB-839 and riluzole leads to enhanced inhibition of GRM1$^+$ melanoma cell proliferation

Suppressive effects of riluzole on GRM1$^+$ melanoma cell proliferation were reported earlier [51, 88, 204]. Here, the consequences of including both CB-839 and riluzole on cell growth of two GRM1-expressing human melanoma cell lines were investigated. As shown in Figure 11, C8161 and 1205LU cells were treated for 7 days with 0.5 μM CB-839, 10 μM riluzole or 0.5 μM CB-839 + 10 μM riluzole. Treatment with either CB-839 or riluzole reduced C8161 cell proliferation by ~40% while combining both CB-839 and riluzole led to an ~85% decrease when compared to vehicle treated control cells. 1205LU cells also displayed a significant reduction in cell proliferation in the presence of both CB-839 and riluzole as compared to either agent alone (Figure 11). As mentioned above, a higher dose of CB839 and riluzole was needed to diminish cell proliferation in UACC903 cells (Figure 12) similar to our earlier observations [205]. The GRM1$^-$ C81-61 and hTERT/CDK^{R24C}/p53^{DD} (AR7119) cells were used as negative controls – these cells did not respond to riluzole plus CB-839 treatment (Figure 11), confirming that GRM1 expression is required to be responsive to these compounds at the indicated doses. Furthermore, increasing evidence illustrates that the presence of a mutation in BRAF frequently makes some cancer cells less responsive to various targeted treatments [206]. Taken together, our results suggest that CB-839 combined with riluzole can enhance the anti-proliferative properties of GRM1$^+$ human melanoma cells and that higher doses are needed for some BRAF-mutated cells.

CB-839 treatment leads to inhibition of glutamate release from GRM1$^+$ human melanoma cells

Earlier we reported elevated levels of extracellular glutamate in human melanoma cell lines that express GRM1 [51]. Inclusion of riluzole in cultured media modulated the amount of glutamate released by these cells [51]. To determine the consequences on the level of glutamate released by GRM1$^+$ melanoma cells upon treatment with CB-839 only or riluzole + CB-839, C8161 cells were plated in glutamate-free MEM media followed by collection of conditioned media at days 0, 2 and 4. We plated a different number of C8161 cells so, at the time of collecting the conditioned-media samples, the cell numbers were very similar among the different days (Figure 13A). In parallel, we also performed cell viability/cell proliferation MTT assays to ensure that the treated cells were viable, as the levels of glutamate release were determined. We showed that extracellular glutamate levels were significantly reduced in the conditioned culture media isolated from CB-839, riluzole or CB-839 + riluzole treated C8161 cells compared to the vehicle treated cells (Figure 13B). We expected to see the lowest glutamate levels in the riluzole + CB-839 treatment group but this was not the case. It is possible that the glutamate concentration in the conditioned media was near the lower limit of quantification for the assay.

Treatment with CB-839 and riluzole slightly enhances apoptotic activity in GRM1$^+$ melanoma cells

Our recent report suggests that CB-839 combined with riluzole can enhance the antiproliferative properties of GRM1$^+$ human melanoma cells [207]. To determine whether GRM1$^+$ melanoma cells respond to riluzole + CB-839 treatment via well-established cell death processes such as apoptosis or necrosis, we utilized a commercially available Apoptosis/Necrosis Kit (ab176749, Abcam) using the GRM1$^+$ 1205LU cells. As shown in

Figure 14, the proliferation of 1205LU cells was reduced by 40% with riluzole, and by 35% with CB-839 single-agent treatments respectively, when compared to DMSO-treated control cells. Expectedly, an 85% reduction in cell proliferation was displayed in the presence of both riluzole and CB-839 when compared to the control. These results validated our previous data from *in vitro* tetrazolium-based proliferation/viability assays shown in Figure 11. As for the level of apoptotic activity in the responding cells, Figure 14 displays a slight increase in apoptotic cell population post riluzole + CB-839 combination treatment (normalized to the total number of cells). Finally, preliminary data from this experiment revealed no major changes in necrotic activity in all the treatment groups when compared to the control (data not shown). For future experiments, we may have to utilize moderately higher concentrations of riluzole and CB-839 or different time points to quantitatively assess and detect significant activation of cell death pathways.

Section II: Perform pre-clinical melanoma treatment studies with a novel combinatorial glutamate signaling blockade in a xenograft melanoma model

Aim 2: Rationale

For many years, designing novel combinatorial strategies to overwhelm the tumor microenvironment has been one of the most sought-after approach. If multiple active pharmaceutical ingredients (APIs) prove safe together, then combination treatments can benefit from multiple or synergistic modes of action. Previously, we have shown that aberrant GRM1 receptor expression as well as excessive production of its ligand, glutamate, by the tumor cells contributes to abnormal glutamatergic signaling and subsequent tumorigenesis. GLS, a critical glutaminolytic enzyme responsible for the conversion of glutamine to glutamate, has elevated activity in numerous tumor types and is positively correlated with cell transformation and oncogenesis [137, 208, 209]. Results from recent studies also propose that combining potent GLS inhibitors with other targeted therapy regiments increases the durability of therapeutic responses in a variety of cancers [143, 144]. Earlier, our group has also shown that inclusion of riluzole, an FDA approved drug for Amyotrophic Lateral Sclerosis that blocks glutamate release, led to a reduction in melanoma cell proliferation *in vitro* and tumor progression *in vivo* [205, 210]. Therefore, functionally, riluzole acts as an indirect antagonist of GRM1. In combination with other small molecule inhibitors, riluzole has also demonstrated synergistic anti-tumor effects *in vitro* and in numerous mouse xenograft model systems [92, 211, 212]. These results prompted us to investigate a novel combinatorial therapeutic approach by inhibition of glutaminolytic glutamate production and utilization in $GRM1^{+}$ melanoma through

combined actions of CB-839 (targeting of glutamate production) and riluzole (glutamate release) (proposed mechanism depicted in Figure 15).

Materials and Methods

Reagents and antibodies

Polyclonal anti-GRM1 antibody was purchased from Lifespan BioSciences (LS-C354444, Seattle, WA). Polyclonal anti-GLS antibody was purchased from Novus Biologicals (NBP1-58044, Littleton, CO). Monoclonal anti-α-tubulin antibody was purchased from Sigma Aldrich (T6074, St. Louis, MO). Monoclonal anti-phospho-T308-AKT (4056), pan-AKT1/2/3 (4691), phospho-ERK1/2-T202/Y204 (4370), pan-ERK1/2 (4695), and anti-PARP (9532) antibodies were purchased from Cell Signaling Technology (Danvers, MA). All primary antibodies recognize human proteins and were either produced in a mouse or rabbit. Peroxidase conjugated secondary goat anti-mouse IgG antibody (A4416, Millipore Sigma, Darmstadt, Germany) or donkey anti-rabbit IgG antibody (AP182P, Millipore Sigma, Darmstadt, Germany) were utilized.

Blood collection

Heparinized capillary tubes (Fisherbrand Heparinized Micro-Hematocrit Capillary Tubes Cat# 22-362-566) were used to retro-orbitally bleed mice. About 300 µL of blood was collected per mouse at each time-point and kept on ice. The refrigerated centrifuge was pre-cooled to 4ºC. Samples were then centrifuged for 8 minutes at 10,000 rpm. The plasma supernatant was separated from the red blood cell pellet and stored at -20ºC.

Xenograft and tumorigenicity study design

The goal of this pre-clinical study was to assess alterations in tumor progression following treatment of tumor-bearing mice with a combination of glutamatergic inhibitors

versus control cohorts. We conducted two autonomous pre-clinical studies in commonly used immunodeficient "nude" mice where two independent (C8161 and 1205LU) subcutaneously implanted human melanoma tumor xenografts were utilized. Male and female mice were used for all groups to excuse gender-related differences. C8161 and 1205LU cells were harvested by trypsinization and resuspended in phosphate buffered saline (PBS) (10^7 cells/ml). 5 to 6-week-old immunodeficient nude male and female mice were subcutaneously injected with 10^6 tumor cells in each dorsal flank. Tumor cell lines for xenograft studies were cultured in RPMI-1640 medium supplemented with 10% FBS. Tumor growth was monitored weekly with a vernier caliper and calculated with the formula ($d2 \cdot D/2$). CB839 (50 mM stock solution) and riluzole (100 mM stock solution) were dissolved in DMSO. Once tumor volumes reached 10 to 30 mm^3, mice were randomly divided into four treatment groups and received control vehicle DMSO, riluzole (10 mg/kg), CB839 (200 mg/kg), or the combination of riluzole (10 mg/kg) and CB839 (200 mg/kg) by oral gavage, daily. We measured tumor volumes twice a week with vernier calipers to monitor tumor progression. In addition, we recorded body weights of these animals weekly. Blood was drawn from these mice via retro-orbital bleeding at the end of the experiment to assess changes in blood plasma metabolite levels analyzed by mass spectrometry. The experiment was terminated when the xenografts in the vehicle group reached maximum allowable size. All animal procedures and studies were performed in strict accordance with the Rutgers institutional animal care and use committee (IACUC). At termination of the studies, tumor samples were isolated and prepared appropriately for further molecular analysis.

Immunohistochemistry

Sectioning, staining and quantitative image analysis of formalin-fixed, paraffin-embedded (FFPE) tumor and liver tissues were performed by Histowiz Inc. (histowiz.com) using a Standard Operating Procedure and fully automated workflow. Briefly, tissue samples were processed and embedded in paraffin blocks and then shipped out to Histowiz on ice where subsequent sectioning at 4 µm and IHC was piloted. FFPE liver sections were stained with hematoxylin and eosin (H&E). IHC on FFPE tumor tissue was performed on a Bond Rx autostainer (Leica Biosystems) with enzyme treatment (1:1000) using standard protocols. Bond Polymer Refine Detection (Leica Biosystems) was used according to the manufacturer's protocol. After staining, sections were dehydrated and film coverslipped using a TissueTek-Prisma and Coverslipper (Sakura). Whole slide scanning (40X) was performed on an Aperio AT2 (Leica Biosystems). Unbiased automated image analysis to obtain the percentage of $Ki67^+$ and Cleaved Caspase 3^+ cells was performed using the HALO image analysis software by Indica Labs.

Determining active drug levels of riluzole and CB-839 in blood plasma

The blood plasma samples were shipped out to Touchstone Biosciences (Plymouth Meeting, PA) for further pharmacokinetic bioanalysis. Plasma samples were prepared as follows. Three volumes of acetonitrile containing internal standard was added to one volume of plasma to precipitate proteins. Samples were centrifuged (3000 g for 10 min) and the supernatant removed for further analysis by LC-MS/MS. Calibration standards and quality controls were made by preparation of a 1 mg/mL stock solution and subsequently a series of working solutions in methanol: water (1:1, v/v) which were spiked into blank plasma to yield a series of calibration standard samples in the range of 1 ng/mL to 10 µg/mL

and quality control samples at three concentration levels (low, middle and high). All incurred plasma samples were treated identically to the calibration standards and quality control samples. LC-MS/MS analysis was performed utilizing multiple reaction monitoring for detection of characteristic ions for each drug candidate, additional related analytes and internal standard.

Quantifying the pool of metabolites in blood plasma

This study was performed in collaboration with Dr. Fabian Filipp (University of California, Merced, CA). The blood plasma samples were shipped out to Dr. Filipp's laboratory for further metabolomic analysis. The metabolomics procedure described below, including GCMS, was executed by Dr. Filipp's laboratory.

5 µL of blood plasma was transferred to microcentrifuge tubes (MT-0200-BC, Biotix, San Diego, CA) with 1 mL of cold -20°C extraction buffer consisting of 50% methanol (A452, Fisher Scientific, Fair Lawn, NJ) in ultrapure (18.2 MΩ x cm) water with 20 µM L-norvaline (N7627 Sigma Merck, Darmstadt, Germany) and 20 µM DL-norleucine (N1398, Sigma Merck, Darmstadt, Germany) and dried by vacuum centrifugation in a speedvac concentrator (DNA120OP115, Savant, Thermo Fisher Scientific, Waltham, MA) overnight. Dried, extracted plasma supernatants were derivatized by the addition of 20 µL of 2.0% methoxyamine-hydrochloride in pyridine (MOX, TS-45950, Thermo Fisher Scientific, Waltham, MA) followed by a 90 min incubation period in a digital shaking drybath at 30°C and 1100 rpm. 90 µL of N-methyl-N-trimethylsilyltrifluoroacetamide (MSTFA, 394866- 10X1ML, Sigma Merck, Darmstadt, Germany) was added and samples incubated at 37°C and 1100 rpm for 30 min before centrifugation for 5 min at 14,000 rpm and 4°C. The supernatant was transferred to an autosampler vial (C4000LV3W, Thermo

Fisher Scientific, Waltham, MA) with screwcap (C5000-53B, Thermo Fisher Scientific, Waltham, MA) for separation by gas chromatography (GC, TRACE 1310, Thermo Fisher Scientific, San Jose, CA) coupled to a triple-quadrupole GC mass spectrometry system for analysis (QQQ GCMS, TSQ8000EI, TSQ8140403, Thermo Fisher Scientific, San Jose, CA). Samples were analyzed on a QQQ GCMS system equipped with a 0.25 mm inner diameter, 0.25 μm film thickness, 30 m length 5% diphenyl/95% dimethyl polysiloxane capillary column (OPTIMA 5 MS Accent, 725820.30, Machery-Nagel) and run under electron ionization at 70 eV. The GC was programed with an injection temperature of 250.0°C and a splitless injection volume of 1.0 μL. The GC oven temperature program started at 50°C for 1 min, rising to 300.0°C at 10 K/min with a final hold at this temperature for 6 min. The GC flow rate with helium carrier gas (HE, HE 5.0UHP, Praxair, Danbury, CT) was 1.2 mL/min. The transfer line temperature was set at 290.0°C and the ion source temperature at 295.0°C. A range of 50-600 m/z was scanned with a scan time of 0.25 seconds. Metabolites were identified using TraceFinder (v3.3, Thermo Fisher Scientific, Waltham, MA) based on libraries of metabolite retention times and fragmentation patterns (Metaflux, Merced, CA). Identified metabolites were quantified using the selected ion count peak area for specific mass ions, and standard curves generated from reference standards run in parallel. Peak intensities were normalized for extraction efficiency using L-norvaline as an internal standard. The mean and standard deviation for each quantified metabolite was calculated. A univariate t-test was used to compare treatment conditions for each metabolite.

Results

Daily oral gavage with riluzole (10mg/kg) and CB-839 (200mg/kg) for 4 weeks displays no apparent toxicity in immunodeficient mice

To confirm *in vitro* anti-tumorigenic potential in GRM1^{+} melanoma cells upon combining CB-839 with riluzole, we conducted *in vivo* experiments on established C8161 and 1205LU xenografts. To ensure that daily administration of 10 mg/kg riluzole and 200 mg/kg CB-839 for a sub-chronic treatment (~30 days) regimen did not result in toxicity, the body weights of the mice were monitored and livers were taken at necropsy, weighed and fixed. All of the treatment groups did not significantly affect the body and liver weights of the mice when compared to the vehicle controls (Figure 16), highlighting that these compounds are not toxic and well tolerated even when administered together. Absence of liver toxicity, such as steatosis or fibrosis, in all treatment groups, was confirmed by hematoxylin and eosin (H&E) staining of fixed liver tissue followed by exhaustive histopathological evaluation of the slides (Figure 17).

Diminished *in vivo* xenograft tumorigenicity with combinatorial treatment targeting glutamate bioavailability

We showed considerable suppression of tumor progression in mice treated with the combination of CB-839 plus riluzole as compared to vehicle treated tumors or tumors treated with riluzole or CB839 alone. C8161 xenograft bearing mice were treated for 28 days. When used as single agents independently, both riluzole (10 mg/kg) and CB-839 (200 mg/kg) resulted in ~50% suppression of implanted xenograft tumor growth. However, a combination of these compounds at the abovementioned dosage resulted in ~75% suppression of tumor growth (Figure 18). For mice implanted with 1205LU xenografts, we were able to conduct treatments for 25 days before tumors in the control mice reached

maximum permissible size. It is noteworthy that a substantially better efficacy of the combination was detected in mice bearing 1205LU xenografts. Specifically, we observed ~95% suppression of tumor volumes in the riluzole plus CB-839 treated cohort compared to 50-60% inhibition of tumor growth in either agent alone (Figure 18). These results run parallel to our *in vitro* findings where we observed that a combination of riluzole (10 μM) and CB-839 (0.5 μM) results in enhanced suppression of cell proliferation (Figure 11). It is astonishing that the *in vivo* combinatorial application reduced tumor progression in both BRAF-wild type (C8161) and BRAF-mutant (1205LU) xenografts as compared with vehicle controls.

Treatment with riluzole and CB-839 results in reduced cell proliferation markers in excised xenograft tumors

Western blot analysis of protein lysates prepared from excised xenografts showed a substantial reduction of ERK phosphorylation with the combination of riluzole and CB839 (Figure 19A). For further confirmation of inhibited cell proliferation, immunohistochemistry (IHC) analysis established reduced cell proliferation with a significant decrease in the number of $Ki67^{+}$ cells in the riluzole plus CB839-treated xenograft tumors compared to vehicle-treated control samples (Figure 19B). Representative high magnification images of IHC staining of the Ki67-stained FFPE sections of the excised xenografts are shown in Figure 19B.

Treatment with riluzole and CB-839 reduces glutamatergic signaling markers in excised xenograft tumors

Molecular analysis of excised tumors allowed for assessment of GRM1-mediated signaling by looking at the overall expression levels of downstream ERK and AKT proteins. Previously, we reported AKT activation in Grm1-mouse melanocytic clones

[213]. Moreover, we have demonstrated a marked reduction in MAPK signaling in riluzole treated human melanoma cells [51]. In the lysates prepared from excised human melanoma xenografts, immunoblot results demonstrate enhanced suppression of both ERK and AKT phosphorylation with the combination of riluzole and CB839 compared to either agent alone (Figure 19A). The immunoblot analyses also revealed reduced expression of GRM1 and GLS in the riluzole plus CB839 treated xenografts that displayed restricted growth (Figure 19A). Treatment with the combination of riluzole and CB839 may have reduced the number of viable $GRM1^{+}$, GLS^{+} tumor cells thus resulting in diminished levels of GRM1 and GLS expression in the residual tumor cells.

Analysis of apoptotic cell death markers in excised xenograft tumors show no change in apoptosis with treatment

In an earlier study conducted in a GRM1-driven breast cancer model, we discovered that mitigation of GRM1 expression significantly attenuated apoptosis (as assessed by cleaved-caspase-3 staining) [58]. Here, we wanted to determine whether abrogation of xenografts through inclusion of both riluzole and CB-839 occurs via apoptosis mediated cell death. In the excised C8161 xenografts, we did not find any evidence of altered cleaved-caspase-3 staining amongst the four treatment arms (Figure 19C). This was confirmed through the absence of PARP cleavage by western blot (Figure 19A). Similar results were obtained from the evaluation of excised 1205LU xenografts (data not shown). The absence of a substantial apoptotic cell population at the end of the experiment may have been underwritten by the death of these cells during the study. It is imperative that revised time-staggered studies be performed in the future to assertively determine the mode of cell death induced by this *in vivo* combinatorial application with riluzole and CB-839.

Reduction of blood plasma amino acid metabolite pool sizes upon treatment

Mass spectrometric analysis of blood plasma by our collaborator (Dr. Fabian Filipp) revealed that glutamate levels react to the administered drugs. Circulating glutamate in blood plasma isolated from tumor-bearing mice is significantly lowered by about 20% on average upon combination treatment with a functional GRM1 inhibitor, riluzole, and glutaminase inhibitor, CB839, with *p* values below 0.05 (Figure 20). Targeted metabolomics revealed that blood plasma pool sizes of hydroxyl-proline, oxalic acid and aspartate also showed a significant reduction in the combination treatment (Figure 20). Their profiles indicate a trend of high responsiveness of plasma metabolite from single-agent treatment and maximum response in the modality of both drugs combined. These results indicate that glutamate and its associated downstream metabolites either within the urea cycle or the citric acid cycle are affected by this drug targeting strategy, such that the mitogenic glutamatergic feedback loop can be broken.

Gender-specific response to riluzole monotherapy detected in xenografts

The aspect of gender origin of cells utilized in experimental biology has been recognized as an important determinant since human cells exhibit wildly different concentrations of many metabolites across the sexes. We identified a major sex-related characteristic in xenograft models contributing to altered drug efficacy - cytotoxicity of a drug, which may be different for each gender depending on differences in xenobiotic metabolism. Specifically, we demonstrated greater inhibition of tumor growth in riluzole-treated male mice due to higher levels of systemically circulating active riluzole (Figure 21). Such cross-sex related modulation of the engraftment efficacy may lower the reported drug efficacy across a cohort average in the absence of gender stratification. No noticeable

differences were detected in the systemically circulating levels of CB839 between male and female mice (Figure 21). By rigorously implementing gender stratification, personalized treatment regimens are facilitated, and reproducibility of disease and developmental models is enabled, consistent with the mandate from the National Institutes of Health to improve scientific rigor and reproducibility in research. Taken together, these results uncovered gender-biased *in vivo* xenograft tumor studies where the enhanced efficacy, especially to riluzole, was dependent on the gender of the recipient mice.

Section III: Elucidate the mechanism(s) responsible for the GRM1-mediated alterations in glutamate bioavailability

Aim 3: Rationale

Numerous molecular mechanisms regulate cancer cells' biological machinery. Determination of all possible regulatory mechanisms of GLS in cancer remains to be fully elucidated. Several studies have shone light on different mechanisms by which GLS is regulated. Figure 3 summarizes various proteins associated with GLS dysregulation. It is not known if any of these regulatory processes are applicable to our system. Our preliminary findings reveal that GLS may be directly or indirectly regulated by GRM1 at the transcriptional or post-transcriptional level. In this aim, we test the involvement of numerous transcription factors implicated in the makeover of GLS-dependent tumor cells. First, participation of the mTORC1/c-Myc axis in regulating GLS expression was explored, as reported by others [145, 169, 186, 190, 214], in a GRM1-driven melanoma system. Moreover, built on findings described by others [191-193], we set off to examine any impending contribution of NF-κB, STAT1, and c-Jun in altering GLS expression. The theme of these studies is to validate innovative discoveries by others that continue to provide paradigms of how GLS is altered in $GRM1^{+}$ melanoma. Understanding these regulatory mechanisms may help open possibilities for novel drug therapies as well as optimize current treatments.

Materials and Methods

Reagents and antibodies

Rapamycin (PubChem CID: 5497196) was purchased from Sigma-Aldrich (St. Louis, MO). Rapamycin was dissolved in dimethyl sulfoxide (DMSO) as a 20 mM stock solution. All inhibitors were used in treatments at the indicated concentrations. Polyclonal anti-GLS antibody was purchased from Novus Biologicals (NBP1-58044, Littleton, CO). Monoclonal a-tubulin antibody was purchased from Sigma-Aldrich (T6074, St. Louis, MO). GRM1 antibody was purchased from Lifespan BioSciences (LS-C354444, Seattle, WA). c-Myc (sc-764) antibody was purchased from Santa Cruz Biotechnology (Dallas, TX). phospho-mTOR (5536) antibody was purchased from Cell Signaling Technology (Danvers, MA). Total mTOR (2972) antibody was also purchased from Cell Signaling Technology (Danvers, MA).

Cell lines and cell culture conditions

C8161 and 1205LU cells were cultured in RPM1-1640 medium supplemented with 10% fetal bovine serum (FBS) and 1% Penicillin-Streptomycin (PS). For experiments involving treatment with rapamycin, 400,000 cells were seeded into an appropriate number of 6 cm dishes. All cells were incubated at 37°C in a humidified 5% CO_2 incubator to prepare for treatment with the 500 nM of rapamycin 24 hours post seeding. Because rapamycin was dissolved in DMSO, the vehicle treated cells were exposed to an equivalent concentration of DMSO. For mRNA isolation and RT-qPCR experiments, C81-61 and C81-61 GRM1-6 (C81-61OE) cells were cultured in RPM1-1640 medium supplemented with 10% FBS and 1% PS. For each cell line, 3,000,000 cells were seeded

into 10 cm dishes and incubated at 37°C in a humidified 5% CO_2 incubator. Cells were allowed to grow to ~85-90% confluency.

RNA extraction, cDNA synthesis, and qRT-PCR

RNA was isolated from C81-61 and C81-61 GRM1-6 cells using RNeasy Mini Kit (Qiagen) according to the manufacturer's instructions and was subsequently treated with Turbo DNA-*free*™ Kit (Invitrogen) to remove any remaining traces of DNA. The RNA concentration and purity were determined by a microvolume Nanodrop spectrophotometer (ThermoFisher Scientific). The concentration of C81-61 RNA was found to be 147.908 ng/µL and the concentration of C81-61 GRM1-6 RNA was found to be 168.199 ng/µL. 1000 ng of RNA sample for each cell line was used for the cDNA synthesis procedure. RNA samples were first subjected to primary reverse transciptase (RT) using the SuperScript® III First-Strand Synthesis System for RT-PCR (Invitrogen) according to the manufacturer's instruction. The reaction mixture contained the sample RNA, 2 µM gene-specific primer, 10 mM deoxyribonucleotide triphosphate mix, and Diethyl pyrocarbonate-treated water. The reaction mixture was incubated at 65ºC for 5 minutes followed by placement on ice for 1 minute. cDNA Synthesis Mix was made adding the following components in the indicated order: 10X Reverse Transcriptase buffer, 25 mM $MgCl_2$, 0.1 M Dithiothreitol, RNaseOUT™ (40 U/µL) and SuperScript® III RT (200 U/µL). 10 µL of the cDNA Synthesis Mix was added to each RNA/primer mixture and then incubated for 50 minutes at 50ºC. The reaction was terminated at 85ºC for 5 minutes and then chilled on ice. This was followed by the addition of 1 µL of RNase H to each sample and incubation at 37ºC for 20 minutes. Samples were used immediately for PCR. A solution of SYBR® Green Master Mix, cDNA, RNase free water, and forward and reverse primers was

prepared for genes targeting GLS (Sigma-Aldrich, Gene ID: 2744) and GAPDH (forward sequence: GTCTCCTCTGACTTCAACAGCG, reverse sequence: ACCACCCTGTTGCTGTAGCCAA). Samples were prepared in triplicates for both cell lines. PCR was done using the StepOne™ Real-Time PCR System and data was collected for quantitative comparison C_T ($\Delta\Delta C_T$).

Production of lentiviral particles

HEK293T cells are human embryonic kidney cells and were used for the production of lentivirus particles. D10 media was used to culture HEK293T cells. D10 media was composed of Dulbecco's modified eagle medium (DMEM) with 10% FBS and 1% Penicillin-Streptomycin. Lentivirus was produced by mixing 1.6 mL DMEM, 80 µL PLUS reagent (Thermo Fisher), 2 µg VSVG, 6 µg delta R8, and 8 µg turbo sh-Myc into one polystyrene tube and 1.6 mL DMEM, 80 µL PLUS reagent, 2 µg VSVG, 6 µg delta R8, and 8 µg PLKO turbo GFP (empty vector) into another polystyrene tube. VSVG is an envelope protein whereas delta R8 is a packaging plasmid for lentivirus production, PLUS reagent is used in conjunction with lipofectamine 2000 to improve transfection efficiency, PLKO is the empty vector without the shRNA that was used as the backbone (negative control), and turbo sh-Myc is the lentiviral shRNA against c-Myc. 120 µL lipofectamine 2000 and 1.6 mL DMEM were mixed in a separate tube and left to incubate for 15 minutes. The mixture was then added dropwise into each tube containing the virus. Eight 100 mm plates of HEK293T cells containing 800,000 cells per plate were prepared the day before transduction. 855 µL of sh-Myc viral mixture was added to 4 plates and 855 µL of PLKO control mixture was added to 4 plates. The plates were left to incubate overnight. Lentiviral

particles were collected from plates with sh-Myc or PLKO at 24 hours, 48 hours, and 72 hours and stored at -80˚C.

Infecting target cells with lentiviral particles

On day 0, C8161 or 1205LU cells were plated as 400,000 cells per 60 mm plate with 3.5 mL of D10 media, two plates for PLKO turbo GFP and two plates for turbo sh-Myc. The plates were left to incubate overnight. On day 1, old media in each plate was replaced with 1 mL D10 media, 2 mL of virus containing DMEM and 7.5 µL polybrene. On day 2, this step was repeated. On days 3 and 4, the protein extraction protocol was performed on the designated plates and extracts were stored at -80˚C.

Results

Concomitant changes in GLS mRNA and protein levels post alterations in GRM1 protein expression

We utilized the aforementioned pair of isogenic cell lines, C81-61 (*GRM1*$^{-}$) and C81-61OE (*GRM1*^{OE}) for this experiment. Consistant with our prior results shown in Figure 9, C81-61OE cells with high levels of GRM1 also had high levels of GLS mRNA and protein when compared to C81-61 cells which displayed low protein levels of GRM1 and GLS along with diminished GLS mRNA expression (Figure 22). This result suggests that there is a positive association between GRM1 protein levels and GLS mRNA levels and that GRM1 may directly or indirectly regulate GLS.

Knockdown of c-Myc does not reduce GLS expression

c-Myc has been demonstrated to promote glutaminolysis through a coordinated transcriptional process that triggers cellular addiction to glutamine [145, 214]. To establish whether this mechanism was functional in our model system, c-Myc was downregulated in

both C8161 and 1205LU cells by infecting with lentiviral particles that were transduced with silencing RNA to c-Myc. Western immunoblots on the extracted proteins were performed. In C8161 cells, band quantification and normalization showed approximately 50% and 65% reduction in c-Myc levels at 72 hours and 96 hours, respectively (Figure 23). Interestingly, 1205LU cells displayed a more robust response (~80% inhibition) in c-Myc expression at both 72 hours and 96 hours post infection (Figure 23). Conflicting with our expectations and previously published data by others [145], c-Myc had no inhibitory effect on GLS expression. In fact, GLS demonstrated a modest 25-50% increase upon c-Myc knockdown at the above-mentioned time points in both cell lines (Figure 23).

The mTORC pathway regulates GLS in GRM1$^+$ melanoma cells

It has been previously demonstrated that mTORC1 is a positive regulator of GLS expression through the c-Myc axis in liver and pancreatic cancer [186, 190]. After the aforesaid unexpected result, we were interested in determining whether this previously defined relationship between mTORC1, c-Myc, and GLS ensues in GRM1$^+$ melanoma. Therefore, we tested the effects of mTORC1 inhibition on c-Myc and GLS protein levels in two GRM1$^+$ human melanoma cell lines. Rapamycin, a well-documented mTORC1 small-molecule inhibitor, was used for this experiment. In 1205LU cells, treatment with 500 nM rapamycin reduced mTOR activation as early as 4 hours post treatment and by 70% at 48 hours post treatment with a 40% suppression of c-Myc. GLS levels were moderately suppressed 4 hours post treatment and by 60% 48 hours after mTOR inhibition (Figure 24). Comparatively, in C8161 cells, treatment with the same dosage of rapamycin for 24 hours reduced mTOR activation by 60% - this led to 8% suppression of c-Myc expression and 50% decrease in GLS levels at 24 hours post mTOR inhibition (Figure 24).

These results suggest that GLS may be a downstream target of the mTORC pathway and its reduced expression may correlate with diminished c-Myc levels in $GRM1^{+}$ melanoma cells. It is also possible that mTORC may directly regulate GLS with c-Myc being an independent target of mTORC. Whether or not c-Myc is involved needs to be further elucidated.

Section IV. Discussion

G-protein coupled receptors (GPCRs) and their downstream effectors represent a class of therapeutic targets in mediating the pathogenesis of melanoma and other malignancies. Previous studies have explored a variety of drugs that affect different cellular processes in hope of attenuating malignancies, however, combination therapy in which two drugs or biologics act in a synergistic manner remains the best therapeutic strategy in the fight against cancer. In melanoma, hyperactive metabotropic glutamate receptor 1 (GRM1) is an oncogenic driver in the neuroectodermal-derived lineage of melanocytes [215]. Ectopic expression of G protein-coupled receptors have the ability to regulate mitogenic signals [43, 44]. Aberrant glutamatergic signaling activates mitogenesis and melanomagenesis independent from canonical mitogen activated protein kinase signaling [216]. Here, we provide a unique focus on non-canonical mitogen-activated protein kinase pathways, G-protein activation independent of BRAF/NRAS genotypes, and metabolic signaling in melanoma. The high frequency of ectopic GRM1 expression in melanoma, and its signaling cascades implicated in cellular transformation, has made it a principal research interest among many groups seeking better therapeutic strategies for the treatment of melanoma. Our group previously demonstrated that expression of GRM1 in melanoma cells results in elevated levels of glutamate, it's natural ligand, in the extracellular space surrounding the receptor [51]. A recent report by Gelb *et al*. has proposed that the GRM1 receptor behaves like a dependence receptor creating dependence on glutamate for sustained growth and viability of human melanomas expressing GRM1 [41]. A switch in cell cycle progression and biosynthetic metabolism may create overflow metabolism, which in turn produces the extracellular signals required for stimulation of the ectopically

expressed glutamate receptor. In this study, the role of GRM1 in modulating glutamate bioavailability in melanoma cells was explored. Our results suggest that GRM1 expression promotes an altered metabolic phenotype that supports increased glutamate production and autocrine glutamatergic signaling. Glutamatergic signaling through GRM1 promotes expression of GLS increasing the conversion of glutamine into glutamate. Melanoma cells heavily depend on anaplerosis via glutamine [111, 217]. $GRM1^{+}$ melanoma cells upregulate GLS to support the increased demand for glutamate. Our metabolomics results reveal that $GRM1^{+}$ melanoma cells exhibit elevated levels of mitochondrial TCA cycle-related amino acids and glutaminolytic intermediates such as glutamate. This finding is comparable to a recent report which suggests that the amino acid signature, especially for glutamic acid and alanine, is different in human melanoma cell lines contingent to their disease stage [119]. Altered levels of these amino acids have been reported to amend the growth and aggressiveness of melanoma cells [119]. The increased intracellular pool of glutamate could be a direct result of increased conversion of glutamine to glutamate via the activity of GLS. Our principle component analysis revealed that modulation of GRM1, in two independent pairs of isogenic melanoma cells, results in metabolic perturbations that overlap with GRM1 expression levels. Surplus quantities of intracellular glutamate are transported to the extracellular environment, where it serves as a trigger for the GRM1 receptor. In neuronal cell lineages, cytoplasmic glutamate is exported via vesicular glutamate transporters or cystine-glutamate exchangers [218]. Specific antagonists of GRM1 and metabolic inhibitors that reduce the availability of glutamate, have provided valuable information alluding to the underlying mechanisms of GRM1's activation, while also providing a basis for pre-clinical research.

We demonstrate elevated glutamate levels in the systemic circulation of heterozygous TGS mice (which harbor only one copy of the disrupted *Grm1*) compared to that of wild type TGS mice (no disrupted *Grm1*) – this was observed in 6 month old TGS mice but no differences were noted in their younger counterparts suggesting time-dependent regulation of blood plasma glutamate levels. The abundant availability of the endogenous ligand for GRM1 leads to constitutive activation of the GRM1 receptor, further promoting cell proliferation and metabolism pathways. To break such positive feedback circuits, we sought after different pharmacological vulnerabilities of glutamate signaling and metabolism. While treatment with a GRM1-specific inhibitor, riluzole, resulted in a significant proliferative disadvantage of tumor cell growth, CB-839 was found to have anti-proliferative effects specifically on $GRM1^{+}$ cell lines that harbored wild type BRAF. In some $GRM1^{+}$, mutated $BRAF^{V600E}$ melanoma cells, a considerably higher concentration of CB-839 was required to detect any noticeable suppression in cell proliferation. Similar results were found in a study by Lee *et al*. depicting the resistance of mutated $BRAF^{V600E}$ to riluzole treatment in a similar set of melanoma cell lines. They illustrated that cell lines containing wild type BRAF were more sensitive to riluzole than those containing mutated $BRAF^{V600E}$ [205]. Cells with mutated $BRAF^{V600E}$ result in constitutive activation of the MAPK pathway, which is also activated by stimulation of GRM1. Therefore, presence of additional downstream gain-of-function mutations in effectors of the MAPK pathway could lead to upregulation of cell proliferation and decreased sensitivity of the pathway to small-molecule inhibitors such as riluzole and CB-839. While inhibition of glutamatergic signaling by decreasing glutamate release via riluzole or inhibition of GLS activity via CB-839 resulted in reduced cell proliferation as well as diminished tumor growth, the

combination of both compounds was most effective. Riluzole and CB-839 aim at complementary aspects of glutamate signaling and metabolism. The combined inhibition of glutamatergic signaling via riluzole and of GLS activity via CB-839 efficiently reduced the conversion of glutamine to glutamate and interrupted export of any residual glutamate. As a consequence, extracellular glutamate concentration was reduced thus lowering the availability of the natural ligand of GRM1. Such rational combination of two complementary drug-targeting approaches disrupted the ability to circumvent individual blockages yielding a robust response, as evidenced by the enhanced reduction of tumor progression. We also expected to see an increased reduction of glutamate in the conditioned media after co-treatment with riluzole and CB-839 but this was not the case. Tumor cells have the ability to compensate for GLS inhibition and can overcome glutamate deprivation under such conditions through increased anaplerosis, for example by asparagine synthetase [182]. This compensatory mechanism may have contributed to intracellular glutamate production and release into the extracellular milieu. Alternatively, other glutamate transport pathways may have been altered to counterbalance the reduced glutamate levels due to the burden exhibited by the combinatorial treatment [180]. Additional metabolic flux analysis would assist in revealing the source of glutamate before and after treatment with riluzole plus CB-839.

Our drug targeting strategy considered different aspects of tumor metabolism. The goal of the study was to limit glutamate supply while reducing circulating glutamate plasma levels, such that the mitogenic glutamatergic feedback loop can be broken. The combined treatment of riluzole and CB839 leads to enhanced inhibition of $GRM1^+$ melanoma cell proliferation *in vitro* and reduction of tumor burden *in vivo*. Most importantly, disruption

of GRM1 signaling through combined actions of CB-839 and riluzole displayed no obvious symptoms of toxicity. The animal models evidenced significant suppression of tumor progression following treatment with the combination of riluzole and CB839. In a few instances, the combination therapy even led to the complete elimination of the tumor mass. Circulating blood plasma glutamate levels were significantly lowered in these tumor xenograft models confirming target engagement. This result runs parallel to our previous finding where we observed diminished glutamate levels in circulating blood plasma of wild type TGS mice compared to their heterozygous TGS counterparts thereby providing prospective for successful translation of this therapy to human patients in the future [219]. In addition to glutamate, plasma pool sizes of hydroxyl-proline, oxoglutarate, oxalic acid, aspartate, and asparagine also showed a significant reduction in the combination treatment. This finding validates a recent report suggesting that addiction to amino acid synthesis (such as proline) from glutamine is associated with response to CB-839 [220] and further confirms on-target activity as the anabolism of these amino acids is reliant on the accessibility of glutamate.

Using phosphorylated-ERK and phosphorylated-AKT levels as markers of glutamatergic signaling, our analysis of excised tumor lysates demonstrated abrogated GRM1-mediated signaling with the combination of CB-839 and riluzole. This was validated through significantly reduced staining of Ki67 indicative of a possible response mechanism through reduced $GRM1^{+}$ tumor cell proliferation. Components of the MAPK pathway have been shown to not only regulate proliferation signals but also function in the control of cell survival by regulating apoptotic activity [221]. Our cell culture studies revealed that apoptosis was marginally elevated in the combination treatment signifying

that the combined targeting of glutamate metabolism and signaling displays enhanced efficacy possibly through a combination of apoptosis-mediated cell death and reduced cell proliferation. Disappointingly, we failed to detect the presence of any apoptosis mediated cell death in the excised tumors exposed to riluzole and CB-839. The absence of any apoptotic tumor cell populations at termination may have been purported by the death of these cells during the course of the study. This can be reassessed by executing time-staggered experiments on various cohorts of mice. Besides, rigorous evaluation of sex differences in drug responses of two independent xenografts revealed a higher tumor burden in the riluzole-treated female mice compared to the analogous male counterparts. This result addresses the subject of drug cytotoxicity, which may be dissimilar for each gender contingent to differences in xenobiotic metabolism [222]. We determined that the blood plasma concentration of unbound riluzole is substantially higher in male mice compared to their female counterparts possibly explaining why riluzole treatment displays a superior response in males. Results like these call for rigorous implementation of gender stratification. By doing so, personalized treatment regimens are facilitated and reproducibility of disease and developmental models is enabled, consistent with the instruction from the National Institutes of Health to improve scientific accuracy and reproducibility in research.

The role of glutamine metabolism in cancer cells is well established. However, it is less clear how its role is influenced by the tumor microenvironment, which is often subject to nutrient and oxygen shortage [223]. Recently, we reported that one of the consequences of aberrant GRM1 signal transduction is downstream activation of the hypoxia-induced transcription factor 1, HIF-1α, which promotes angiogenesis even in normoxic conditions

[199]. Glutamine metabolism is strongly coupled to HIF-1α activity and enhanced in tumors [116]. Metabolomics data show that pool sizes of TCA cycle intermediates are increased by GRM1 expression, while glycolytic intermediates are unaffected. This further suggests that GRM1 signaling is tightly connected to glutaminolysis.

In our attempt to dig deeper into the regulatory mechanism of GLS, our preliminary findings revealed elevated levels of GLS mRNA transcripts in $GRM1^+$ melanoma cells suggesting that GLS may be directly or indirectly regulated by GRM1 at the transcriptional or post-transcriptional level. It has been previously demonstrated that mTOR complex 1 (mTORC1) is a positive regulator of GLS expression through the c-Myc axis [186, 190]. Importantly, mTORC1 has been shown to act as a critical molecular link between growth signals including lipids, nucleic acids and proteins, and the processes underlying anabolic cell growth and differentiation [224]. Other studies have shown a direct relationship between c-Myc and GLS expression - Gao *et al*. reported that c-Myc transcriptionally represses miR-23a and miR-23b leading to higher expression of GLS, which upregulates the glutamine catabolism in human P-493B lymphoma cells and PC3 prostate cancer cells [225]. Surprisingly, our results showed that independent knockdown of c-Myc did not lead to a parallel downregulation of GLS expression suggesting that a concomitant decrease in mTORC may be essential. Others have postulated that there needs to be simultaneous suppression of mTORC and c-Myc in order to perceive a subsequent decrease in GLS expression [169, 186, 190]. We established that GLS overexpression, in $GRM1^+$ cell lines, transpires, at least in part, through the mTORC axis, as seen through reduced phosphorylation of mTORC and subsequent downregulation of GLS. Whether or not c-Myc is involved in this process needs to be further elucidated. Current work is focused on

determining whether mTOR-mediated regulation of GLS occurs through mTORC1 or mTORC2. These results are crucial in understanding the underlying molecular mechanisms of GRM1-mediated alterations in the glutaminolytic activity of melanoma cells. This research, combined with our previous data, may aid in our understanding of these regulatory mechanisms and could possibly help open up opportunities for novel drug therapies as well as optimize current treatments.

Conclusions

The overall goal of this dissertation was to investigate how ectopic GRM1 expression leads to rewiring of metabolic processes, especially in glutamate metabolism, and how this may contribute to deregulated tumor cell proliferation. We have heretofore exposed a positive correlation between the expression of GRM1 and GLS, the pivotal enzyme in glutaminolysis. We then went on to establish why and how the GRM1 receptor is able to disrupt glutamate bioavailability. Moreover, we uncovered the underlying mechanism by which the GLS-mediated glutaminolytic glutamate production is altered by GRM1 in GRM1-expressing melanoma cells. We are the first group to propose that modulation of glutamatergic signaling by blocking independent but complementary pathways with the combinatorial use of two small molecule inhibitors, riluzole and CB-839, may offer therapeutic benefits to patients with GRM1-expressing cancers, especially melanoma. Altered metabolisms have been observed in many cancers, therefore, the knowledge we gain from our studies in melanoma may be applicable to other malignancies.

Future Directions

Accompanied by the onset of the post-genome era, scientists are now beginning to divert their attention from conventional "one-size-fits-all" therapy to personalized medicine. As the first one to discover that ectopic expression of GRM1 is the driving basis for melanoma development, our group has been devoted to utilizing glutamatergic signaling inhibitor riluzole to treat melanoma patients for a while. Previously, our group had reported on completed Phase 0 and Phase 2 trials using single agent riluzole in late stage melanoma patients [90, 91]. Based on results we reported earlier where we observed correlations between GRM1 and GLS expression levels [207], it will be interesting to see if similar observations may be made with multiple sets of paired pre- and post-treatment tumor samples. Currently, CB-839 is also in clinical trials in combination with other compounds for patients with advanced, metastatic, solid and hematopoietic tumors [226, 227], where glutamine metabolism has been identified as a suitable drug target; it will be of great interest to see if we could initiate a clinical trial in melanoma combining two relatively non-toxic drugs, riluzole and CB-839. We predict enhanced efficacy compared to the previously completed monotherapy trial with riluzole in Phase 0 and 2. Furthermore, we would like to incorporate anti-PD-1/anti-PD-L1 checkpoint therapy in combination with riluzole and CB-839 as targeted therapy has been postulated to prime the immune system and improve patients' responsiveness [83, 84].

In the treatment of amyotrophic lateral sclerosis (ALS), riluzole contains neurotoxic excretion of glutamate [86, 87, 228]. The underlying mechanism by which riluzole inhibits the release of glutamate is largely unknown. A recent report by our group demonstrated that *in vitro* treatment of two melanoma cell lines with riluzole altered

expression of the cysteine-glutamate amino acid transporter, xCT (SLC7A11) [229]. Additional xenograft studies revealed that riluzole down-regulated xCT expression suggesting that xCT is a molecular target of riluzole [229, 230]. To investigate this further, we have obtained mouse melanocytes that lack xCT expression. Current work is focused on utilizing genetic means to influence these xCT-null cells with GRM1 and determine whether xCT is functionally altered by riluzole in $GRM1^{+}$ melanoma. Moreover, it is possible that riluzole may condense extracellular glutamate concentrations by promoting reuptake of glutamate. The excitatory amino acid transporters 1-4 (EAAT1-4) are typically found on neuronal cells to help reduce the excitotoxic effects of excess glutamate [231-233]. To start, it will be interesting to determine if there are any correlations between EAAT and GRM1 expression. Depending on these results, modulation of EAAT and/or GRM1 levels by genetic approaches may enable us to determine whether one or more of these transporters are involved in riluzole-mediated diminution of extracellular glutamate levels.

The high metabolic demand of cancer results in increased production of ROS. To combat this, tumors increase antioxidant production via hyperactivation of the nuclear factor erythroid 2-related factor 2 (NRF2) pathway. NRF2 is the master regulator of a cell's endogenous antioxidant response. Kelch-like ECH-associated protein 1 (Keap1) has been shown to interact with and directly promote proteosomal degradation of NRF2 by cooperating with Cul3, an important compotent of the E3 ubiquitin ligase complex [234]. Keap1-mutant (loss-of-function mutation) lung cancer cells have been shown to demonstrate increased sensitivity to GLS inhibition and glutamine deprivation [235]. This sensitivity to GLS inhibition is the result of Keap1-mutated (loss of Keap1) cells being

overly dependent on glutaminolysis through proper functioning of xCT transporter [236]. A previous report by our group has revealed that riluzole treatment can also increase ROS accumulation in $GRM1^+$ melanoma cells by diminishing intracellular glutathione levels [237]. We have also illustrated that treatment of $GRM1^+$ melanoma cells with riluzole reduces xCT expression [229]. It would be interesting to determine whether combined treatment with riluzole and CB-839 mediates its anti-tumorigenic potential by altering the Keap1/NRF2 axis. In fact, preliminary crossing of $GRM1^+$ TG-3 mice with NRF2-null mice resulted in extreme sickness and even lethality in some of the ensuing mice (data unpublished). We should begin the investigation by checking the status of Keap1 in $GRM1^+$ melanoma cells. Results from this exploration may help uncover novel regulatory mechanisms of GRM1 and GLS mediated tumorigenesis.

Last but not least, unraveling alternate mechanisms underlying GRM1 and GLS mediated glutamatergic signaling is still crucial. Potential factors that influence communication between GRM1 and GLS should be investigated. Redis *et al*. uncovered an allele-specific regulatory mechanism that the long ncRNA *CCAT2* interacts with the Cleavage Factor I complex and then fine-tunes the alternative splicing of *GLS* by selecting the poly (A) site in intron 14 of the precursor mRNA [238]. Recently, Edwards *et al.* reported that the receptor tyrosine kinase EphA2 activates the TEAD family transcriptional coactivators YAP and TAZ and further overexpresses *GLS*, the regulatory DNA elements of which contains TEAD binding site [239]. Another recent study demonstrated that heat shock factor 1 (HSF1) stimulates GLS-dependent mTOR activation by means of recruiting DNA transferase 3a (DNMT3a) to epigenetically deregulate the expression of microRNA137 (MIR137) which targets GLS in colorectal cancer [240]. Our future

research may interrogate whether these molecules play a role in the metabolic rewiring of $GRM1^{+}$ melanoma cells. One rational approach would be to conduct RNA-seq analysis to determine the various genes that are altered upon ectopic expression of GRM1 and/or GLS inhibition in melanoma. Once we can fully disclose the atlas of the whole regulatory pathway, our current combinatorial therapy can be optimized for melanoma patients to prolong their response and survival.

References

1. Siegel, R.L., K.D. Miller, and A. Jemal, *Cancer statistics, 2016.* CA: A Cancer Journal for Clinicians, 2016. **66**(1): p. 7-30.
2. Siegel, R.L., K.D. Miller, and A. Jemal, *Cancer statistics, 2020.* CA: A Cancer Journal for Clinicians, 2020. **70**(1): p. 7-30.
3. Dickson, P.V. and J.E. Gershenwald, *Staging and prognosis of cutaneous melanoma.* Surgical oncology clinics of North America, 2011. **20**(1): p. 1-17.
4. Greenwald, H.S., E.B. Friedman, and I. Osman, *Superficial spreading and nodular melanoma are distinct biological entities: a challenge to the linear progression model.* Melanoma research, 2012. **22**(1): p. 1-8.
5. Weinberg, R., *The Nature of Cancer* in *The Biology of Cancer*. 2014, Garland Science New York.
6. Cichorek, M., et al., *Skin melanocytes: biology and development.* Postepy Dermatol Alergol, 2013. **30**(1): p. 30-41.
7. Brenner, M. and V.J. Hearing, *The protective role of melanin against UV damage in human skin.* Photochem Photobiol, 2008. **84**(3): p. 539-49.
8. Karasarides, M., et al., *B-RAF is a therapeutic target in melanoma.* Oncogene, 2004. **23**(37): p. 6292-8.
9. Burow, M.E., et al., *PI3-K/AKT regulation of NF-kappaB signaling events in suppression of TNF-induced apoptosis.* Biochem Biophys Res Commun, 2000. **271**(2): p. 342-5.
10. McCubrey, J.A., et al., *Ras/Raf/MEK/ERK and PI3K/PTEN/Akt/mTOR cascade inhibitors: how mutations can result in therapy resistance and how to overcome resistance.* Oncotarget, 2012. **3**(10): p. 1068-111.
11. Davies, H., et al., *Mutations of the BRAF gene in human cancer.* Nature, 2002. **417**(6892): p. 949-54.
12. Pollock, P.M., et al., *High frequency of BRAF mutations in nevi.* Nat Genet, 2003. **33**(1): p. 19-20.
13. Cheng, L., et al., *Molecular testing for BRAF mutations to inform melanoma treatment decisions: a move toward precision medicine.* Modern pathology : an official journal of the United States and Canadian Academy of Pathology, Inc, 2018. **31**(1): p. 24-38.
14. Jakob, J.A., et al., *NRAS mutation status is an independent prognostic factor in metastatic melanoma.* Cancer, 2012. **118**(16): p. 4014-23.
15. Curtin, J.A., et al., *Distinct sets of genetic alterations in melanoma.* N Engl J Med, 2005. **353**(20): p. 2135-47.
16. Dankort, D., Curley, D.P., Cartlidge, R.A., Nelson, B., Karnezis, A.N., Damsky, W.E., You, M.J., DePinho, R.A., McMahon, M., Bosenberg, M. , *Braf(V600E) cooperates with Pten loss to induce metastatic melanoma.* Nat Genet 2009, 2009.
17. Chin, L., et al., *Cooperative effects of INK4a and ras in melanoma susceptibility in vivo.* Genes Dev, 1997. **11**(21): p. 2822-34.
18. Tachibana, M., et al., *Ectopic expression of MITF, a gene for Waardenburg syndrome type 2, converts fibroblasts to cells with melanocyte characteristics.* Nat Genet, 1996. **14**(1): p. 50-4.

19. Levy, C., M. Khaled, and D.E. Fisher, *MITF: master regulator of melanocyte development and melanoma oncogene.* Trends Mol Med, 2006. **12**(9): p. 406-14.
20. Garraway, L.A., et al., *Integrative genomic analyses identify MITF as a lineage survival oncogene amplified in malignant melanoma.* Nature, 2005a. **436**(7047): p. 117-22.
21. Loercher, A.E., et al., *MITF links differentiation with cell cycle arrest in melanocytes by transcriptional activation of INK4A.* The Journal of cell biology, 2005. **168**(1): p. 35-40.
22. Aoude, L.G., et al., *Genetics of familial melanoma: 20 years after CDKN2A.* Pigment Cell Melanoma Res, 2015. **28**(2): p. 148-60.
23. Sharpless, N.E. and L. Chin, *The INK4a/ARF locus and melanoma.* Oncogene, 2003. **22**(20): p. 3092-3098.
24. Rozengurt, E., *Signal transduction pathways in the mitogenic response to G protein- coupled neuropeptide receptor agonists.* J Cell Physiol, 1998. **177**(4): p. 507-17.
25. Kroeze, W.K., D.J. Sheffler, and B.L. Roth, *G-protein-coupled receptors at a glance.* Journal of Cell Science, 2003. **116**(24): p. 4867.
26. Hamm, H.E., *The many faces of G protein signaling.* J Biol Chem, 1998. **273**(2): p. 669-72.
27. Bunemann, M., M. Frank, and M.J. Lohse, *Gi protein activation in intact cells involves subunit rearrangement rather than dissociation.* Proc Natl Acad Sci U S A, 2003. **100**(26): p. 16077-82.
28. Rosenbaum, D.M., S.G.F. Rasmussen, and B.K. Kobilka, *The structure and function of G-protein-coupled receptors.* Nature, 2009. **459**(7245): p. 356-363.
29. Fredriksson, R., et al., *The G-protein-coupled receptors in the human genome form five main families. Phylogenetic analysis, paralogon groups, and fingerprints.* Mol Pharmacol, 2003. **63**(6): p. 1256-72.
30. Khan, M.Z., *Ionotropic glutamate receptors (iGluRs) of the delta family (GluD1 and GluD2) and synaptogenesis.* Alexandria Journal of Medicine, 2017. **53**(3): p. 201-206.
31. Dingledine, R., et al., *The glutamate receptor ion channels.* Pharmacol Rev, 1999. **51**(1): p. 7-61.
32. Bortolotto, Z.A., et al., *Kainate receptors are involved in synaptic plasticity.* Nature, 1999. **402**(6759): p. 297-301.
33. Gouaux, E., *Structure and function of AMPA receptors.* The Journal of physiology, 2004. **554**(Pt 2): p. 249-253.
34. Young, D., et al., *Isolation and characterization of a new cellular oncogene encoding a protein with multiple potential transmembrane domains.* Cell, 1986. **45**(5): p. 711-9.
35. Julius, D., et al., *Ectopic expresion of the serotonin 1c receptor and the triggering of malignant transformation.* Science, 1989. **244**: p. 1057-1062.
36. Gutkind, J.S., et al., *Muscarinic acetylcholine receptor subtypes as agonist-dependent oncogenes.* Proc. Natl. Acad. Sci., 1991. **88**: p. 4703-4707.
37. Allen, L.F., et al., *G-protein-coupled receptor genes as protooncogenes: constitutively activating mutation of the alpha 1B-adrenergic receptor enhances*

mitogenesis and tumorigenicity. Proc Natl Acad Sci U S A, 1991. **88**(24): p. 11354-8.

38. Rigi-Ladiz, M.A., et al., *DNA methylation and expression status of glutamate receptor genes in patients with oral squamous cell carcinoma.* Meta Gene, 2019. **20**: p. 100545.
39. Aiba, A., et al., *Reduced hippocampal long-term potentiation and ontext-specific deficit in associative learning in mGluR1 mutant mice.* Cell, 1994. **79**: p. 365-375.
40. Conquet, F., et al., *Motor deficit and impairment of synaptic plasticity in mice lacking mGluR1*. Nature, 1994. **372**: p. 237-243.
41. Gelb, T., et al., *Metabotropic glutamate receptor 1 acts as a dependence receptor creating a requirement for glutamate to sustain the viability and growth of human melanomas.* Oncogene, 2015. **34**(21): p. 2711-20.
42. Chen, S., et al., *Spontaneous melanocytosis in transgenic mice.* J Invest Dermatol, 1996. **106**(5): p. 1145-51.
43. Marin, Y.E. and S. Chen, *Involvement of metabotropic glutamate receptor 1, a G protein coupled receptor, in melanoma development.* J Mol Med (Berl), 2004. **82**(11): p. 735-49.
44. Marin, Y.E., et al., *Stimulation of oncogenic metabotropic glutamate receptor 1 in melanoma cells activates ERK1/2 via PKCepsilon.* Cell Signal, 2006. **18**(8): p. 1279-86.
45. Zhu, H., et al., *Development of heritable melanoma in transgenic mice.* J Invest Dermatol, 1998. **110**(3): p. 247-52.
46. Pollock, P.M., et al., *Melanoma mouse model implicates metabotropic glutamate signaling in melanocytic neoplasia.* Nat Genet, 2003. **34**(1): p. 108-12.
47. Ohtani, Y., et al., *Metabotropic glutamate receptor subtype-1 is essential for in vivo growth of melanoma.* Oncogene, 2008. **27**: p. 7162-7170.
48. Teh, J.L. and S. Chen, *Glutamatergic signaling in cellular transformation.* Pigment Cell Melanoma Res, 2012. **25**(3): p. 331-42.
49. Shin, S.S., et al., *AKT2 is a downstream target of metabotropic glutamate receptor 1 (Grm1).* Pigment Cell Melanoma Res, 2010. **23**(1): p. 103-11.
50. Gilman, A.G., *G proteins: transducers of receptor-generated signals.* Annu Rev Biochem, 1987. **56**: p. 615-49.
51. Namkoong, J., et al., *Metabotropic glutamate receptor 1 and glutamate signaling in human melanoma.* Cancer Research, 2007. **67**(5): p. 2298-305.
52. Marin, Y.E., et al., *Stimulation of oncogenic metabotropic glutamate receptor 1 in melanoma cells activates ERK1/2 via PKCepsilon.* Cell Signaling, 2006. **18**: p. 1279-1286.
53. Shin, S.S., et al., *Oncogenic activities of metabotropic glutamate receptor 1 (Grm1) in melanocyte transformation.* Pigment Cell Melanoma Res, 2008a. **21**(3): p. 368-78.
54. Speyer, C.L., et al., *Metabotropic glutamate receptor-1: a potential therapeutic target for the treatment of breast cancer.* Breast Cancer Res Treat, 2012. **132**: p. 565-73.
55. Banda, M., et al., *Metabotropic glutamate receptor-1 contributes to progression in triple negative breast cancer.* PLoS One, 2014. **9**(1): p. e81126.

56. Dolfi, S.C., et al., *Riluzole exerts distinct antitumor effects from a metabotropic glutamate receptor 1-specific inhibitor on breast cancer cells.* Oncotarget, 2017. **8**(27): p. 44639-44653.
57. Sexton, R.E., et al., *Metabotropic glutamate receptor-1 regulates inflammation in triple negative breast cancer.* Sci Rep, 2018. **8**(1): p. 16008.
58. Teh, J.L., et al., *Metabotropic glutamate receptor 1 disrupts mammary acinar architecture and initiates malignant transformation of mammary epithelial cells.* Breast Cancer Res Treat, 2015. **151**: p. 57-73.
59. Martino, J., et al., *Metabotropic Glutamate Receptor 1 (Grm1) Is An Oncogene In Epithelial Cells.* Oncogene, 2013. **32**: p. 4366-4376.
60. Herner, A., et al., *Glutamate increases pancreatic cancer cell invasion and migration via AMPA receptor activation and Kras-MAPK signaling.* Int J Cancer, 2011. **129**(10): p. 2349-59.
61. Valiya Veettil, M., et al., *Glutamate secretion and metabotropic glutamate receptor 1 expression during Kaposi's sarcoma-associated herpesvirus infection promotes cell proliferation.* PLoS Pathog, 2014. **10**(10): p. e1004389.
62. de Groot, J.F., et al., *Knockdown of GluR1 expression by RNA interference inhibits glioma proliferation.* J Neurooncol, 2008. **88**(2): p. 121-33.
63. Zhang, C., et al., *Anti-cancer effect of metabotropic glutamate receptor 1 inhibition in human glioma U87 cells: involvement of PI3K/Akt/mTOR pathway.* Cell Physiol Biochem, 2015. **35**(2): p. 419-32.
64. Pereira, M.S.L., et al., *Metabotropic glutamate receptors as a new therapeutic target for malignant gliomas.* Oncotarget, 2017. **8**(13): p. 22279-22298.
65. Sabel, M.S., Y. Liu, and D.M. Lubman, *Proteomics in Melanoma Biomarker Discovery: Great Potential, Many Obstacles.* International Journal of Proteomics, 2011. **2011**: p. 181890.
66. Danson, S. and P. Lorigan, *Improving outcomes in advanced malignant melanoma: update on systemic therapy.* Drugs, 2005. **65**(6): p. 733-43.
67. Eisen, T., et al., *Sorafenib in advanced melanoma: a Phase II randomised discontinuation trial analysis.* Br J Cancer, 2006. **95**(5): p. 581-6.
68. Bucheit, A.D. and M.A. Davies, *Emerging insights into resistance to BRAF inhibitors in melanoma.* Biochem Pharmacol, 2014. **87**.
69. Johnson, D.B. and J.A. Sosman, *Therapeutic Advances and Treatment Options in Metastatic Melanoma.* JAMA Oncol, 2015. **1**(3): p. 380-6.
70. Bollag, G., et al., *Clinical efficacy of a RAF inhibitor needs broad target blockade in BRAF-mutant melanoma.* Nature, 2010. **467**(7315): p. 596-9.
71. Flaherty, K.T., et al., *Inhibition of mutated, activated BRAF in metastatic melanoma.* N Engl J Med, 2010. **363**(9): p. 809-19.
72. Chapman, P.B., et al., *Improved survival with vemurafenib in melanoma with BRAF V600E mutation.* N Engl J Med, 2011. **364**(26): p. 2507-16.
73. Siegel, R.L., K.D. Miller, and A. Jemal, *Cancer statistics, 2016.* CA Cancer J Clin, 2016. **66**(1): p. 7-30.
74. Beloueche-Babari, M., et al., *Acute tumour response to the MEK1/2 inhibitor selumetinib (AZD6244, ARRY-142886) evaluated by non-invasive diffusion-weighted MRI.* Br J Cancer, 2013. **109**(6): p. 1562-9.

75. Hatzivassiliou, G., et al., *RAF inhibitors prime wild-type RAF to activate the MAPK pathway and enhance growth.* Nature, 2010. **464**(7287): p. 431-5.
76. Baines, A.T., D. Xu, and C.J. Der, *Inhibition of Ras for cancer treatment: the search continues.* Future Med Chem, 2011. **3**(14): p. 1787-808.
77. Christensen, J.G., et al., *The KRASG12C Inhibitor, MRTX849, Provides Insight Toward Therapeutic Susceptibility of KRAS Mutant Cancers in Mouse Models and Patients.* Cancer Discovery, 2019: p. CD-19-1167.
78. Haanen, J.B.A.G., *Immunotherapy of melanoma.* EJC Supplements, 2013. **11**(2): p. 97-105.
79. Simeone, E. and P.A. Ascierto, *Immunomodulating antibodies in the treatment of metastatic melanoma: the experience with anti-CTLA-4, anti-CD137, and anti-PD1.* J Immunotoxicol, 2012. **9**(3): p. 241-7.
80. Kaufman, H.L., et al., *The Society for Immunotherapy of Cancer consensus statement on tumour immunotherapy for the treatment of cutaneous melanoma.* Nat Rev Clin Oncol, 2013. **10**(10): p. 588-98.
81. Carretero-González, A., et al., *Analysis of response rate with ANTI PD1/PD-L1 monoclonal antibodies in advanced solid tumors: a meta-analysis of randomized clinical trials.* Oncotarget, 2018. **9**(9): p. 8706-8715.
82. Okazaki, T. and T. Honjo, *PD-1 and PD-1 ligands: from discovery to clinical application.* Int Immunol, 2007. **19**(7): p. 813-24.
83. Keir, M.E., et al., *PD-1 and its ligands in tolerance and immunity.* Annu Rev Immunol, 2008. **26**: p. 677-704.
84. Alsaab, H.O., et al., *PD-1 and PD-L1 Checkpoint Signaling Inhibition for Cancer Immunotherapy: Mechanism, Combinations, and Clinical Outcome.* Front Pharmacol, 2017. **8**: p. 561.
85. Namkoong, J., et al., *Metabotropic glutamate receptor 1 and glutamate signaling in human melanoma.* Cancer Res, 2007. **67**(5): p. 2298-305.
86. Bensimon, G., et al., *A study of riluzole in the treatment of advanced stage or elderly patients with amyotrophic lateral sclerosis.[see comment]*. Journal of Neurology, 2002. **249**(5): p. 609-15.
87. Bensimon, G., L. Lacomblez, and V. Meininger, *A controlled trial of riluzole in amyotrophic lateral sclerosis. ALS/Riluzole Study Group.* N Engl J Med, 1994. **330**(9): p. 585-91.
88. Le, M.N., et al., *The Glutamate Release Inhibitor Riluzole Decreases Migration, Invasion and Proliferation of Melanoma Cells.* The Journal of investigative dermatology, 2010. **130**(9): p. 2240-2249.
89. Cheah, B.C., et al., *Riluzole, neuroprotection and amyotrophic lateral sclerosis.* Curr Med Chem, 2010. **17**(18): p. 1942-199.
90. Yip, D., et al., *A phase 0 trial of riluzole in patients with resectable stage III and IV melanoma.* Clin Cancer Res, 2009. **15**(11): p. 3896-902.
91. Mehnert, J.M., et al., *A phase II trial of riluzole, an antagonist of metabotropic glutamate receptor 1 (GRM1) signaling, in patients with advanced melanoma.* Pigment Cell Melanoma Res, 2018. **31**(4): p. 534-540.
92. Mehnert, J.M., et al., *A phase I trial of riluzole and sorafenib in patients with advanced solid tumors and melanoma.* Journal of Clinical Oncology, 2012. **30**(15_suppl): p. TPS3112-TPS3112.

93. Pelletier, J.C., et al., *Dipeptide Prodrugs of the Glutamate Modulator Riluzole.* ACS Med Chem Lett, 2018. **9**(7): p. 752-756.
94. Silk, A.W., et al., *A phase Ib study of troriluzole (BHV-4157) in combination with nivolumab.* Journal of Clinical Oncology, 2020. **38**(5_suppl): p. 79-79.
95. Hanahan, D. and R.A. Weinberg, *Hallmarks of cancer: the next generation.* Cell, 2011. **144**(5): p. 646-74.
96. Zheng, J., *Energy metabolism of cancer: Glycolysis versus oxidative phosphorylation (Review).* Oncology letters, 2012. **4**(6): p. 1151-1157.
97. Hampsey, M., *Cancer Cell Metabolism 16:695:624*. 2019.
98. Vander Heiden, M.G., L.C. Cantley, and C.B. Thompson, *Understanding the Warburg Effect: The Metabolic Requirements of Cell Proliferation.* Science (New York, N.Y.), 2009. **324**(5930): p. 1029-1033.
99. Lunt, S.Y. and M.G.V. Heiden, *Aerobic Glycolysis: Meeting the Metabolic Requirements of Cell Proliferation.* Annual Review of Cell and Developmental Biology, 2011. **27**(1): p. 441-464.
100. Warburg, O., *On the origin of cancer cells.* Science, 1956. **123**(3191): p. 309-14.
101. Warburg, O., *On respiratory impairment in cancer cells.* Science, 1956. **124**(3215): p. 269-70.
102. Pfeiffer, T., S. Schuster, and S. Bonhoeffer, *Cooperation and Competition in the Evolution of ATP-Producing Pathways.* Science, 2001. **292**(5516): p. 504-507.
103. Locasale, J.W. and L.C. Cantley, *Metabolic flux and the regulation of mammalian cell growth.* Cell metabolism, 2011. **14**(4): p. 443-451.
104. Dang, C.V., *Links between metabolism and cancer.* Genes Dev, 2012. **26**(9): p. 877-90.
105. Altman, B.J., Z.E. Stine, and C.V. Dang, *From Krebs to clinic: glutamine metabolism to cancer therapy.* Nat Rev Cancer, 2016. **16**(10): p. 619-34.
106. Deberardinis, R.J., et al., *Brick by brick: metabolism and tumor cell growth.* Curr Opin Genet Dev, 2008. **18**(1): p. 54-61.
107. Stein, W.H. and S. Moore, *The free amino acids of human blood plasma.* J Biol Chem, 1954. **211**(2): p. 915-26.
108. Biolo, G., et al., *Transmembrane transport and intracellular kinetics of amino acids in human skeletal muscle.* Am J Physiol, 1995. **268**(1 Pt 1): p. E75-84.
109. DeBerardinis, R.J. and T. Cheng, *Q's next: the diverse functions of glutamine in metabolism, cell biology and cancer.* Oncogene, 2010. **29**(3): p. 313-24.
110. Michalak, K.P., et al., *Key Roles of Glutamine Pathways in Reprogramming the Cancer Metabolism.* Oxid Med Cell Longev, 2015. **2015**: p. 964321.
111. Filipp, F.V., et al., *Reverse TCA cycle flux through isocitrate dehydrogenases 1 and 2 is required for lipogenesis in hypoxic melanoma cells.* Pigment cell & melanoma research, 2012. **25**(3): p. 375-383.
112. Bertout, J.A., S.A. Patel, and M.C. Simon, *The impact of O2 availability on human cancer.* Nature Reviews Cancer, 2008. **8**(12): p. 967-975.
113. Thompson, C.B., *Rethinking the regulation of cellular metabolism.* Cold Spring Harb Symp Quant Biol, 2011. **76**: p. 23-9.
114. Semenza, G.L., *Defining the role of hypoxia-inducible factor 1 in cancer biology and therapeutics.* Oncogene, 2010. **29**(5): p. 625-34.

115. Semenza, G.L., *HIF-1: upstream and downstream of cancer metabolism.* Current Opinion in Genetics & Development, 2010. **20**(1): p. 51-56.
116. Metallo, C.M., et al., *Reductive glutamine metabolism by IDH1 mediates lipogenesis under hypoxia.* Nature, 2012. **481**(7381): p. 380-4.
117. Liou, G.-Y. and P. Storz, *Reactive oxygen species in cancer.* Free radical research, 2010. **44**(5): p. 479-496.
118. Seidlitz, E.P., et al., *Cancer cell lines release glutamate into the extracellular environment.* Clin Exp Metastasis, 2009. **26**(7): p. 781-7.
119. Wasinger, C., et al., *Amino Acid Signature in Human Melanoma Cell Lines from Different Disease Stages.* Scientific Reports, 2018. **8**(1): p. 6245.
120. DeBerardinis, R.J. and T. Cheng, *Q's next: the diverse functions of glutamine in metabolism, cell biology and cancer.* Oncogene, 2009. **29**(3): p. 313-324.
121. Rzeski, W., C. Ikonomidou, and L. Turski, *Glutamate antagonists limit tumor growth.* Biochem Pharmacol, 2002. **64**(8): p. 1195-200.
122. Baenke, F., et al., *Resistance to BRAF inhibitors induces glutamine dependency in melanoma cells.* Molecular Oncology, 2016. **10**(1): p. 73-84.
123. Hernandez-Davies, J.E., et al., *Vemurafenib resistance reprograms melanoma cells towards glutamine dependence.* Journal of Translational Medicine, 2015. **13**(1): p. 210.
124. Ratnikov, B., et al., *Right on TARGET: glutamine metabolism in cancer.* Oncoscience, 2015. **2**(8): p. 681-3.
125. Teh, J. and S. Chen, *mGlu Receptors and Cancerous Growth.* Wiley Interdiscip Rev Membr Transp Signal, 2012. **1**(2): p. 211-220.
126. Wall, B.A., et al., *Riluzole is a radio-sensitizing agent in an in vivo model of brain metastasis derived from GRM1 expressing human melanoma cells.* Pigment Cell Melanoma Res, 2015. **28**(1): p. 105-9.
127. van Geldermalsen, M., et al., *ASCT2/SLC1A5 controls glutamine uptake and tumour growth in triple-negative basal-like breast cancer.* Oncogene, 2016. **35**(24): p. 3201-8.
128. Jin, L., G.N. Alesi, and S. Kang, *Glutaminolysis as a target for cancer therapy.* Oncogene, 2016. **35**(28): p. 3619-25.
129. Yang, L., S. Venneti, and D. Nagrath, *Glutaminolysis: A Hallmark of Cancer Metabolism.* Annu Rev Biomed Eng, 2017. **19**: p. 163-194.
130. Marie, S.K.N. and S.M.O. Shinjo, *Metabolism and Brain Cancer.* Clinics, 2011. **66**(Suppl 1): p. 33-43.
131. DeBerardinis, R.J., et al., *Beyond aerobic glycolysis: transformed cells can engage in glutamine metabolism that exceeds the requirement for protein and nucleotide synthesis.* Proc Natl Acad Sci U S A, 2007. **104**(49): p. 19345-50.
132. Katt, W.P. and R.A. Cerione, *Glutaminase regulation in cancer cells: a druggable chain of events.* Drug Discov Today, 2014. **19**(4): p. 450-7.
133. Christa, L., et al., *Overexpression of glutamine synthetase in human primary liver cancer.* Gastroenterology. **106**(5): p. 1312-1320.
134. Osada, T., et al., *Acquisition of glutamine synthetase expression in human hepatocarcinogenesis.* Cancer, 1999. **85**(4): p. 819-831.

135. Sappington, D.R., et al., *Glutamine drives glutathione synthesis and contributes to radiation sensitivity of A549 and H460 lung cancer cell lines.* Biochimica et biophysica acta, 2016. **1860**(4): p. 836-843.
136. Katt, W.P., M.J. Lukey, and R.A. Cerione, *A tale of two glutaminases: homologous enzymes with distinct roles in tumorigenesis.* Future Medicinal Chemistry, 2017. **9**(2): p. 223-243.
137. Wang, J.B., et al., *Targeting mitochondrial glutaminase activity inhibits oncogenic transformation.* Cancer Cell, 2010. **18**(3): p. 207-19.
138. van den Heuvel, A.P., et al., *Analysis of glutamine dependency in non-small cell lung cancer: GLS1 splice variant GAC is essential for cancer cell growth.* Cancer Biol Ther, 2012. **13**(12): p. 1185-94.
139. Seltzer, M.J., et al., *Inhibition of glutaminase preferentially slows growth of glioma cells with mutant IDH1*. Cancer Res, 2010. **70**(22): p. 8981-7.
140. Zhang, J., et al., *Inhibition of GLS suppresses proliferation and promotes apoptosis in prostate cancer.* Bioscience reports, 2019. **39**(6): p. BSR20181826.
141. Xiang, Y., et al., *Targeted inhibition of tumor-specific glutaminase diminishes cell-autonomous tumorigenesis.* J Clin Invest, 2015. **125**(6): p. 2293-306.
142. Masamha, C.P. and P. LaFontaine, *Molecular targeting of glutaminase sensitizes ovarian cancer cells to chemotherapy.* Journal of Cellular Biochemistry. **0**(0).
143. Momcilovic, M., et al., *Targeted inhibition of EGFR and glutaminase induces metabolic crisis in EGFR mutant lung cancer.* Cell reports, 2017. **18**(3): p. 601-610.
144. Xie, C., et al., *Inhibition of mitochondrial glutaminase activity reverses acquired erlotinib resistance in non-small cell lung cancer.* Oncotarget, 2016. **7**(1): p. 610-621.
145. Gao, P., et al., *c-Myc suppression of miR-23a/b enhances mitochondrial glutaminase expression and glutamine metabolism.* Nature, 2009. **458**: p. 762-766.
146. Briggs, K.J., et al., *Paracrine Induction of HIF by Glutamate in Breast Cancer: EglN1 Senses Cysteine.* Cell, 2016. **166**(1): p. 126-39.
147. Dancey, J., *mTOR signaling and drug development in cancer.* Nat Rev Clin Oncol, 2010. **7**(4): p. 209-19.
148. Sommer, L., *Generation of melanocytes from neural crest cells.* Pigment Cell & Melanoma Research, 2011. **24**(3): p. 411-421.
149. Prickett, T.D. and Y. Samuels, *Molecular pathways: dysregulated glutamatergic signaling pathways in cancer.* Clin Cancer Res, 2012. **18**(16): p. 4240-6.
150. Lyons, S.A., et al., *Autocrine glutamate signaling promotes glioma cell invasion.* Cancer Res, 2007. **67**(19): p. 9463-71.
151. Pei, Z., et al., *Pathway analysis of glutamate-mediated, calcium-related signaling in glioma progression.* Biochemical Pharmacology, 2020: p. 113814.
152. Sontheimer, H., *A role for glutamate in growth and invasion of primary brain tumors.* J Neurochem, 2008. **105**(2): p. 287-95.
153. Ye, Z.C., J.D. Rothstein, and H. Sontheimer, *Compromised glutamate transport in human glioma cells: reduction-mislocalization of sodium-dependent glutamate transporters and enhanced activity of cystine-glutamate exchange.* J Neurosci, 1999. **19**(24): p. 10767-77.

154. Takano, T., et al., *Glutamate release promotes growth of malignant gliomas.* Nat Med, 2001. **7**(9): p. 1010-5.
155. Xie, T.X., et al., *Activation of stat3 in human melanoma promotes brain metastasis.* Cancer Res, 2006. **66**(6): p. 3188-96.
156. Group, F.-N.B.W., *Understanding Prognostic versus Predictive Biomarkers*, F.a.D. Adminstration, Editor. 2016, National Institutes of Health Silver Spring (MD).
157. Perng, P., C. Marcus, and R.M. Subramaniam, *18F-FDG PET/CT and Melanoma: Staging, Immune Modulation and Mutation-Targeted Therapy Assessment, and Prognosis.* American Journal of Roentgenology, 2015. **205**(2): p. 259-270.
158. Zhu, L., et al., *Metabolic Imaging of Glutamine in Cancer.* Journal of nuclear medicine : official publication, Society of Nuclear Medicine, 2017. **58**(4): p. 533-537.
159. Huang, J., C. Plass, and C. Gerhauser, *Cancer chemoprevention by targeting the epigenome.* Curr Drug Targets, 2011. **12**(13): p. 1925-56.
160. Proenza, A.M., et al., *Breast and lung cancer are associated with a decrease in blood cell amino acid content.* J Nutr Biochem, 2003. **14**(3): p. 133-8.
161. Koochekpour, S., et al., *Serum glutamate levels correlate with Gleason score and glutamate blockade decreases proliferation, migration, and invasion and induces apoptosis in prostate cancer cells.* Clin Cancer Res, 2012. **18**(21): p. 5888-901.
162. Droge, W., et al., *Elevated plasma glutamate levels in colorectal carcinoma patients and in patients with acquired immunodeficiency syndrome (AIDS).* Immunobiology, 1987. **174**(4-5): p. 473-9.
163. Vanhove, K., et al., *The plasma glutamate concentration as a complementary tool to differentiate benign PET-positive lung lesions from lung cancer.* BMC Cancer, 2018. **18**(1): p. 868.
164. Rodríguez-Tomàs, E., et al., *Alterations in plasma concentrations of energy-balance-related metabolites in patients with lung, or head & neck, cancers: Effects of radiotherapy.* Journal of Proteomics, 2020. **213**: p. 103605.
165. Saha, S.K., et al., *Multiomics Analysis Reveals that GLS and GLS2 Differentially Modulate the Clinical Outcomes of Cancer.* Journal of clinical medicine, 2019. **8**(3): p. 355.
166. Cheng, L., et al., *Molecular testing for BRAF mutations to inform melanoma treatment decisions: a move toward precision medicine.* Mod Pathol, 2018. **31**(1): p. 24-38.
167. Bolzoni, M., et al., *Dependence on glutamine uptake and glutamine addiction characterize myeloma cells: a new attractive target.* Blood, 2016. **128**(5): p. 667.
168. Xiang, L., et al., *Glutaminase 1 expression in colorectal cancer cells is induced by hypoxia and required for tumor growth, invasion, and metastatic colonization.* Cell Death Dis, 2019. **10**(2): p. 40.
169. Lampa, M., et al., *Glutaminase is essential for the growth of triple-negative breast cancer cells with a deregulated glutamine metabolism pathway and its suppression synergizes with mTOR inhibition.* PLOS ONE, 2017. **12**(9): p. e0185092.
170. Choi, Y.-K. and K.-G. Park, *Targeting Glutamine Metabolism for Cancer Treatment.* Biomolecules & therapeutics, 2018. **26**(1): p. 19-28.

171. Robinson, Mary M., et al., *Novel mechanism of inhibition of rat kidney-type glutaminase by bis-2-(5-phenylacetamido-1,2,4-thiadiazol-2-yl)ethyl sulfide (BPTES).* Biochemical Journal, 2007. **406**(3): p. 407-414.
172. Gross, M.I., et al., *Antitumor Activity of the Glutaminase Inhibitor CB-839 in Triple-Negative Breast Cancer.* 2014. **13**(4): p. 890-901.
173. Abu Aboud, O., et al., *Glutamine Addiction in Kidney Cancer Suppresses Oxidative Stress and Can Be Exploited for Real-Time Imaging.* 2017. **77**(23): p. 6746-6758.
174. Bromley-Dulfano, S., et al., *Antitumor Activity Of The Glutaminase Inhibitor CB-839 In Hematological Malignances.* 2013. **122**(21): p. 4226-4226.
175. Ramachandran, S., et al., *Structural basis for exploring the allosteric inhibition of human kidney type glutaminase.* Oncotarget, 2016. **7**(36): p. 57943-57954.
176. Song, M., et al., *Recent Development of Small Molecule Glutaminase Inhibitors.* Curr Top Med Chem, 2018. **18**(6): p. 432-443.
177. Lukey, M.J., et al., *Liver-Type Glutaminase GLS2 Is a Druggable Metabolic Node in Luminal-Subtype Breast Cancer.* Cell Rep, 2019. **29**(1): p. 76-88.e7.
178. Leone, R.D., et al., *Glutamine blockade induces divergent metabolic programs to overcome tumor immune evasion.* Science, 2019: p. eaav2588.
179. Gross, M., et al., *Abstract 2329: Glutaminase inhibition with CB-839 enhances anti-tumor activity of PD-1 and PD-L1 antibodies by overcoming a metabolic checkpoint blocking T cell activation.* Cancer Research, 2016. **76**: p. 2329-2329.
180. Shin, C.S., et al., *The glutamate/cystine xCT antiporter antagonizes glutamine metabolism and reduces nutrient flexibility.* Nat Commun, 2017. **8**: p. 15074.
181. Mackinnon, A., et al., *Biomarkers of Response to the Glutaminase Inhibitor CB-839 in Multiple Myeloma Cells.* 2014. **124**(21): p. 3429-3429.
182. Krall, A.S., et al., *Asparagine promotes cancer cell proliferation through use as an amino acid exchange factor.* Nature Communications, 2016. **7**: p. 11457.
183. MacKinnon, A.L., et al., *Metabolomic, Proteomic and Genomic Profiling Identifies Biomarakers of Sensitivity to Glutaminase Inhibitor CB-839 in Multiple Myeloma.* Blood, 2015. **126**(23): p. 1802-1802.
184. Davidson, S.M., et al., *Environment Impacts the Metabolic Dependencies of Ras-Driven Non-Small Cell Lung Cancer.* Cell Metab, 2016. **23**(3): p. 517-28.
185. Sullivan, M.R., et al., *Quantification of microenvironmental metabolites in murine cancers reveals determinants of tumor nutrient availability.* Elife, 2019. **8**.
186. Liu, P., et al., *A functional mammalian target of rapamycin complex 1 signaling is indispensable for c-Myc-driven hepatocarcinogenesis.* Hepatology, 2017. **66**(1): p. 167-181.
187. Sarbassov, D.D., et al., *Prolonged rapamycin treatment inhibits mTORC2 assembly and Akt/PKB.* Mol Cell, 2006. **22**(2): p. 159-68.
188. Arriola Apelo, S.I., et al., *Alternative rapamycin treatment regimens mitigate the impact of rapamycin on glucose homeostasis and the immune system.* Aging cell, 2016. **15**(1): p. 28-38.
189. Busca, R., et al., *Inhibition of the phosphatidylinositol 3-kinase/p70(S6)-kinase pathway induces B16 melanoma cell differentiation.* J Biol Chem, 1996. **271**(50): p. 31824-30.

190. Csibi, A., et al., *The mTORC1/S6K1 pathway regulates glutamine metabolism through the eIF4B-dependent control of c-Myc translation.* Curr Biol, 2014. **24**(19): p. 2274-80.
191. Rathore, M.G., et al., *The NF-kappaB member p65 controls glutamine metabolism through miR-23a.* Int J Biochem Cell Biol, 2012. **44**(9): p. 1448-56.
192. Zhao, L., et al., *Interferon-alpha regulates glutaminase 1 promoter through STAT1 phosphorylation: relevance to HIV-1 associated neurocognitive disorders.* PLoS One, 2012. **7**(3): p. e32995.
193. Lukey, M.J., et al., *The oncogenic transcription factor c-Jun regulates glutaminase expression and sensitizes cells to glutaminase-targeted therapy.* Nat Commun, 2016. **7**: p. 11321.
194. Verma, M., *Personalized medicine and cancer.* Journal of personalized medicine, 2012. **2**(1): p. 1-14.
195. Haas, H., et al., *The non-competitive metabotropic glutamate receptor-1 antagonist CPCCOEt inhibits the in vitro growth of human melanoma.* Oncol Rep, 2007. **17**: p. 1399-1404.
196. Haq, R., D.E. Fisher, and H.R. Widlund, *Molecular pathways: BRAF induces bioenergetic adaptation by attenuating oxidative phosphorylation.* Clin Cancer Res, 2014. **20**(9): p. 2257-63.
197. Hall, A., et al., *Dysfunctional oxidative phosphorylation makes malignant melanoma cells addicted to glycolysis driven by the (V600E)BRAF oncogene.* Oncotarget, 2013. **4**(4): p. 584-99.
198. Wangari-Talbot, J., et al., *Functional effects of GRM1 suppression in human melanoma cells.* Mol Cancer Res, 2012. **10**(11): p. 1440-50.
199. Wen, Y., et al., *Activation of the glutamate receptor GRM1 enhances angiogenic signaling to drive melanoma progression.* Cancer Res, 2014. **74**(9): p. 2499-509.
200. Hsu, M.Y., et al., *E-cadherin expression in melanoma cells restores keratinocyte-mediated growth control and down-regulates expression of invasion-related adhesion receptors.* Am J Pathol, 2000. **156**(5): p. 1515-25.
201. Chen, S., et al., *Spontaneous melanocytosis in transgenic mice.* J. Invest. Dermatol., 1996. **106**: p. 1145-1150.
202. Zhu, H., et al., *Development of heritable melanoma in transgenic mice.* J. Invest. Dermatol., 1998. **110**: p. 247-252.
203. Tang, Z., et al., *GEPIA: a web server for cancer and normal gene expression profiling and interactive analyses.* Nucleic Acids Res, 2017. **45**(W1): p. W98-w102.
204. Isola, A.L., et al., *Exosomes released by metabotropic glutamate receptor 1 (GRM1) expressing melanoma cells increase cell migration and invasiveness.* Oncotarget, 2018. **9**(1): p. 1187-1199.
205. Lee, H.J., et al., *Glutamatergic pathway targeting in melanoma; single agent and combinatorial therapies.* Clin Cancer Res, 2011. **17**: p. 7080-7092.
206. Spagnolo, F., et al., *BRAF-mutant melanoma: treatment approaches, resistance mechanisms, and diagnostic strategies.* OncoTargets and therapy, 2015. **8**: p. 157-168.

207. Shah, R., et al., *Concurrent Targeting of Glutaminolysis and Metabotropic Glutamate Receptor 1 (GRM1) Reduces Glutamate Bioavailability in GRM1+ Melanoma.* Cancer Research, 2019. **79**(8): p. 1799-1809.
208. Lora, J., et al., *Antisense glutaminase inhibition decreases glutathione antioxidant capacity and increases apoptosis in Ehrlich ascitic tumour cells.* European Journal of Biochemistry, 2004. **271**(21): p. 4298-4306.
209. Cairns, R.A., I.S. Harris, and T.W. Mak, *Regulation of cancer cell metabolism.* Nat Rev Cancer, 2011. **11**(2): p. 85-95.
210. Khan, A., et al., *Riluzole enhances ionizing radiation–induced cytotoxicity in human melanoma cells that ectopically express metabotropic glutamate receptor 1 in vitro and in vivo.* Clin Can Res, 2011. **17**: p. 1807-14.
211. Benavides-Serrato, A., et al., *Repurposing Potential of Riluzole as an ITAF Inhibitor in mTOR Therapy Resistant Glioblastoma.* International Journal of Molecular Sciences, 2020. **21**(1): p. 344.
212. Speyer, C.L., et al., *Riluzole synergizes with paclitaxel to inhibit cell growth and induce apoptosis in triple-negative breast cancer.* Breast Cancer Research and Treatment, 2017. **166**(2): p. 407-419.
213. Shin, S.S., et al., *AKT2 is a downstream target of metabotropic glutamate receptor 1 (mGluR1)* Pigment Cell Melanoma Res, 2010. **23**: p. 103-111.
214. Wise, D.R., et al., *Myc regulates a transcriptional program that stimulates mitochondrial glutaminolysis and leads to glutamine addiction.* Proc Natl Acad Sci U S A, 2008. **105**(48): p. 18782-7.
215. Filipp, F.V., et al., *Frontiers in pigment cell and melanoma research.* Pigment Cell Melanoma Res, 2018. **31**(6): p. 728-735.
216. Filipp, F.V., *Precision medicine driven by cancer systems biology.* Cancer Metastasis Reviews, 2017. **36**(1): p. 91-108.
217. Scott, D.A., et al., *Comparative Metabolic Flux Profiling of Melanoma Cell Lines: BEYOND THE WARBURG EFFECT.* The Journal of Biological Chemistry, 2011. **286**(49): p. 42626-42634.
218. Schallier, A., et al., *Region- and age-specific changes in glutamate transport in the AbetaPP23 mouse model for Alzheimer's disease.* J Alzheimers Dis, 2011. **24**(2): p. 287-300.
219. Kuzu, O.F., et al., *Current State of Animal (Mouse) Modeling in Melanoma Research.* Cancer Growth Metastasis, 2015. **8**(Suppl 1): p. 81-94.
220. Grinde, M.T., et al., *Glutamine to proline conversion is associated with response to glutaminase inhibition in breast cancer.* Breast Cancer Res, 2019. **21**(1): p. 61.
221. Marani, M., et al., *Role of Bim in the survival pathway induced by Raf in epithelial cells.* Oncogene, 2004. **23**(14): p. 2431-41.
222. Rinn, J.L., et al., *Major molecular differences between mammalian sexes are involved in drug metabolism and renal function.* Dev Cell, 2004. **6**(6): p. 791-800.
223. Mayers, J.R. and M.G. Vander Heiden, *Famine versus feast: understanding the metabolism of tumors in vivo.* Trends in biochemical sciences, 2015. **40**(3): p. 130-140.
224. Howell, Jessica J., et al., *A growing role for mTOR in promoting anabolic metabolism.* Biochemical Society Transactions, 2013. **41**(4): p. 906-912.

225. Gao, P., et al., *c-Myc suppression of miR-23a/b enhances mitochondrial glutaminase expression and glutamine metabolism.* Nature, 2009. **458**(7239): p. 762-5.
226. Meric-Bernstam, F., et al., *CB-839, a glutaminase inhibitor, in combination with cabozantinib in patients with clear cell and papillary metastatic renal cell cancer (mRCC): Results of a phase I study.* Journal of Clinical Oncology, 2019. **37**(7_suppl): p. 549-549.
227. Kalinsky, K., et al., *Abstract PD3-13: Phase 1 study of CB-839, a first-in-class oral inhibitor of glutaminase, in combination with paclitaxel in patients with advanced triple negative breast cancer.* Cancer Research, 2018. **78**(4 Supplement): p. PD3-13-PD3-13.
228. Lacomblez, L., et al., *Long-term safety of riluzole in amyotrophic lateral sclerosis.* Amyotrophic Lateral Sclerosis & Other Motor Neuron Disorders, 2002. **3**(1): p. 23-9.
229. Shin, S.-S., et al., *Participation of xCT in melanoma cell proliferation in vitro and tumorigenesis in vivo.* Oncogenesis, 2018. **7**(11): p. 86-86.
230. Mizoule, J., et al., *2-Amino-6-trifluoromethoxy benzothiazole, a possible antagonist of excitatory amino acid neurotransmission--I. Anticonvulsant properties.* Neuropharmacology, 1985. **24**(8): p. 767-73.
231. Lin, C.L., et al., *Aberrant RNA processing in a neurodegenerative disease: the cause for absent EAAT2, a glutamate transporter, in amyotrophic lateral sclerosis.* Neuron, 1998. **20**(3): p. 589-602.
232. Jacob, C.P., et al., *Alterations in expression of glutamatergic transporters and receptors in sporadic Alzheimer's disease.* J Alzheimers Dis, 2007. **11**(1): p. 97-116.
233. de Groot, J.F., et al., *The excitatory amino acid transporter-2 induces apoptosis and decreases glioma growth in vitro and in vivo.* Cancer Res, 2005. **65**(5): p. 1934-40.
234. McMahon, M., et al., *Keap1-dependent proteasomal degradation of transcription factor Nrf2 contributes to the negative regulation of antioxidant response element-driven gene expression.* J Biol Chem, 2003. **278**(24): p. 21592-600.
235. Romero, R., et al., *Keap1 loss promotes Kras-driven lung cancer and results in dependence on glutaminolysis.* Nat Med, 2017. **23**(11): p. 1362-1368.
236. Sayin, V.I., et al., *Activation of the NRF2 antioxidant program generates an imbalance in central carbon metabolism in cancer.* Elife, 2017. **6**.
237. Wall, B.A., et al., *Disruption of GRM1-mediated signalling using riluzole results in DNA damage in melanoma cells.* Pigment Cell & Melanoma Research, 2014. **27**(2): p. 263-274.
238. Redis, R.S., et al., *Allele-Specific Reprogramming of Cancer Metabolism by the Long Non-coding RNA CCAT2.* Mol Cell, 2016. **61**(4): p. 520-534.
239. Edwards, D.N., et al., *The receptor tyrosine kinase EphA2 promotes glutamine metabolism in tumors by activating the transcriptional coactivators YAP and TAZ.* Science Signaling, 2017. **10**(508): p. eaan4667.
240. Li, J., et al., *Heat Shock Factor 1 Epigenetically Stimulates Glutaminase-1-Dependent mTOR Activation to Promote Colorectal Carcinogenesis.* Mol Ther, 2018. **26**(7): p. 1828-1839.

Figures

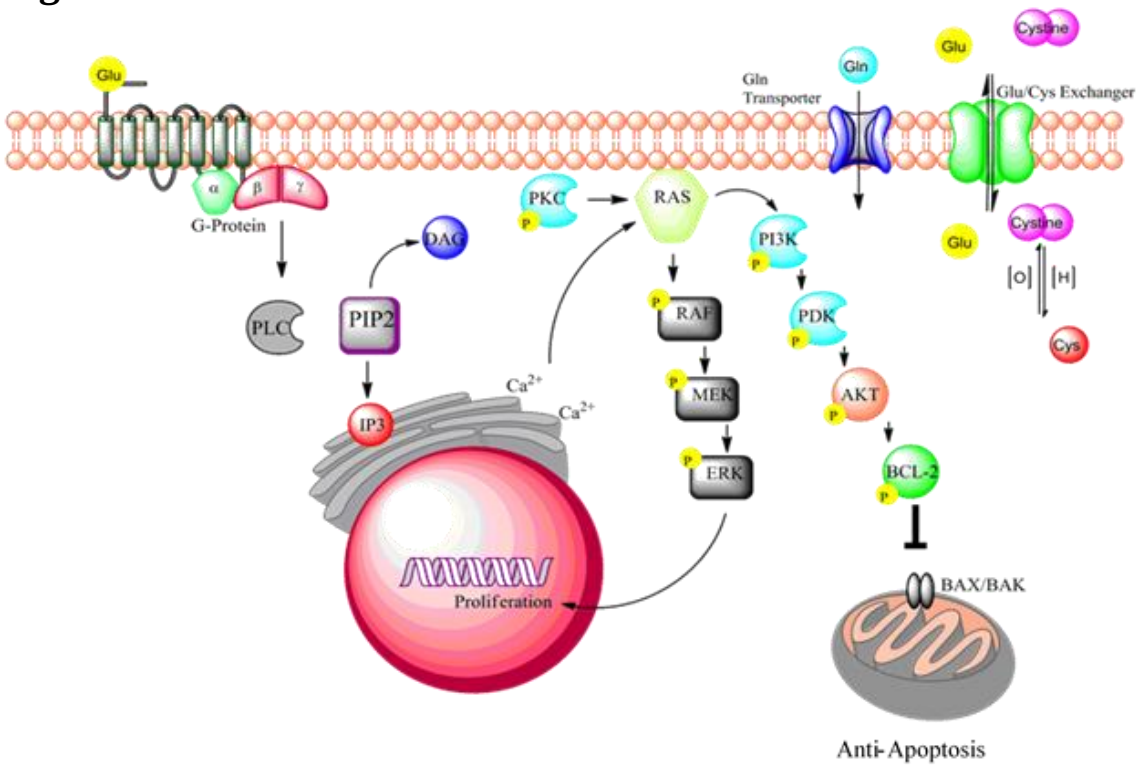

Figure 1: GRM1-mediated signal transduction pathways: Upon ligand binding, GRM1 activates two major signaling pathways implicated in several cancers, MAPK and PI3K/AKT (Adapted with permission from Wall *et al*, 2012).

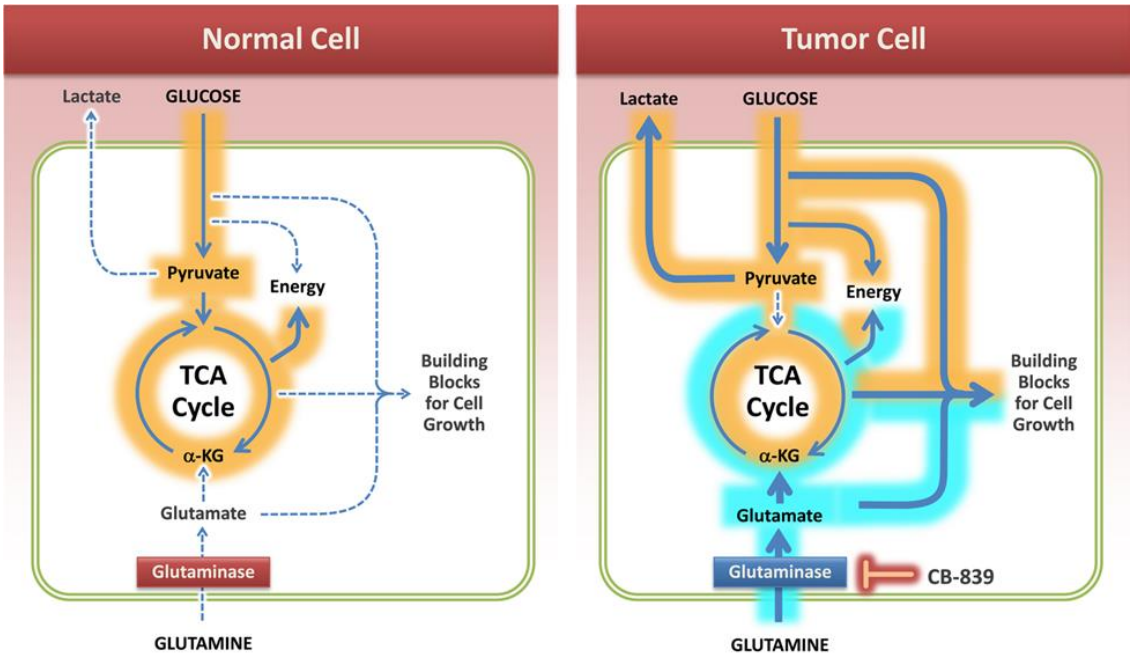

Figure 2: Tumor cells exhibit increased glutamine and glucose consumption: Cancer cells undergo a 'metabolic switch' that utilizes glutamine as well as glucose to meet the increased demand for intermediates needed for growth and energy production. CB-839 targets glutaminolysis mediated glutamate production as indicated (Adapted with permission from Parlati *et al*, 2015).

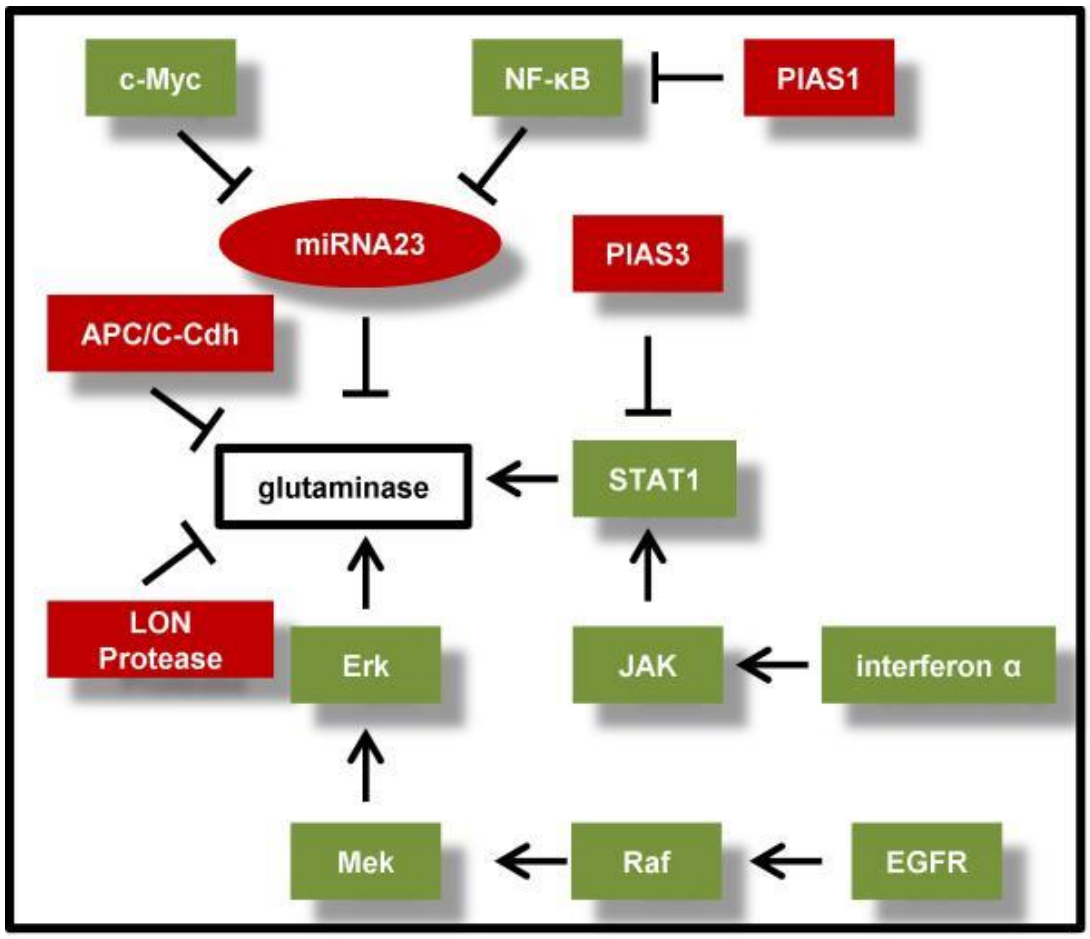

Figure 3: Pathways that regulate GLS in different cancer types: A summary of the proposed proteins/pathways responsible for regulation of GLS in cancer (Adapted with permission from Katt and Cerione *et al*, 2014).

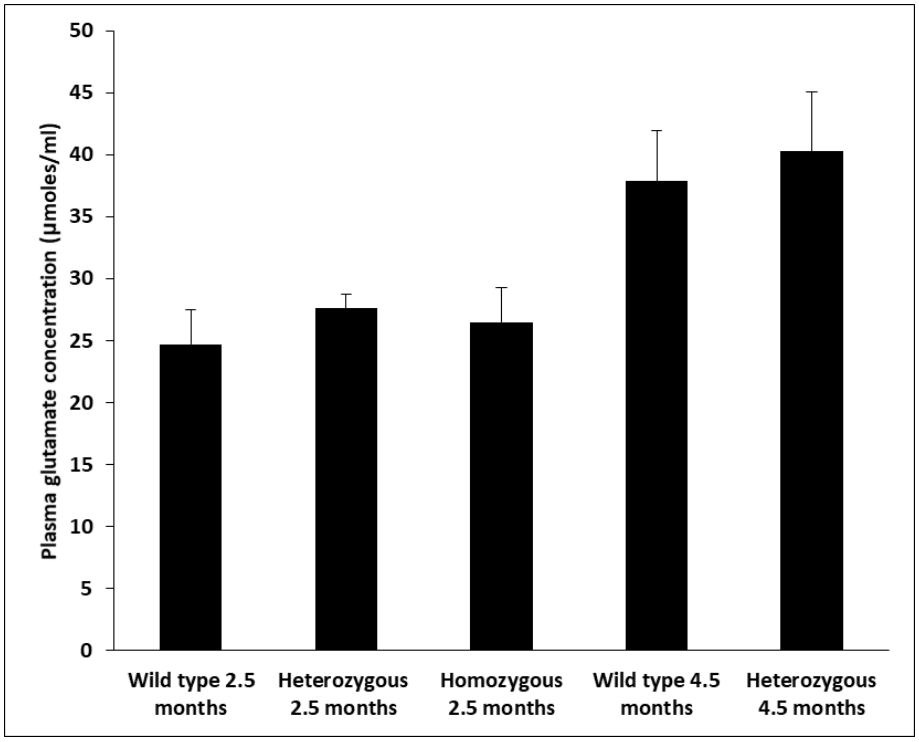

Figure 4: Unchanged plasma glutamate levels between young wild type and melanoma-prone TGS mice: We examined circulating plasma glutamate concentrations in 2.5-month old wild type, heterozygous and homozygous TGS mice and the differences were not statistically significant. We also analyzed glutamate levels in circulating blood plasma in 4.5-month old wild type and heterozygous TGS mice and no statistically significant changes were detected at both time points. Glutamate concentration in plasma isolated from 2.5 month and 4.5 month old TGS mice was measured using the Glutamate Determination Kit (GLN1, Sigma-Aldrich) according to the manufacturer's instructions. Data are given as µmoles of glutamate per mL of plasma and represented as mean ± STDEV (n=3).

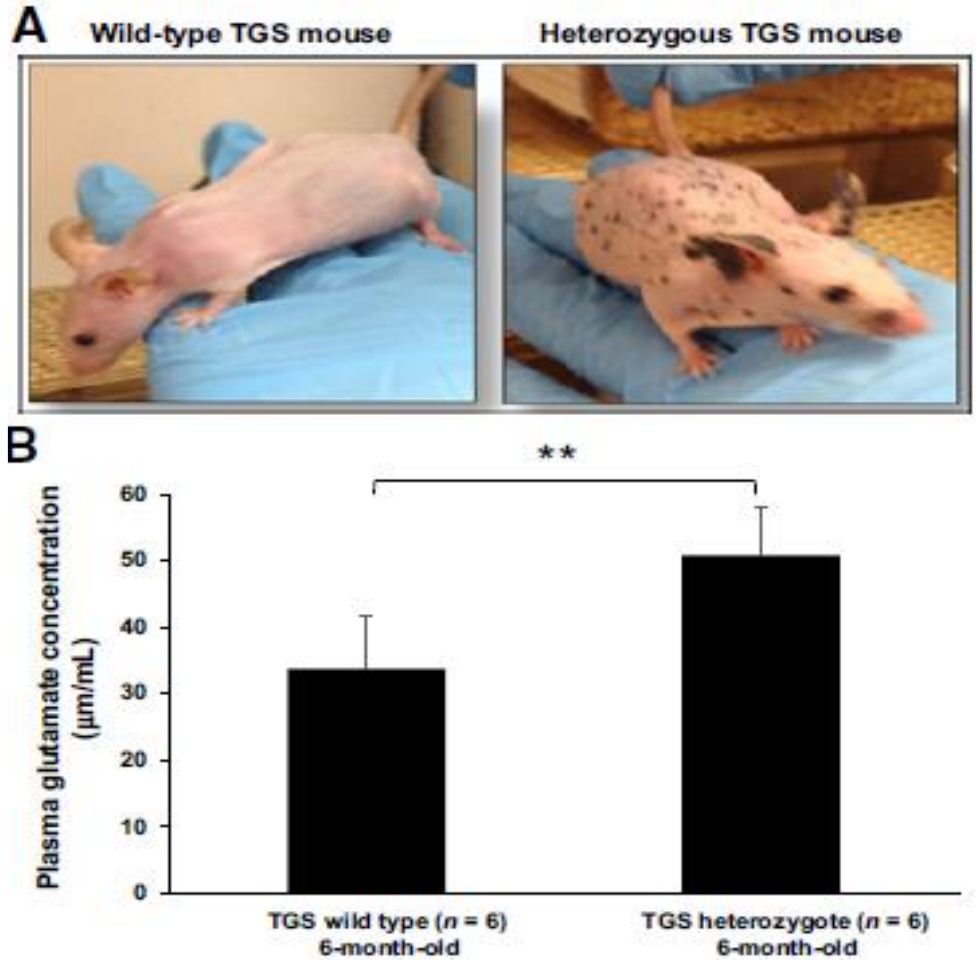

Figure 5: (A) Phenotypes of wild type and heterozygous TGS genotypes: Pigmented lesions on the skin of heterozygous TGS mice are easily visualized compared to the WT without any copies of the disrupted endogenous *Grm1* gene. Homozygous and heterozygous TGS mice are indistinguishable in the progression of the disease; the major difference is the onset of the disease, 2-3 months for homozygous TGS, and 5-7 months for heterozygous TGS. (**B) Elevated circulating glutamate levels in blood plasma isolated from heterozygous TGS mice:** Glutamate concentration in plasma isolated from wild type (6 month old) or heterozygous TGS mice (6 month old) was measured using the Glutamate Determination Kit (GLN1, Sigma-Aldrich) according to the manufacturer's instructions. Data are given as µmoles of glutamate per mL of plasma and represented as mean ± STDEV (n=6). Student's t-test was used to calculate statistical significance. ***p* value < 0.01.

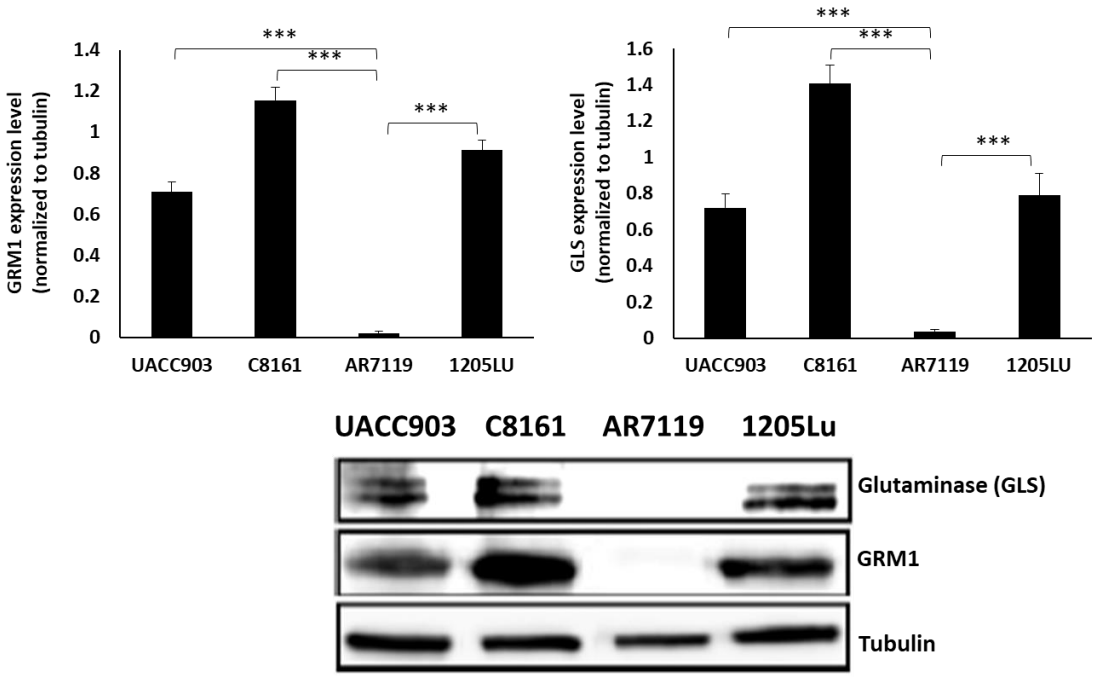

Figure 6: A link between GLS and GRM1 levels in human melanoma cells: Western immunoblots of GRM1 and glutaminase (GLS) on protein lysates from three different human melanoma cell lines (C8161, UACC903 and 1205LU) and one normal immortalized melanocyte cell line, hTERT/CDK^{R24C}/p53^{DD} (AR7119). Lysates were probed with the indicated antibodies. GLS expression correlated with GRM1 levels. Quantification of the intensity of GRM1 and GLS bands normalized to tubulin is displayed above the gel on a bar graph. Data are expressed as a mean ± STDEV of three independent experiments. Student's t-test was used to calculate statistical significance. ****p* value < 0.001.

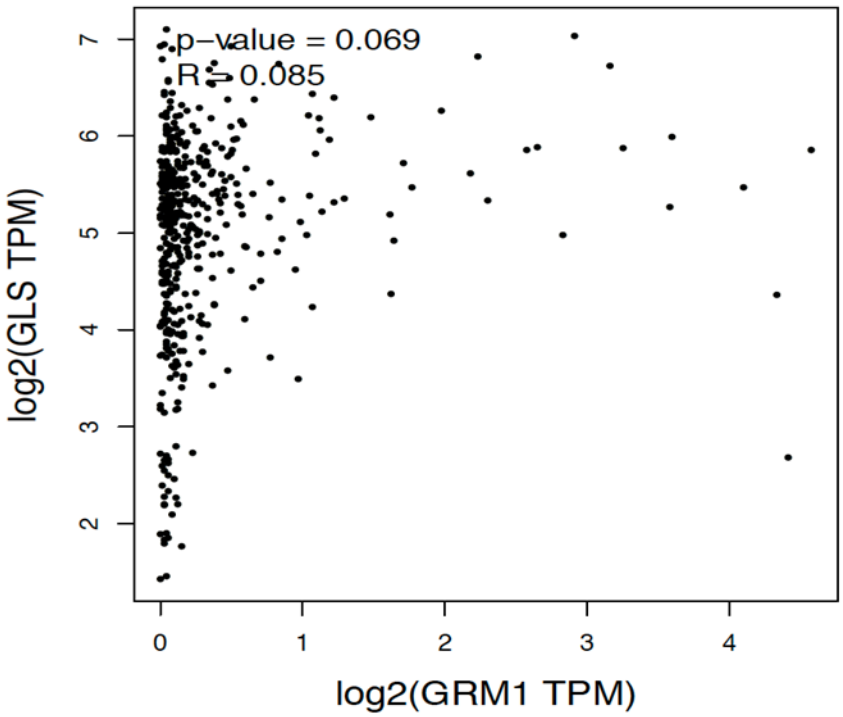

Figure 7: No correlation detected between GRM1 and GLS in patient tumors: 461 melanoma patient tumor samples were examined utilizing GEPIA, which uses RNA sequencing data from the TCGA database. Absence of any correlation between GRM1 and GLS was detected (Pearson's correlation coefficient = 0.085).

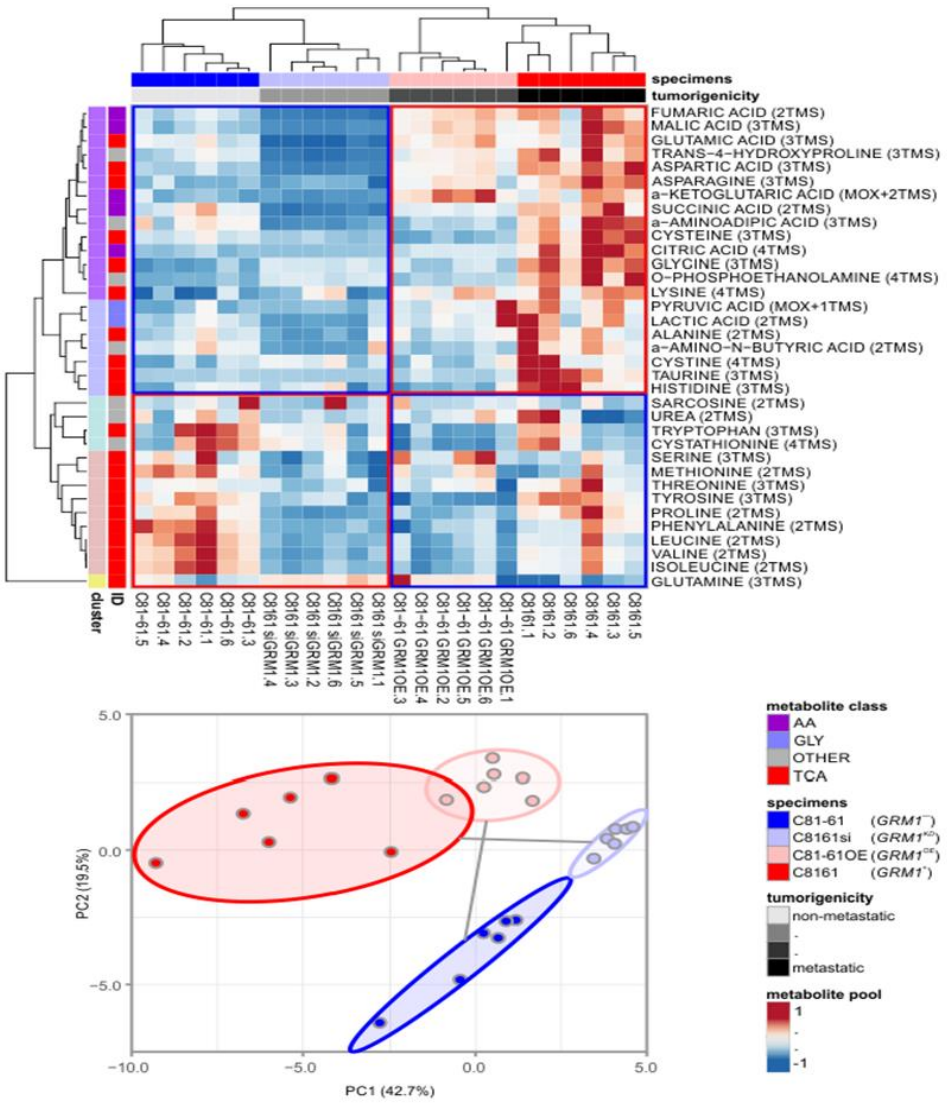

Figure 8: Metabolic profiling of the GRM1-driven melanoma model: A patient-derived early stage melanoma cell line C81-61 (*GRM1*$^{-}$) does not express endogenous GRM1 and is non-tumorigenic (blue). In contrast, after disease progression of the patient, a second specimen, tumorigenic C8161 (*GRM1*$^{+}$), was derived from the same patient (red). The panel of human cell lines, C81-61 (*GRM1*$^{-}$), C8161si (*GRM1*^{KD}), C81-61OE (*GRM1*^{OE}), and C8161 (*GRM1*$^{+}$) color-coded in blue, light blue, light red, and red respectively. Heat map representation of metabolomics profiling of isogenic human melanoma cell lines resembles tumorigenic properties of specimens. A cluster of tricarboxylic acid cycle (TCA) cycle-related organic and amino acids (AA) and glycolytic (GLY) metabolites show increased pool sizes in the cancer progression model. In the bottom panel, principle component analysis of melanoma specimens shows a directed shift upon genetic manipulation of the cancer metabolism driver GRM1. In this reduced dimensionality space of metabolomics measurements, tumorigenic (red and light red) and non-tumorigenic (blue and light blue) specimens cluster together.

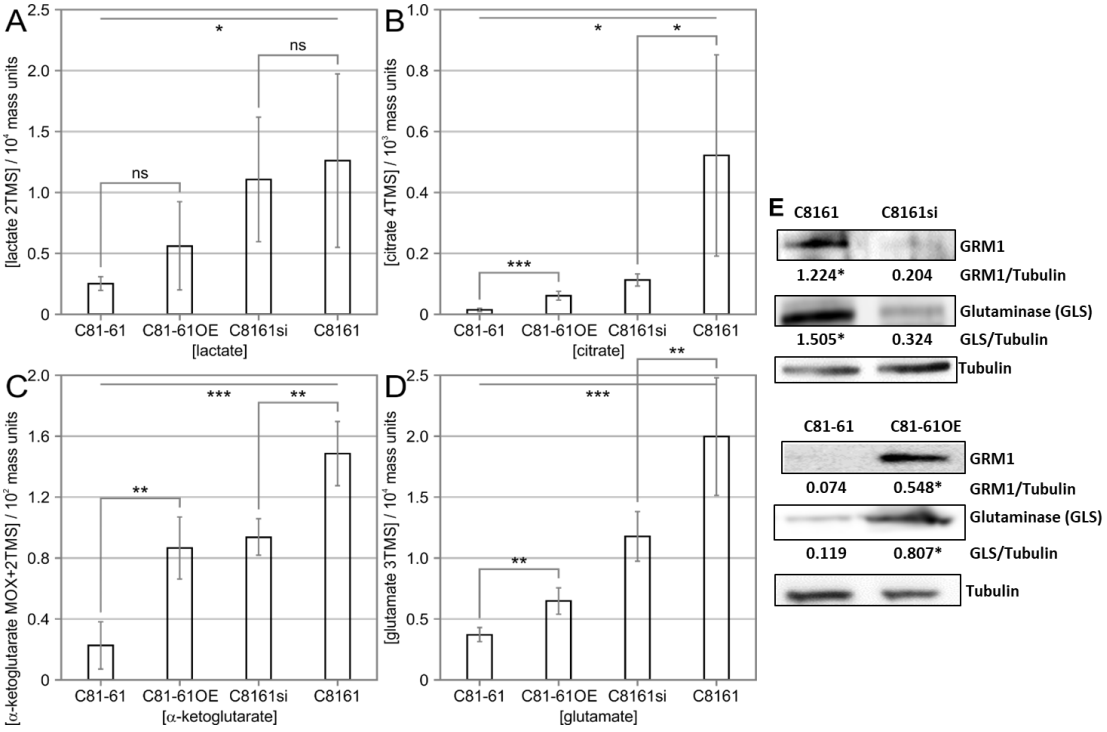

Figure 9: Modulation of GRM1 alters the intracellular production of glutaminolytic and glycolytic metabolites in human melanoma cells: The intracellular concentrations of lactate (A), citrate (B), α-ketoglutarate (C), and glutamate (D) were detected in C81-61, C81-61OE (C81-61 GRM1-6), C8161 and C8161si (C8161 TetR siGRM1 B22-20) cells by GCMS analysis. Data represent the average of six independent reads (mean ± STDEV). (E) Modulations in GRM1 and subsequent changes in glutaminase protein levels in C81-61, C81-61OE, C8161, and C8161si cells were determined by Western blot. Tubulin was used as the loading control. Numerical values indicating quantified intensity of GRM1 and GLS bands normalized to tubulin are displayed below the gel. Data are expressed as a mean ± STDEV of three independent experiments. Paired, homoscedastic Student's t-test was used to calculate statistical significance with *p* value threshold levels. **p* value < 0.05, ***p* value < 0.01, ****p* value < 0.001, and ns = no significance.

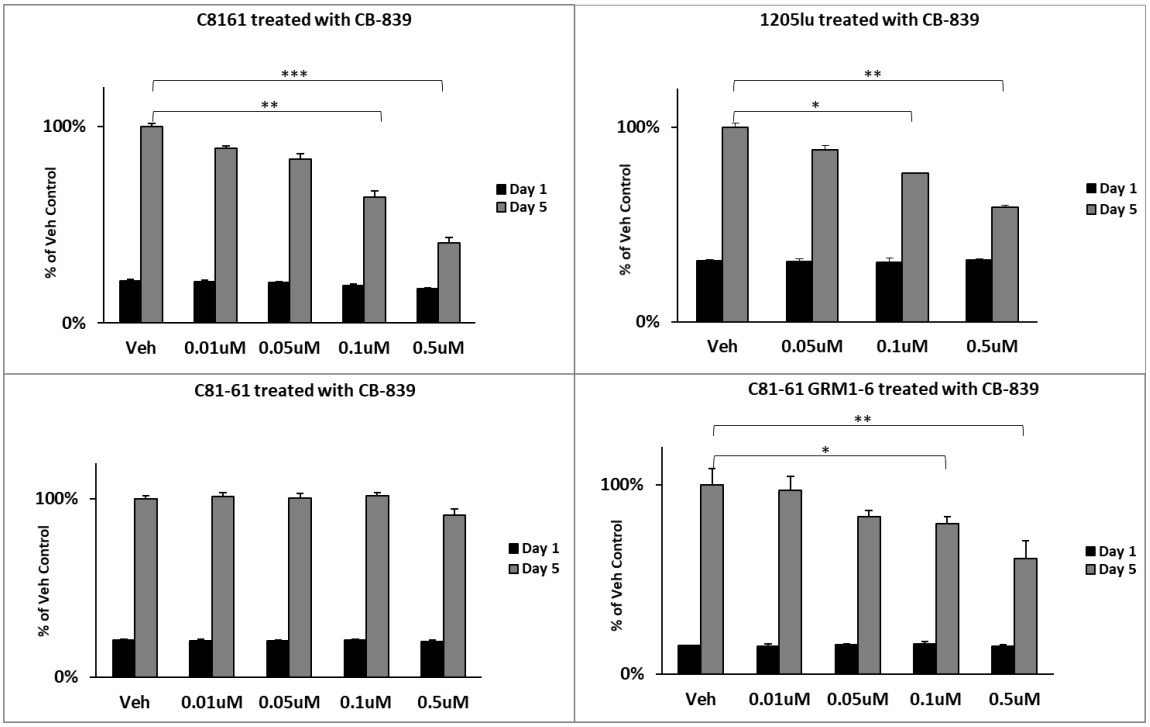

Figure 10: Inhibition of GLS reduces proliferation of GRM1-expressing melanoma cells: MTT cell viability/proliferation assays were performed on GRM1-positive C8161, 1205LU and C81-61OE (C81-61 GRM1-6) cell lines, and GRM1-negative C81-61 cells. Treatment conditions for all cells were vehicle (DMSO) or CB-839 at 0.01, 0.05, 0.1 and 0.5 μM. Each time point and concentration represents a mean ± STDEV of four independent measurements of the absorbance. A one-way ANOVA test with Bonferroni's post-hoc analysis was used to calculate statistical significance between experimental and control groups. **p* value < 0.05, ***p* value < 0.01, and ****p* value < 0.001.

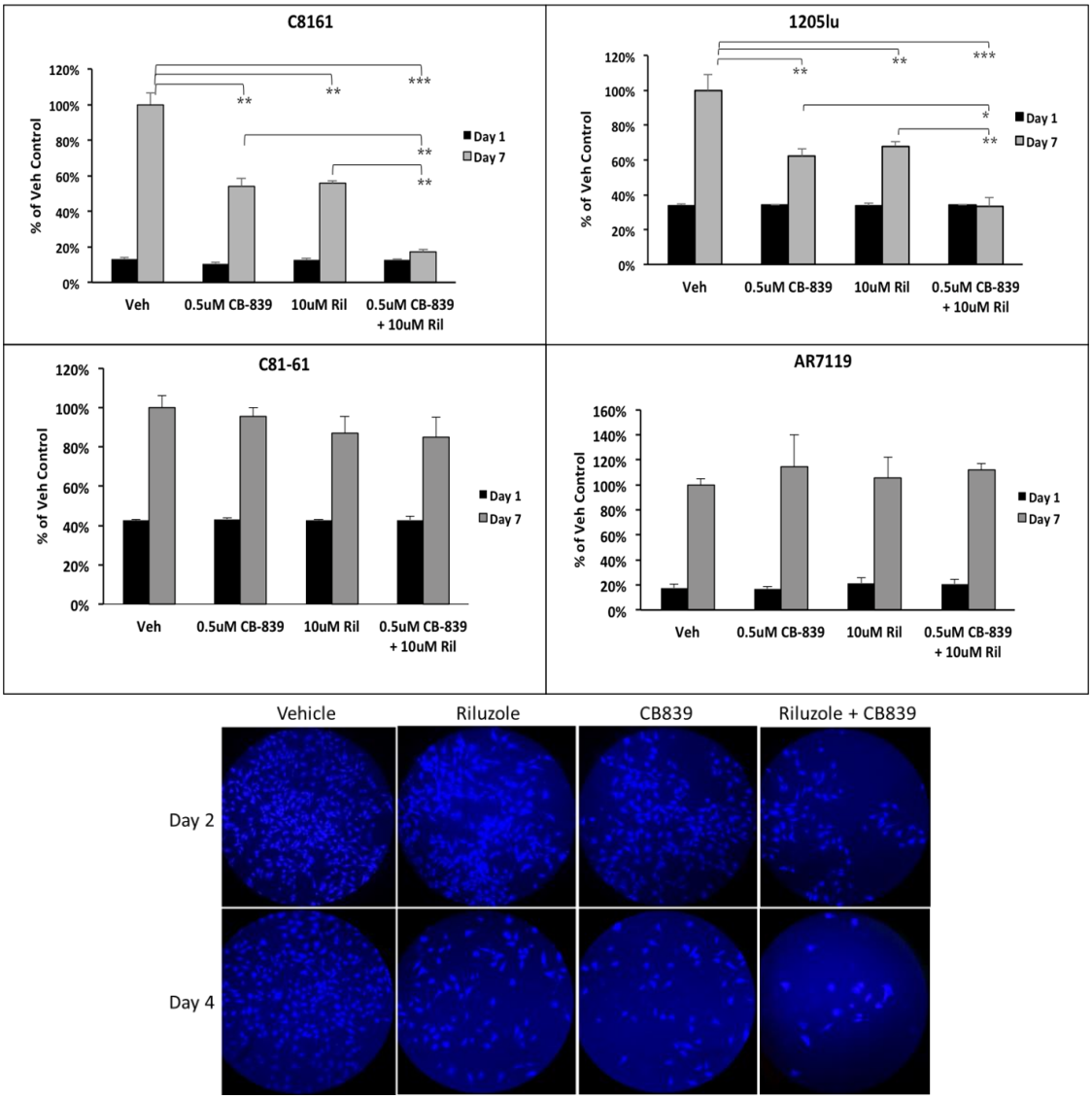

Figure 11: Enhanced suppression of proliferation of GRM1-expressing human melanoma cells with CB-839 and riluzole: Top panel displays MTT cell viability/proliferation assays that were performed on GRM1-expressing C8161 and 1205LU cells. GRM1-negative C81-61 and AR7119 cells were used as controls. Since AR7119 cells do not readily take up the tetrazolium MTT reagent, the trypan blue exclusion assay was performed on these cells as an alternative. The treatment conditions were vehicle (DMSO), CB-839 or/and riluzole at 0.5 μM and 10 μM respectively. Each time point and concentration represents a mean ± STDEV of four independent measurements of the absorbance. A two-way ANOVA test with Bonferroni's post-hoc analysis was used to calculate statistical significance between experimental and control groups. **p* value < 0.05, ***p* value < 0.01, and ****p* value < 0.001. The bottom panel shows a visual representation of viable 1205LU cells stained with CytoCalcein450 (blue color) from an independent experiment. Images were captured on days 2 and 4 post treatment on a Confocal florescence microscope.

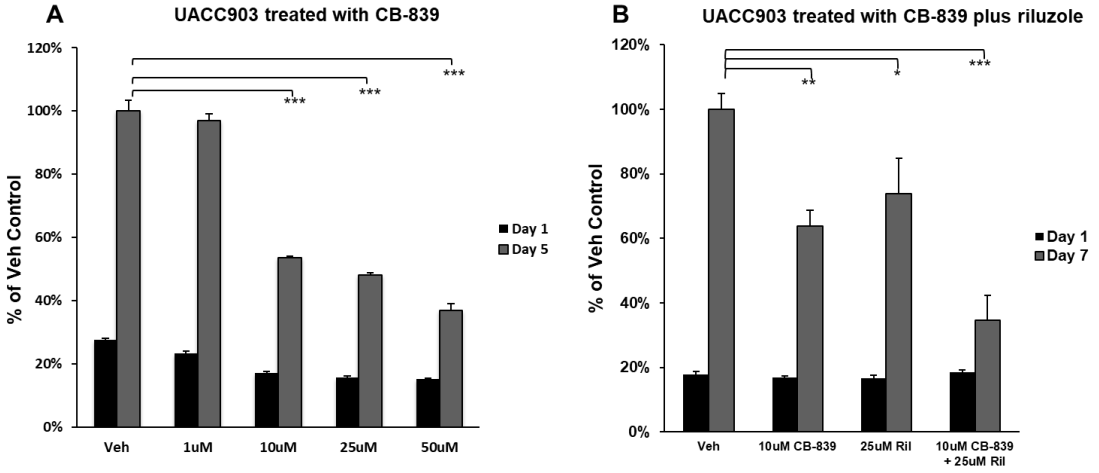

Figure 12: GRM1-expressing UACC903 cells respond to riluzole and CB-839 at higher doses: MTT cell viability/proliferation assays were performed on UACC903 cells. (A) The treatment conditions were vehicle (DMSO) or CB-839 at 1, 10, 25 and 50 μM. Absorbance was measured at Day 5. (B) The treatment conditions were vehicle (DMSO), CB-839 or/and riluzole at 10 μM and 25 μM respectively. Each time point and concentration represents a mean ± STDEV of four independent measurements of the absorbance. A two-way ANOVA test with Bonferroni's post-hoc analysis was used to calculate statistical significance between experimental and control groups. **p* value < 0.05, ***p* value < 0.01, ****p* value < 0.001, and ns = no significance.

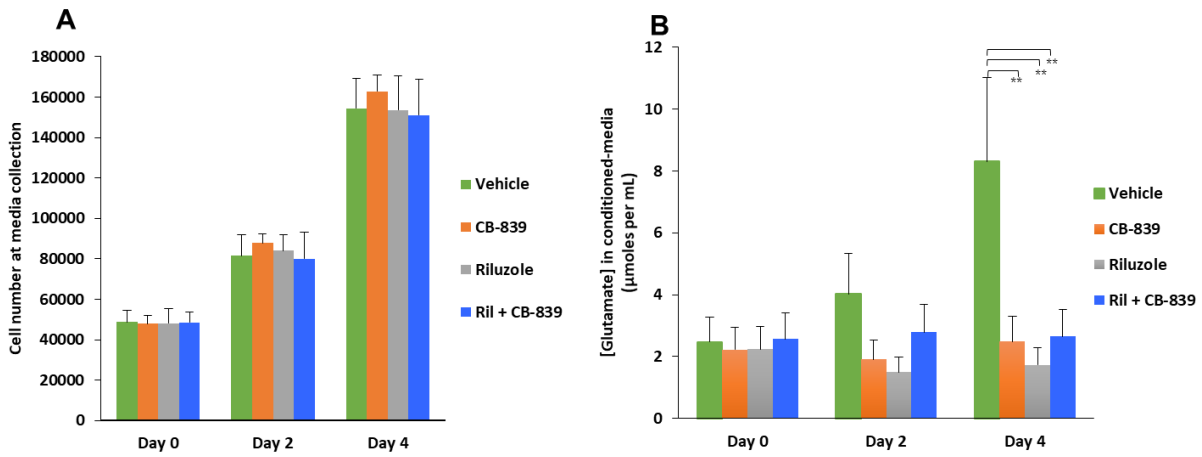

Figure 13: CB-839 treatment leads to inhibition of glutamate release in GRM1$^+$ human melanoma cells: Human melanoma C8161 cells were assessed for the amount of glutamate they release into the extracellular medium after treatment with CB-839, riluzole or CB-839 + riluzole. (A) Different number of cells was plated such that comparable numbers of cells were present at the time of sample (conditioned medium) collection. The bar graph represents the number of viable cells during sample collection at day 0, day 2 or day 4. (B) Concentrations of extracellular glutamate within each treatment group are shown. Statistical analysis was performed between control (vehicle) and treated pairs to show significance. Each bar represents mean ± STDEV, n=3. **p* value < 0.05, ***p* value < 0.01, ****p* value < 0.001, and ns = no significance.

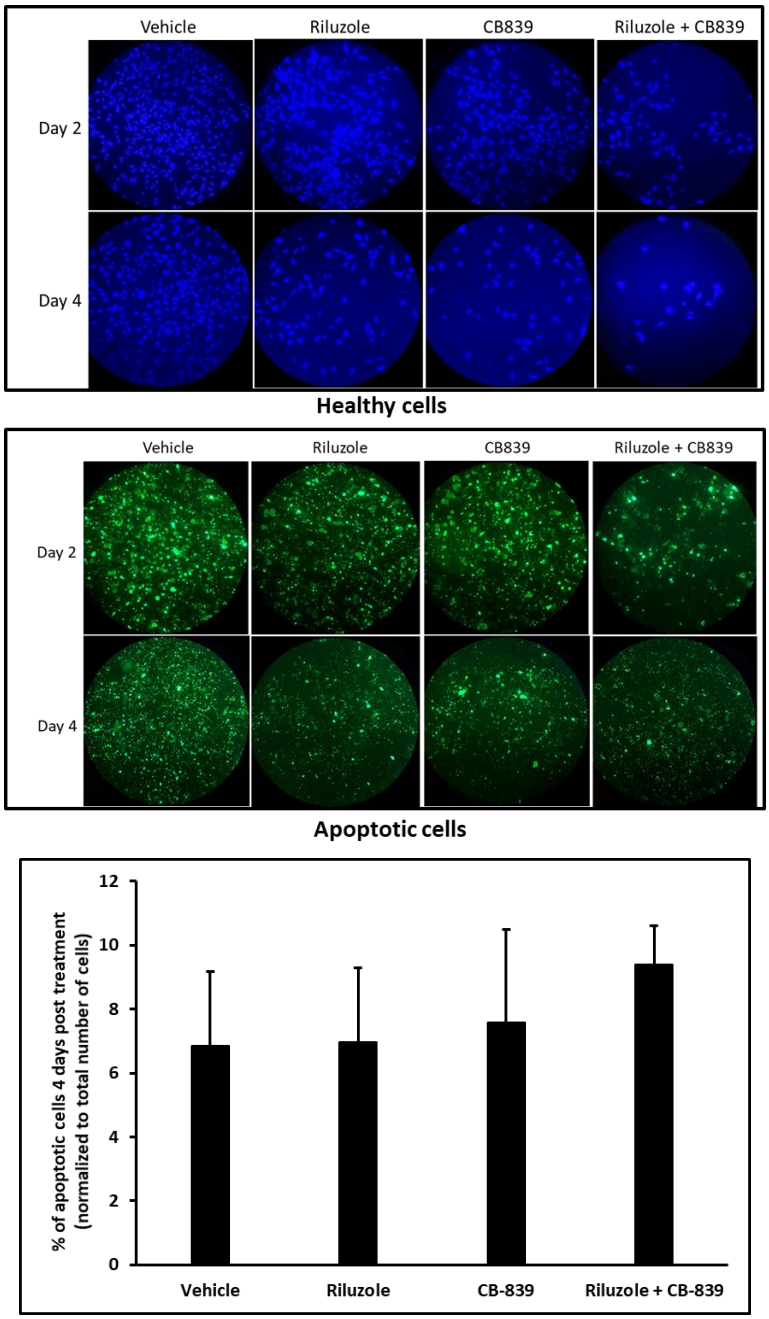

Figure 14: Treatment with CB-839 and riluzole slightly enhances apoptotic activity in GRM1^{+} melanoma cells: 1205LU cells were seeded in a 96-well black plate with a clear bottom. The treatment conditions were vehicle (DMSO), CB-839 or/and riluzole at 0.5 μM and 10 μM respectively. The experiment was conducted twice in triplicates for each time point and concentration (n=6). Blue fluorescence represents a visual representation of 1205LU cells stained with CytoCalcein450 (healthy cells) whereas green fluorescence indicates staining with Apopxin Green (apoptotic cells). Images were captured on days 2 and 4 post treatment on a Confocal florescence microscope. Quantification of apoptotic cells normalized to the total number of cells is shown in the bar graph.

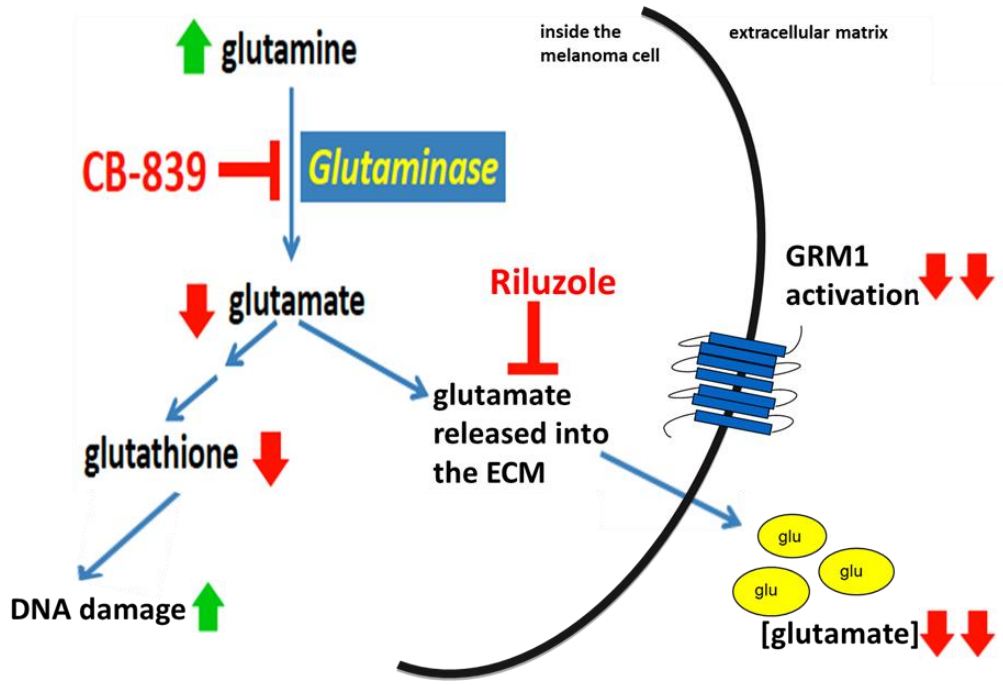

Figure 15: Proposed rationale/mechanism for utilizing a combination of riluzole and CB-839: Cancer cells undergo a 'metabolic switch' that utilizes glutamine in addition to glucose to meet the increased demand for biomass. With the goal of limiting tumor glutamate bioavailability, CB-839 targeted glutamate production and riluzole attacked glutamate release.

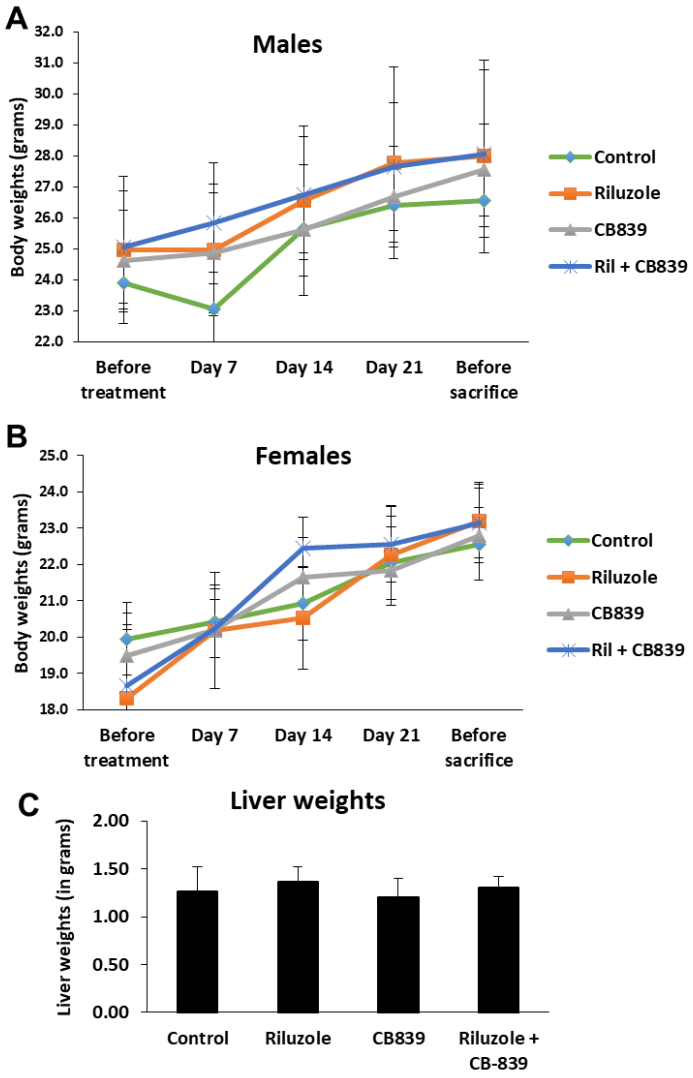

Figure 16: No apparent toxicity due to daily treatment with riluzole and CB-839: Two independent xenografts were established in male (n=20) and female (n=20) mice using either C8161 or 1205LU human melanoma cells. The treatment groups were vehicle control (DMSO + PBS), riluzole (10 mg/kg), CB-839 (200 mg/kg), or the combination of riluzole (10 mg/kg) and CB-839 (200 mg/kg). All agents were given daily by p.o. gavage. All tumor-bearing mice were euthanized after 28 days due to tumor burden in the control (vehicle) group. (A, B) Whole body weights and (C) liver weights of male and female mice were monitored throughout the course of treatment administration. No significant differences in body weights or liver weights were observed with treatment. A two-way ANOVA test with Bonferroni's post-hoc analysis was used to calculate statistical significance between all treated pairs.

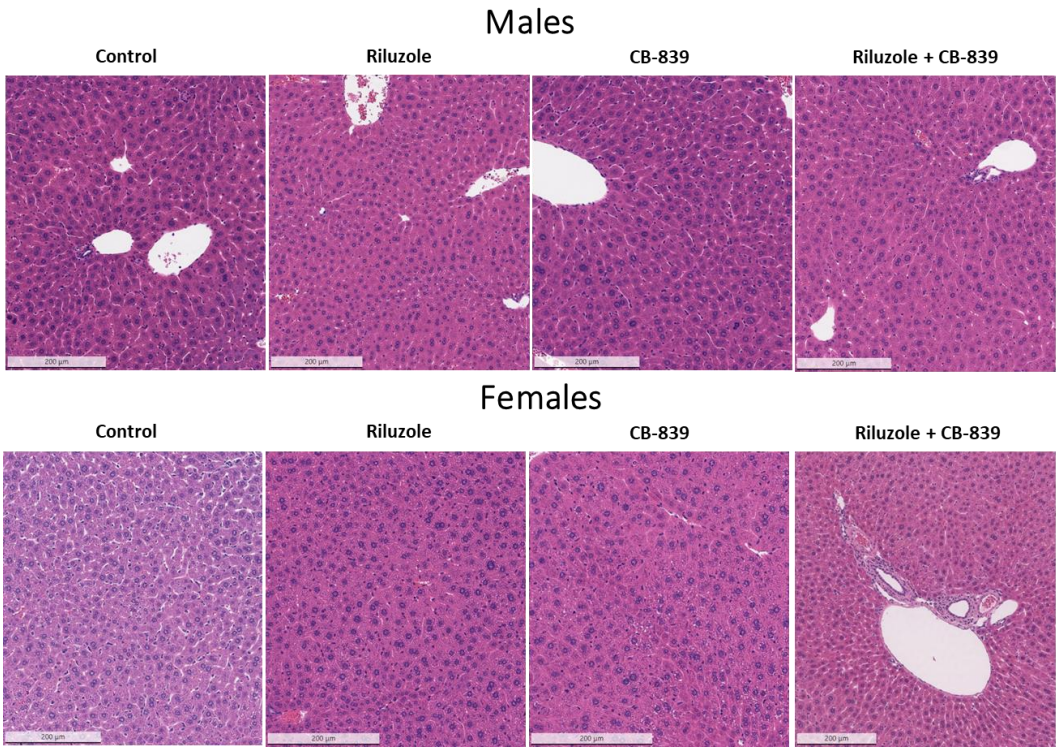

Figure 17: Daily administration of riluzole and CB-839 does not induce liver toxicity: Hematoxylin and eosin (H&E)-stained liver sections from mice treated with vehicle control (DMSO + PBS), riluzole (10 mg/kg), CB-839 (200 mg/kg), or the combination of riluzole (10 mg/kg) and CB-839 (200 mg/kg). All livers display normal hepatic architecture. Livers (n=3 for each group) from male and female mice were harvested and analyzed upon termination of the experiment.

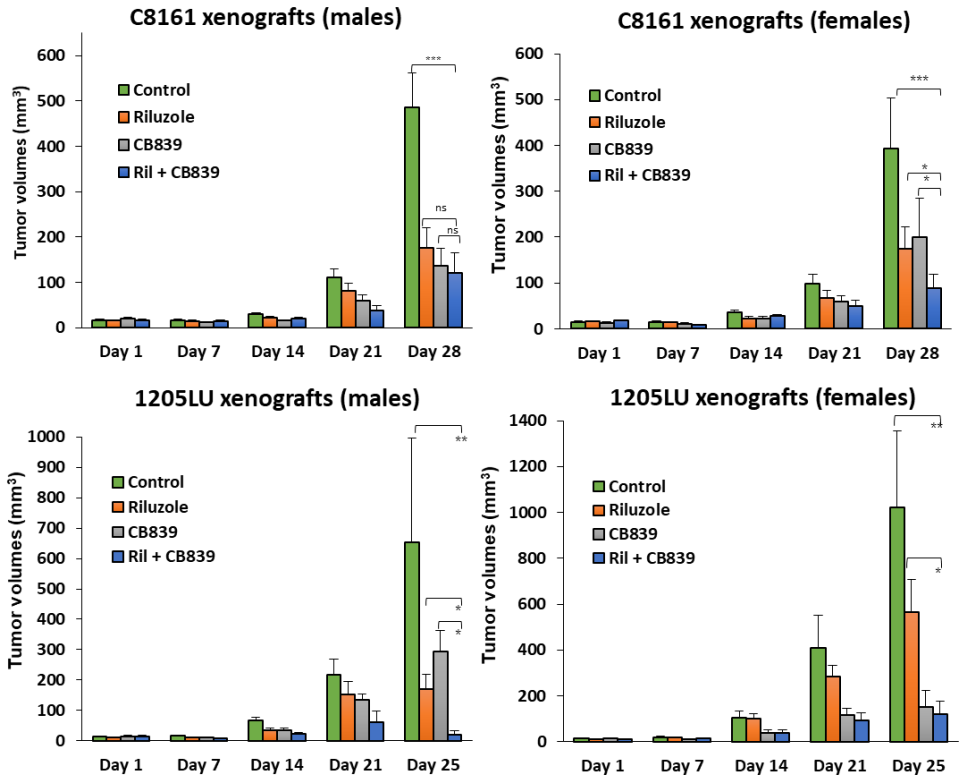

Figure 18: ***In vivo*** **xenograft tumorigenicity assay:** Two independent xenografts were established in male (n=20) and female (n=20) mice using either C8161 or 1205LU human melanoma cells. The groups were vehicle control (DMSO + PBS), riluzole (10 mg/kg), CB-839 (200 mg/kg), or the combination of riluzole (10 mg/kg) and CB-839 (200 mg/kg). All agents were given daily by p.o. gavage. All tumor-bearing mice were euthanized due to large tumor burden in the control (vehicle) group. A two-way ANOVA test with Bonferroni's post-hoc analysis was used to calculate statistical significance between all treated pairs. Each bar represents volumes of tumors (mean ± SE), n=5 for each of the four treatment groups for males or females.

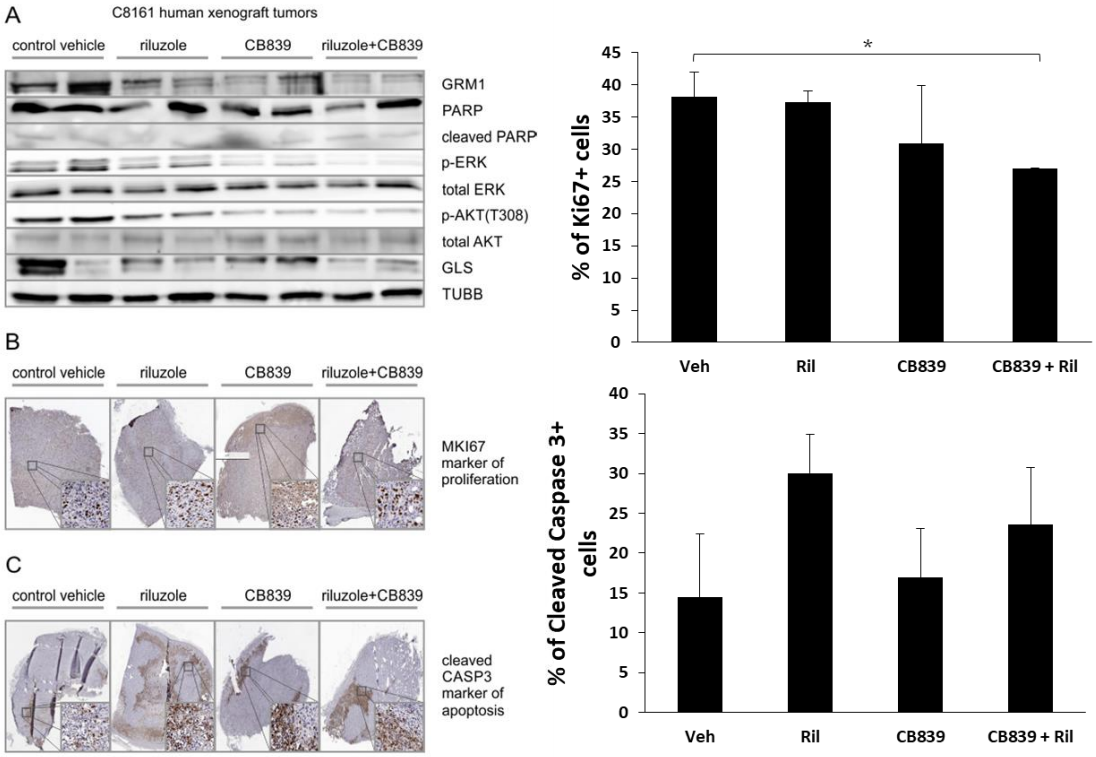

Figure 19: Molecular characterization of excised tumor xenografts post treatment: (A) Levels of GRM1, GLS, phosphorylated-AKT, phosphorylated-ERK and cleaved PARP in the excised xenografts were examined by western immunoblots. IHC staining of tumors with (B) Ki67 and (C) Cleaved Caspase 3. Graphs displaying the percentage of positively stained tumor cells are shown to the right of the representative images. Three tumor specimens (n=3) for all of the treatment groups. *p value < 0.05.

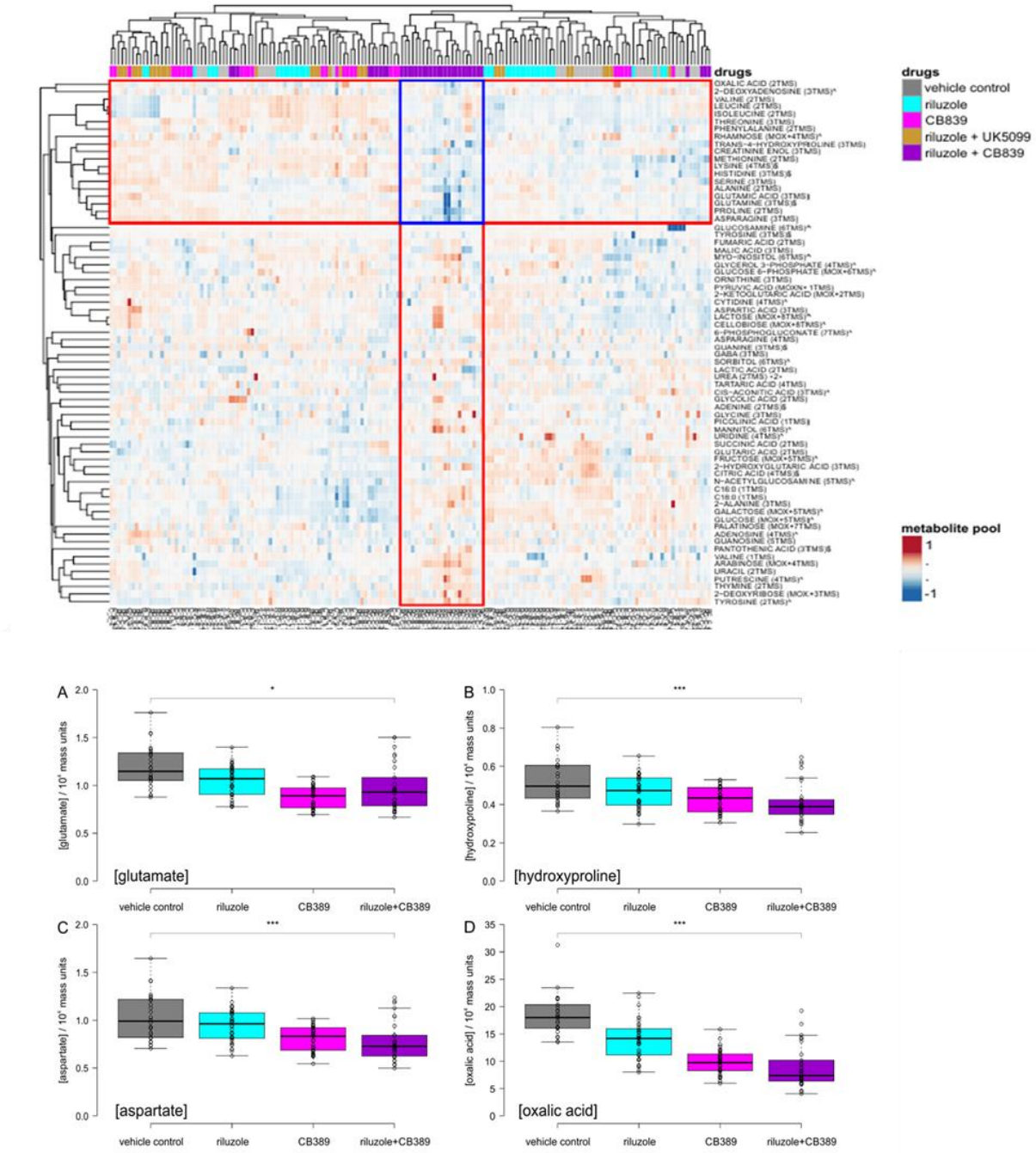

Figure 20: Decoding circulating metabolite levels in combination modality of riluzole and CB839 targeting GRM1$^+$ melanoma: Top panel displays the metabolomic profile of blood plasma isolated from xenografted mice – shows major cluster response of TCA cycle and glutamate-related metabolites upon drug treatment. The bottom panel displays metabolites that stand out markedly as quantified in the A, B, C and D. n=3 for each of the tested drug conditions (vehicle control, riluzole, CB-839, and riluzole + CB-839). Riluzole + UK5099 (gold color in top panel) was part of another study irrelevant to this thesis. **p* value < 0.05, ****p* value < 0.001.

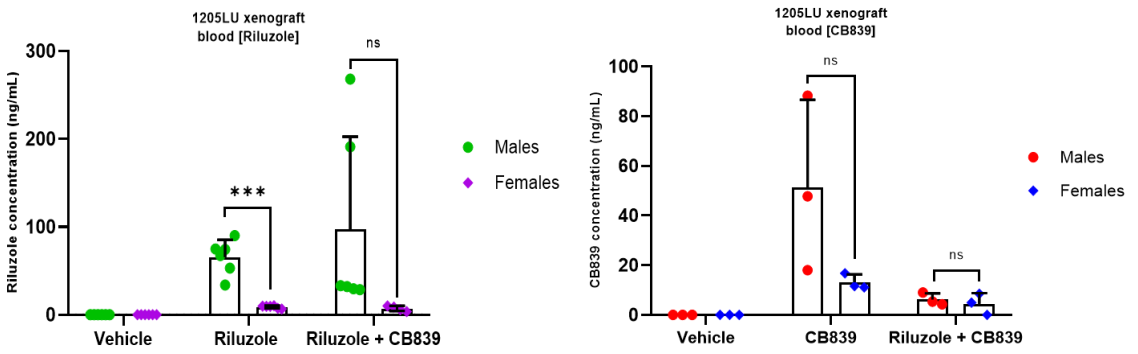

Figure 21: Determination of unbound active riluzole and CB-839 in blood plasma: LC-MS profiles of blood plasma isolated from xenografted mice show active riluzole (left) and/or CB-839 (right) levels in nanograms per mL of blood plasma in their respective treatment groups (single treatments of riluzole, CB839, as well as in combination with riluzole and CB839). when compared to vehicle control. The active compound data is further classified into males/females (green/purple for riluzole and red/blue for CB-839). n=3, ****p* value < 0.001, ns = no significance.

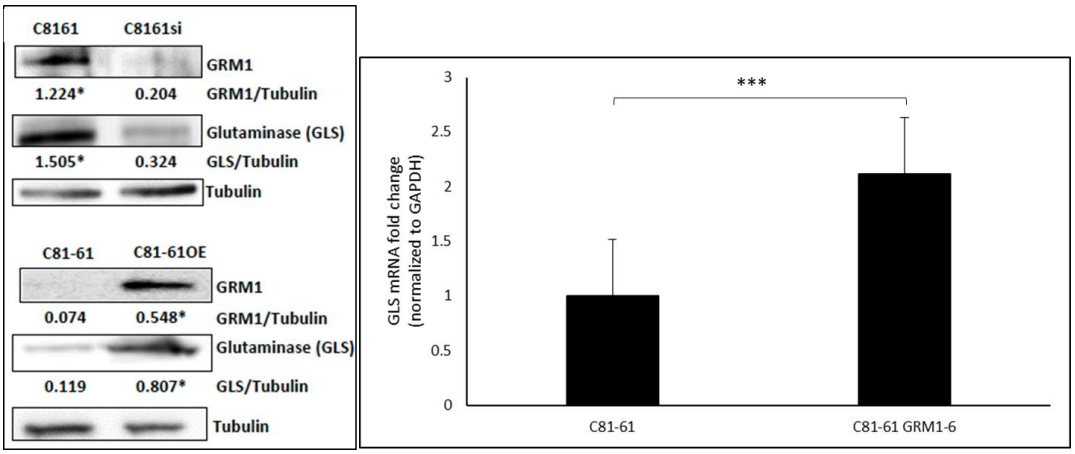

Figure 22: Changes in GLS mRNA and protein levels post alterations in GRM1 protein expression: Modulations in GRM1 protein expression and subsequent changes in GLS protein levels, in C81-61 and C81-61 GRM1-6 (C81-61OE), were determined via western immunoblots. Tubulin was used as the loading control. Fluctuations in mRNA transcript levels were determined via RT-qPCR and normalized to GAPDH. n=3, **p* value < 0.05, ****p* value < 0.001

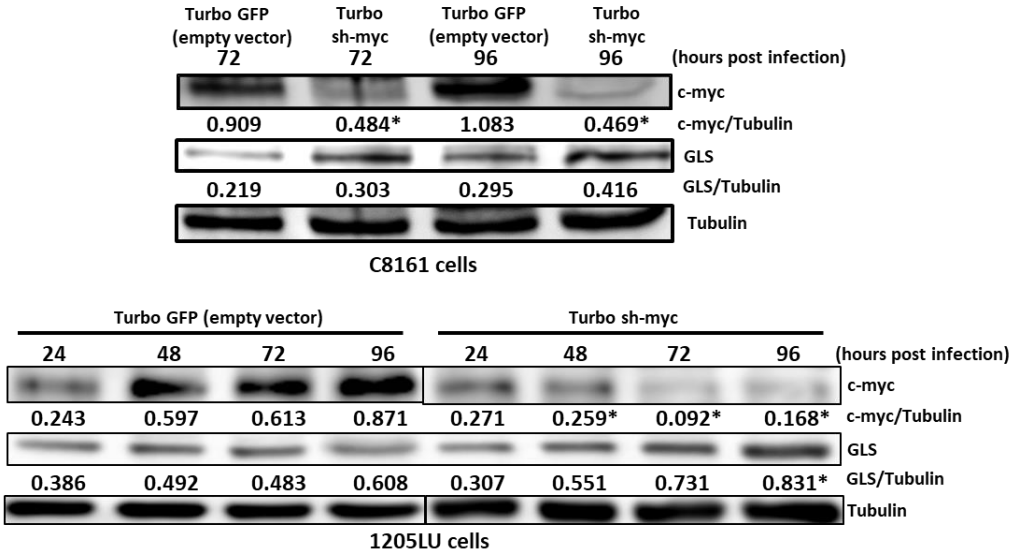

Figure 23: Knockdown of c-Myc does not reduce GLS expression: C8161 and 1205LU cells were transiently infected with lentiviral particles against c-Myc (Turbo sh-myc). Turbo GFP was used as the empty vector. Cells were lysed and blotted with the indicated antibodies. Tubulin was used as the loading control. The experiment was performed in biological triplicates. n=3, **p* value < 0.05

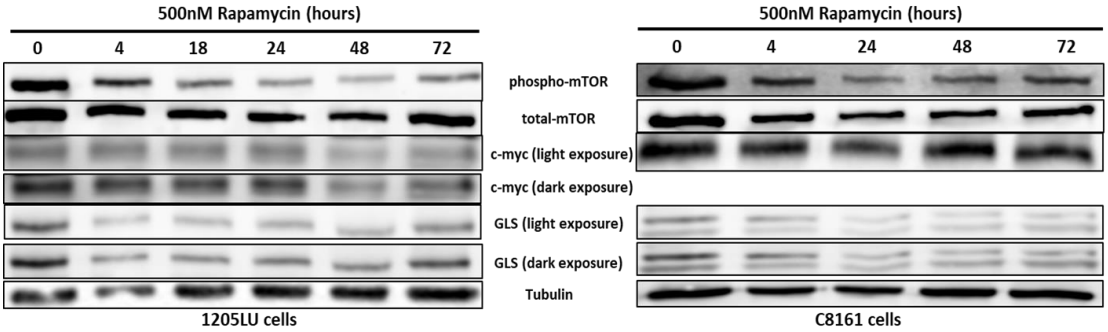

Figure 24: The mTORC pathway regulates GLS in GRM1^{+} melanoma cells: C8161 and 1205LU cells were treated with 500 nM rapamycin. Protein lysates were collected and prepared at the indicated time points. Specified antibodies were utilized for western blotting. Tubulin was used as the loading control. The experiment was performed in biological duplicates.